FEASIBILITY STUDY ON CONCENTRATED SOLAR POWER PLANTS IN MALAYSIA

CHOY DE JEN

FACULTY OF ENGINEERING
UNIVERSITY OF MALAYA
KUALA LUMPUR

2020

FEASIBILITY STUDY ON CONCENTRATED SOLAR POWER PLANTS IN MALAYSIA

CHOY DE JEN

RESEARCH REPORT SUBMITTED IN PARTIAL FULFILMENT OF THE REQUIREMENTS FOR THE DEGREE OF MASTER OF MECHANICAL ENGINEERING

FACULTY OF ENGINEERING
UNIVERSITY OF MALAYA
KUALA LUMPUR

2020

UNIVERSITY OF MALAYA

ORIGINAL LITERARY WORK DECLARATION

Name of Candidate: CHOY DE JEN

Matric No: 17202145/1

Name of Degree: Master of Mechanical Engineering

Title of Project Paper/Research Report/Dissertation/Thesis ("this Work"):

Feasibility Study on Concentrated Solar Power Plants in Malaysia

Field of Study: Renewable Energy

I do solemnly and sincerely declare that:

(1) I am the sole author/writer of this Work;
(2) This Work is original;
(3) Any use of any work in which copyright exists was done by way of fair dealing and for permitted purposes and any excerpt or extract from, or reference to or reproduction of any copyright work has been disclosed expressly and sufficiently and the title of the Work and its authorship have been acknowledged in this Work;
(4) I do not have any actual knowledge nor do I ought reasonably to know that the making of this work constitutes an infringement of any copyright work;
(5) I hereby assign all and every rights in the copyright to this Work to the University of Malaya ("UM"), who henceforth shall be owner of the copyright in this Work and that any reproduction or use in any form or by any means whatsoever is prohibited without the written consent of UM having been first had and obtained;
(6) I am fully aware that if in the course of making this Work I have infringed any copyright whether intentionally or otherwise, I may be subject to legal action or any other action as may be determined by UM.

Candidate's Signature Date: 8.9.2020

Subscribed and solemnly declared before,

Witness's Signature Date: 8.9.2020

Name: Choy Sher Rin

Designation: Miss

FEASIBILITY STUDY ON CONCENTRATED SOLAR POWER PLANTS IN MALAYSIA

ABSTRACT

The rapidly growing economy and population in Southeast Asia has elevated the need for affordable, secured, sustainable and environmentally friendly energy sources. One such energy source is solar energy which is a suitable energy source for most Southeast Asian countries which are within the Sun Belt region. This study performs a performance and financial analysis on concentrated solar power (CSP) technologies, specifically the solar power tower (SPT) in the Malaysian environment through the use of simulation software. The significance of the study lies in the fact that limited research has been done on CSP technologies in Malaysia and the study is in-line with the government's effort to achieve 20% electricity generation from renewable energy by 2035. The layout optimization of the solar field was done using the SolarPILOT software which served as an input to the System Advisory Model (SAM) software where the performance and financial analysis were performed. Results based on the analysis showed that the capacity of the CSP models for KLIA and Gaya Island are 13.7 MWe with an annual energy production of 41,145,964 kWh and 57,999,736 kWh respectively. The net capital cost for both plants are RM 368,563,644 and RM 352,014,120 with a positive NPV of RM 32,649,339 and RM 30,965,316 respectively. The PPA price for the KLIA plant was found to exceed the Malaysian government's Feed-in-Tariff (FiT) rate while the Gaya Island plant maintained below that rate. LCOE values for both CSP models were found to exceed the national average value of 0.78 RM/kWh. The study showed that the Solar Power Tower (SPT) technology is feasible in both the performance and economical aspects provided the required PPA price is agreed upon. However, it may not be the best option due to the higher cost and labor requirements compared to technologies like solar PV.

Keywords: feasibility, SPT, simulation, SolarPILOT, SAM

KAJIAN KEBOLEHLAKSANAAN LOJI PENJANAKUASA TENAGA SURIA TERTUMPU DI MALAYSIA

ABSTRAK

Ekonomi dan penduduk yang berkembang pesat di Asia Tenggara telah meningkatkan keperluan sumber tenaga yang berpatutan, terjamin, lestari dan mesra alam. Salah satu sumber tenaga tersebut adalah tenaga suria yang merupakan sumber tenaga yang sesuai untuk kebanyakan negara Asia Tenggara yang berada di wilayah "Sun Belt". Kajian ini melakukan analisis terhadap prestasi dan kewangan mengenai teknologi tenaga suria tertumpu (TST), khususnya menara tenaga suria (MTS) di persekitaran Malaysia dengan menggunakan simulasi. Kepentingan kajian adalah kerana penyelidikan terhadap teknologi TST yang terhad di Malaysia dan kajian ini sejajar dengan usaha pemerintah untuk mencapai 20% penjanaan elektrik dari tenaga yang boleh diperbaharui menjelang tahun 2035. Pengoptimuman tata letak medan suria dilakukan dengan menggunakan program SolarPILOT yang berfungsi sebagai input kepada program Model Advisory Model (SAM) di mana analisis prestasi dan kewangan akan dijalankan. Analisis menunjukkan bahawa kapasiti model TST untuk KLIA dan Pulau Gaya adalah 13.7 MWe dengan pengeluaran tenaga tahunan 41,145,964 kWh dan 57,999,736 kWh masing-masing. Kos modal bersih untuk kedua-dua loji tersebut adalah RM 368,563,644 dan RM 352,014,120 dengan nilai NPV positif RM 32,649,339 dan RM 30,965,316 masing-masing. Harga PPA untuk loji KLIA didapati melebihi kadar Feed-in-Tariff (FiT) kerajaan Malaysia sementara loji Pulau Gaya kekal di bawah kadar tersebut. Nilai LCOE untuk kedua-dua model TST didapati melebihi nilai purata nasional, iaitu 0.78 RM/kWh. Kajian ini telah menunjukkan bahawa teknologi MTS dapat dilaksanakan dari aspek prestasi dan juga ekonomi. Namun, ini bukan pilihan terbaik kerana kos dan keperluan tenaga pekerja yang tinggi berbanding dengan teknologi seperti solar PV.

Keywords: kebolehlaksanaan, MTS, Simulasi, SolarPILOT, SAM

ACKNOWLEDGEMENTS

I would like to thank my university for giving me the opportunity to conduct this study and my supervisor, Dr. Mohd Nashrul Mohd Zubir for guiding me throughout my research. I would also like to thank the team at SOLCAST for providing me with the weather data and the team at NREL for providing support for SolarPILOT and SAM where needed. Finally, I would like to thank my parents and my friends for their continuous support.

TABLE OF CONTENTS

LIST OF FIGURES

LIST OF TABLES

LIST OF SYMBOLS AND ABBREVIATIONS

CO_2	:	Carbon dioxide
PV	:	Photovoltaic
CSP	:	Concentrated solar power
SAM	:	System Advisor Model
SPT	:	Solar power tower
PD	:	Parabolic trough
LFR	:	Linear Fresnel reflector
HTF	:	Heat transfer fluid
PML	:	Profiled multi-layer
SiSiC	:	Siliconized silicon carbide
SiC	:	Silicon carbide
DIAPR	:	Directly Irradiated Annular Pressurized Receiver
REFOS	:	Solar-Hybrid Gas Turbine and CC systems
TES	:	Thermal energy storage
DNI	:	Direct Normal Irradiance
GHI	:	Total global horizontal irradiance
DHI	:	Total diffused horizontal irradiance
NaNO3	:	Sodium nitrate
KNO3	:	Potassium nitrate
PCM	:	Phase-change materials
SM	:	Solar multiple
HECTOR	:	Heliostat Cleaning Team Oriented Robot
MEF	:	Multi-effect distillation
MSF	:	Multi-stage flash

VC	:	Vapor compression
RO	:	Reverse osmosis
SWRO	:	Sea and Brackish Water Reverse Osmosis
MD	:	Membrane Distillation
TOU	:	time-of-use
MCRT	:	Monte-Carlo Raytracing
ROI	:	Return of investment
LCOE	:	Levelized cost of electricity
PPA	:	Power purchase agreement
IRR	:	Internal rate of return
NPV	:	Net present value
LSS	:	Large Scale Solar
KLIA	:	Kuala Lumpur International Airport
RE	:	Renewable energy
GITA	:	Green Investment Tax Allowance
O&M	:	Operation & maintenance

CHAPTER 1: INTRODUCTION

1.1 Background

Energy sufficiency and provision has been an important topic throughout history as it has a critical and large impact on human lives and economic growth. In 2018, the majority of global energy is produced from coal (38%) and natural gas (23.2%), with renewable energy only supplying 9.3% of the global energy demand (BP, 2019). The total global CO_2 emission due to energy generation in 2018 is 33890.8 million tonnes, with the Asia Pacific region producing a total of 16744.1 million tonnes, which is 49.4% of the total global emission (BP, 2019). It is widely recognized that CO_2 is the main cause of global warming and as such, the excessive use of coal and natural gas could be directly attributed to the cause of climate change. Thus, more emphasis should be placed on the development and implementation of renewable energy.

The Southeast Asian region has experienced rapid economic growth in the last few decades which has driven up the energy use over the past few decades (International Renewable Energy Agency (IRENA), 2018). The region, including Malaysia, has an abundance of natural resources, with hard coal, lignite, natural gas and oil as shown in figure 1.1 (ASEAN Centre for Energy, 2015). Though not evenly distributed, the countries in this region are also relatively rich is renewable energy sources (ASEAN Centre for Energy, 2017). Since the natural resources are highly accessible and inexpensive in some of these countries, no emphasis was made on the development on alternative, renewable energy generation.

In the past year, the total renewable energy production capacity from all the Southeast Asian countries is around 57,427 MW, with Vietnam having the highest capacity at 18,523 MW (IRENA, 2019). It is a respectable value which had a steady growth over the last 10 years. However, as fossil fuels are not infinite, they will be fully depleted in the future and this process will be accelerated by the ever-growing energy demand. In short, a higher growth rate is needed to account for the rapid increase in energy demand and to reduce the amount of non-renewable modes of energy generation which directly contributes to global warming through the emission of CO_2.

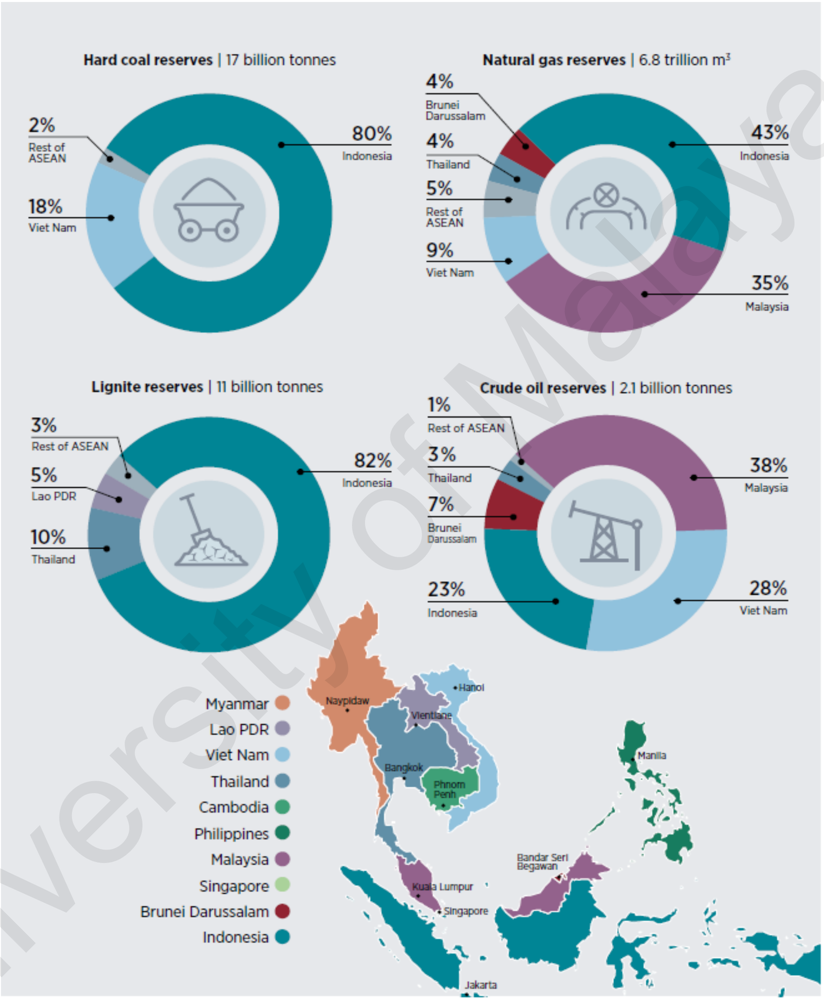

Figure 1.1: Fossil-fuel reserves in Southeast Asia (International Renewable Energy Agency (IRENA), 2018)

Malaysia possesses the largest amount of oil and natural gas reserves among the Southeast Asian countries. As of 2016, 61% of the energy production in Malaysia is generated with natural gas, followed by 32.3% with crude oil, 1.5% with coal and a total of 5.2% from all renewable energy sources (Energy Commission, 2018). In 2017, Malaysia's population was 31.6 million with a total electricity consumption of 152 TWh (Terawatt/hour) and a total CO_2 emission of 211 Mt (Mega-tonne). The CO_2 emission that year was the 3rd highest among the Southeast Asian countries (Energy Agency, 2019).

As Malaysia is situated within the latitude of 4.21 degrees North and 101.98 degrees East, it is located within the Sun Belt or Solar Belt region and is listed under “suitable” for solar power plants as shown in figure 1.2 (Kodama, 2018). As such, various solar energy generation methods can be explored, such as solar farms which uses solar photovoltaic (PV) panels and concentrated solar power plants (CSP).

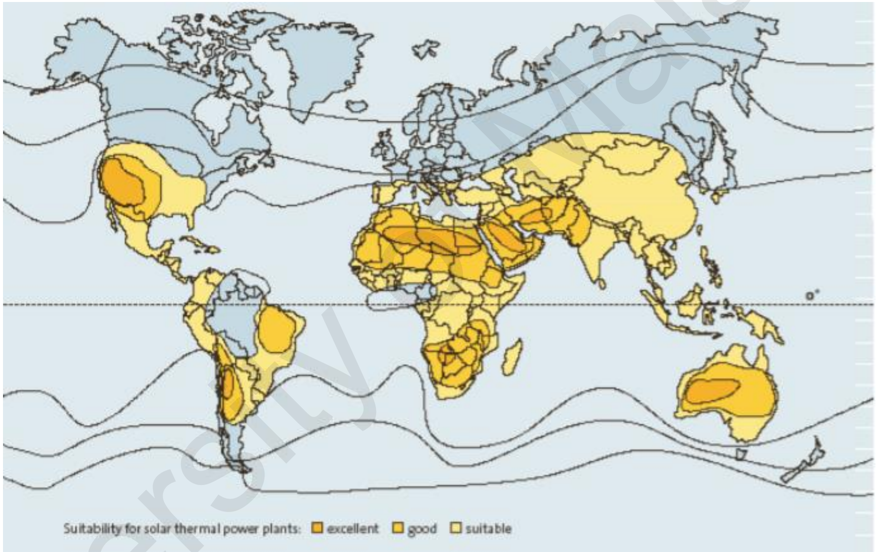

Figure 1.2: Sun-Belt region and location suitability for thermal power plants (Kodama, 2018)

Concentrated solar power plant systems are a popular and rapidly expanding trend worldwide. Based on the SolarPaces web database, as of June 2019, the worldwide CSP plants have a combined capacity of 9,603 MW, with 5,769 MW operational, 2,242 MW under construction and 15,952 MW is currently under planning or development. The two largest adopters of the CSP technology are Spain and the USA, respectively.

The concept of CSP involves the use of mirrors or reflectors to reflect or concentrate solar radiation onto a receiver, which is used to absorb the heat energy. The gathered heat energy heats up the heat transfer fluid (usually water/steam) within the receiver and the fluid is then directed to a conventional steam turbine. The steam turbine drives an electric generator which generates electricity, and the efficiency of such machines are limited by the Carnot cycle. CSP systems can be integrated with conventional power plants that utilizes heat transfer fluids such as steam by functioning as an alternate heat source instead of using boilers in a coal or natural gas power plant. However, unlike solar photovoltaics, only direct solar radiation can be used as it is the only portion of the available solar radiation that can be used in the CSP concept.

The potential for electricity generation using CSP technology in most of the countries in the Sun Belt region is typically many times higher than their electricity demand, creating opportunities for electricity export through high-voltage lines (IEA-ETSAP & IRENA, 2013).

The four main types of solar concentrator systems are parabolic trough, power tower, linear Fresnel, and dish (Santos et al., 2018a). The feasibility study shall be conducted specifically on the solar power tower.

1.2 Problem Statement

The rapidly growing economy of Malaysia has raised concerns regarding the need for affordable, secured and environmentally sustainable energy. Malaysia's over-reliance on fossil fuel and hydroelectric power generation may not be optimal long term solutions to the growing energy demand due to the negatives effects such as the release of greenhouse gasses (CO_2) from the burning of fossil fuel as well as the destruction of natural habitat and landscape from flooding due to the construction of the hydroelectric dam. A possible solution and option for a clean energy generation method is the concentrated solar power (CSP) technology as CSP plants have proven to be an effective technology for the generation of clean and renewable energy. Currently, concentrated solar power generation technology have not been implemented or tested in full scale in Malaysia. There are also not many researches being done on the technology in Malaysia. Therefore, this project aims to study the concept of the concentrated solar power plant and the feasibility of its implementation in Malaysia. It is expected that concentrated solar power plants are a viable power generation option as the geographical location of Malaysia is situated within the Sun Belt region.

1.3 Objectives of the study

1. To select suitable areas in Malaysia based on the basic requirements of a CSP plant.
2. To design a concentrated solar power plant model using simulation software based on the geographical and weather data available.
3. To obtain the performance and financial metrics of the CSP plant models.
4. To investigate the feasibility of CSP implementation in Malaysia.

1.4 Scope of the Study

1. The feasibility study will only be conducted on locations within Malaysia.
2. The design of the concentrated solar power plant model will only be done on locations deemed suitable for CSP implementation.
3. The study will only be done on Solar Tower CSP plants.

CHAPTER 2: LITERATURE REVIEW

2.1 Introduction

As global warming worsens and the topic of climate change becomes the mainstream topic discussed in every environmental forums and conferences, it is important to research on topics related to clean energy. One such topic is the concentrated solar power generation technology (CSP).

In this chapter, the types of CSP technology as well as the main components of a CSP plant will be described. Then, studies done on the desalination process of sea water will be discussed. The heliostat cleaning process along with the different technologies available as well as their performance will be reviewed. Following that, validation of the simulation software used in this study will be described. Next, existing research on the prospective of Concentrated Solar Power (CSP) technologies will be discussed, along with the solar to electricity efficiency for each type of CSP. Lastly, the gaps in knowledge will be discussed along with the significance of the study, and a summary of the literature review will be given.

2.2 CSP Technologies

There are currently four different arrangements being used in CSPs around the world. These arrangements can be distinguished by two different categories, the concentrator focus method and the mobility of the receiver (IEA-ETSAP & IRENA, 2013). As shown in Figure 2.1 below, Parabolic Trough and Linear Fresnel Reflector plants concentrate sun rays into a focal line absorber. For the Power Tower and Solar Dish plants, the sun rays are focused onto a focal point absorber as shown in Figure 2.2 (IEA-ETSAP &

IRENA, 2013). Linear Fresnel Reflector plants and Solar Power Tower plants have fixed receivers while Parabolic Trough and Solar Dish plants have solar tracking abilities (Lovegrove & Stein, 2012b).

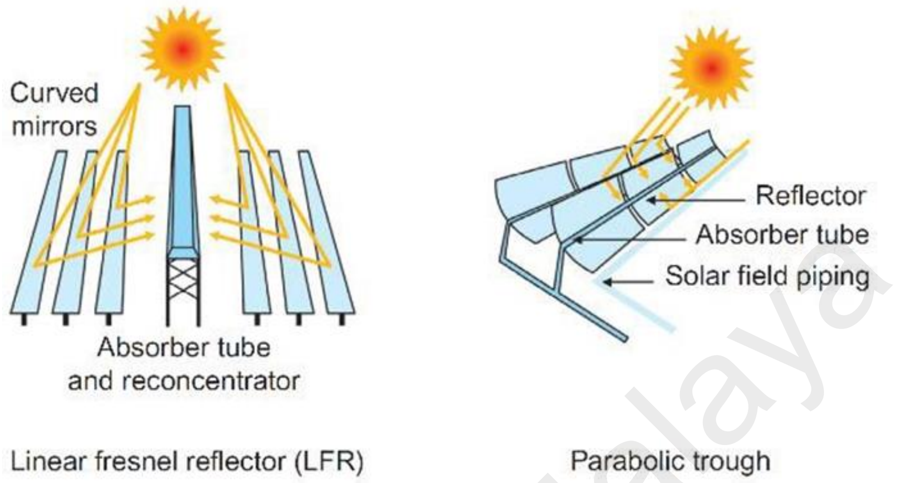

Figure 2.1: LFR and Parabolic Trough focal line absorber (IEA-ETSAP & IRENA, 2013)

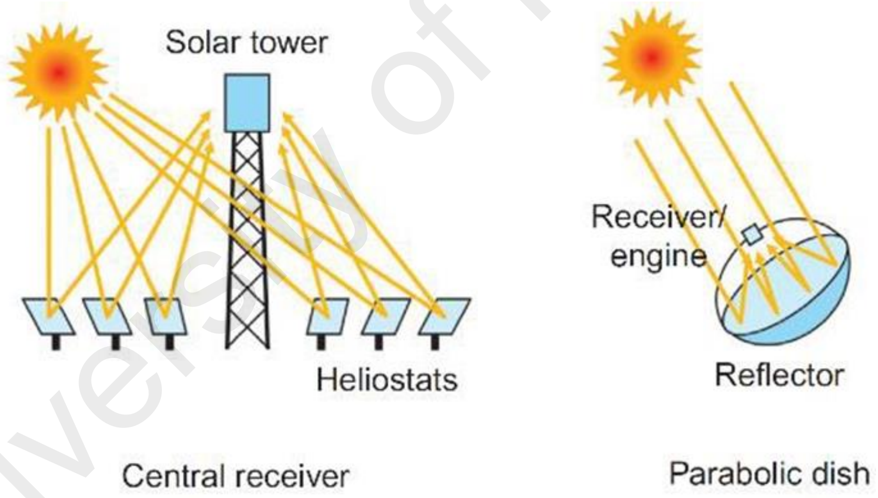

Figure 2.2: Solar Tower and Parabolic Dish focal point absorber (IEA-ETSAP & IRENA, 2013)

2.2.1 Linear Fresnel Reflector

Linear Fresnel reflector (LFR) systems have rows of flat mirror which are positioned at a precise angle that reflects the sun's rays onto the receiver (Pitz-Paal, 2014). For thermal systems, the fixed receiver does not only avoid the requirement of rotary joints for the heat transfer fluid, but it can also reduce convection losses from a thermal receiver because of its permanently down-facing cavity (Lovegrove & Stein, 2012b). Linear Fresnel Reflectors have simple designs which are low in cost to fabricate and build (Santos et al., 2018b). However, it has one of the lowest optical efficiencies among the different types of CSP technologies (Lovegrove & Stein, 2012b). The benefit of having a fixed receiver is that higher pressures can be sustained for the process fluid which allows for steam generation instead of using heat transfer fluids. This excludes the need for heat transfer fluids and heat exchangers, which in-turn reduces the overall maintenance and operating costs (ELBEH, 2017).

2.2.2 Parabolic Dish

Parabolic dishes utilize multiple small flat mirrors, which are placed together to form a dish shape that is able to concentrate sun rays onto a thermal receiver located in-front or above the centre of the dish (B Hoffschmidt, Alexopoulos, Göttsche, Sauerborn, & Kaufhold, 2012). It is similar to how a satellite dish functions. The Parabolic Dish system offer the highest potential solar conversion efficiencies of all the CSP technologies due to the fact that their full aperture is always facing directly at the sun and avoids the 'cosine lost effect' present in the other systems (Lovegrove & Stein, 2012b).

3.2.3 Parabolic Trough

The Parabolic Trough system is the most mature CSP technology and it is widely used in many existing commercial power plants (ELBEH, 2017). Similar to the Linear Fresnel Reflectors, this system has long rows of reflectors which reflects sun rays onto the central heat receiver. The difference is that the reflectors are parabolic trough shaped. Overall, the optical efficiency Parabolic Trough system is higher compared to some of the other technologies, along with the ability to have a storage system. The concentration of solar irradiance on the receiver with the parabolic design can achieve values up to 70 to 100 times the initial value of solar irradiance received by the reflectors (*Concentrating Solar Power*, 2016).

2.2.4 Solar Power Tower

A solar power tower system utilizes a large field, better known as the solar field, which consists of large numbers of stationary flat mirrors that track the sun, known as heliostats. These mirrors functions like a magnifying glass and concentrate solar radiation onto a receiver on a solar tower. The arrangement for this system is a shown in Figure 2.3. The heliostats can vary greatly in size, depending on the layout of the solar field and plant design. The size of the heliostats has a significant trade-off in terms of advantages and disadvantages. Large heliostats have larger power outputs, but they require stronger structures with powerful motors and are more expensive to build and maintain. Small heliostats are lighter, which requires less powerful motors and are less expensive. However, to achieve the same power output as a large heliostat, many smaller mirrors are required.

High solar concentration factors of up to 1000 can be achieved due to the relatively large size of the solar field and the small central receiver (B Hoffschmidt, Alexopoulos, Rau, et al., 2012). Due to these high concentration factors, a 15% to 17% annual solar to electricity conversion efficiency could be achieved (Brussels & Ce, 2011). Such high levels of solar concentration on a receiver results in high temperatures similar to that of boilers. As such this technology is used as an environmentally friendly alternative in a conventional steam turbine power plant.

There are three main heat transfer fluids (HTF) currently in use in CSP plants, namely steam, molten salt, and air. Most SPT plants use molten salt as the HTF, where two separate loops will be connected to a heat exchanger. The primary loop uses molten salt which transfers heat from the receiver to the water in the secondary loop, which turns the water into steam.

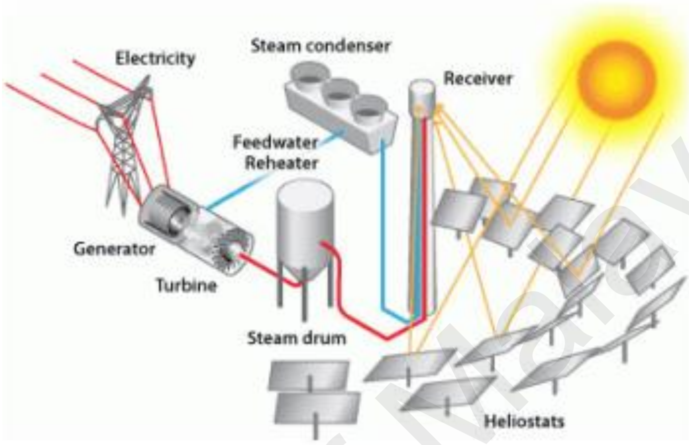

Figure 2.3: Plant layout for solar power tower CSP plants ("Power Tower System Concentrating Solar Power Basics | Department of Energy," n.d.)

2.2 Primary Components of CSP plants

2.2.1 Solar Reflector

The solar reflector, also known as heliostats in SPT applications, is an integral part of a CSP system that reflects the incoming sunlight onto the components which absorbs it. The material used to manufacture these reflectors are required to have high reflectivity and are sturdy enough to withstand the harsh outdoor conditions. Solar collectors that are currently used in CSP systems around the world can be classified into two different types, namely, flat plate or concentrating plate. In most plants, the concentrating plate which curvature is based on a parabolic concentrator, is used. A solar collector based on a parabolic concentrator can either be a trough with a two-dimensional parabolic shape, a three-dimensional dish with dual axis tracking heliostats or multiple arrays of mirrors with single axis tracking (Pihl & Frescativägen, n.d.).

The Linear Fresnel reflector is a reflector that is derived based on the Fresnel lens which can be described as a lens that is divided into multiple concentric annular sections. Fresnel lenses essentially functions like a convex lens, but with reduced thickness. The various different types of solar reflectors used in CSP plants such as the parabolic trough, linear Fresnel, solar power tower and solar dish are as shown in Figure 2.4 along with the respective concentration ratio and indicative temperature obtained for the respective reflector types.

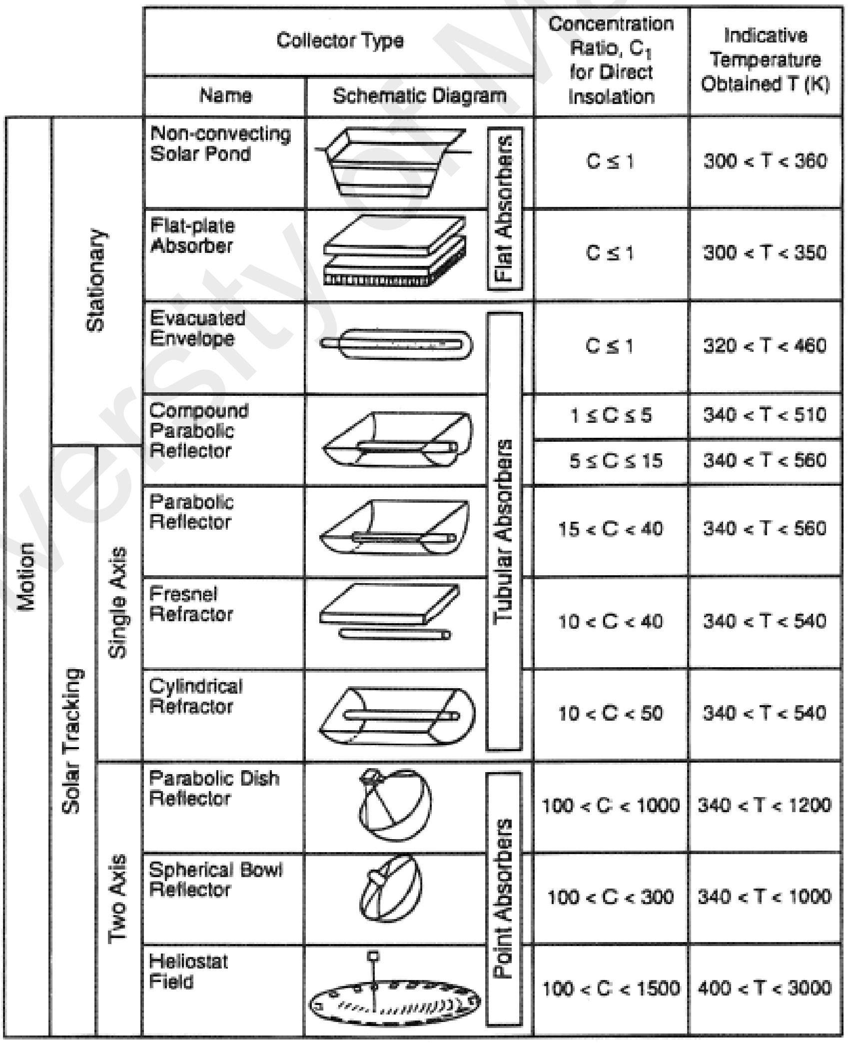

Motion			Collector Type: Name	Collector Type: Schematic Diagram	Concentration Ratio, C_1 for Direct Insolation	Indicative Temperature Obtained T (K)
Motion	Stationary		Non-convecting Solar Pond	Flat Absorbers	$C \leq 1$	$300 < T < 360$
	Stationary		Flat-plate Absorber	Flat Absorbers	$C \leq 1$	$300 < T < 350$
	Stationary		Evacuated Envelope	Tubular Absorbers	$C \leq 1$	$320 < T < 460$
	Stationary		Compound Parabolic Reflector	Tubular Absorbers	$1 \leq C \leq 5$	$340 < T < 510$
	Solar Tracking	Single Axis			$5 \leq C \leq 15$	$340 < T < 560$
	Solar Tracking	Single Axis	Parabolic Reflector	Tubular Absorbers	$15 < C < 40$	$340 < T < 560$
	Solar Tracking	Single Axis	Fresnel Refractor	Tubular Absorbers	$10 < C < 40$	$340 < T < 540$
	Solar Tracking	Single Axis	Cylindrical Refractor	Tubular Absorbers	$10 < C < 50$	$340 < T < 540$
	Solar Tracking	Two Axis	Parabolic Dish Reflector	Point Absorbers	$100 < C < 1000$	$340 < T < 1200$
	Solar Tracking	Two Axis	Spherical Bowl Reflector	Point Absorbers	$100 < C < 300$	$340 < T < 1000$
	Solar Tracking	Two Axis	Heliostat Field	Point Absorbers	$100 < C < 1500$	$400 < T < 3000$

Figure 2.4: Types of solar reflector and the respective parameters (Norton, n.d.)

In order to be able to receive and reflect the highest possible amount of solar energy, a solar reflector should be designed to track the sun position instead of being in a stationary position. To accomplish this, tracking mechanisms were developed and they can be categorized based on the tracking modes, i.e. single or dual axis tracking. Figure 2.5 below shows a flat reflector and its variation between 4 different tracking modes.

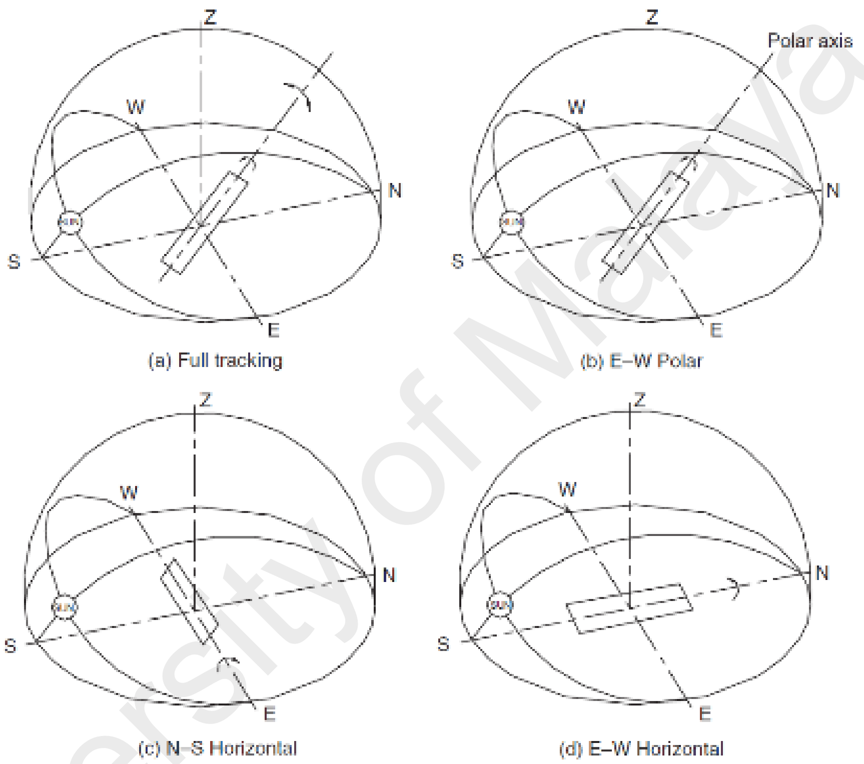

Figure 2.5: Solar reflector geometry for various tracking modes (Kalogirou, 2012)

Figure 2.5 (a) shows dual axes tracking, which allows the reflector to perform a full tracking of the sun's path. Figure 2.5 (b), (c) and (d) shows single axis tracking mechanisms where the reflector is partially fixed and can only follow part of the sun's path by tilting. The figures show the tilting direction of East-West (Polar), North South and East-West (Earth Axis) respectively.

Each mode of tracking yields different amounts of direct solar radiation on the reflectors surface which is directly related to the cosine of the incidence angle. The dual axis tracking system will have the highest incident radiation yields while the other methods fluctuates based on the seasons and equinoxes. However, the effect of cloud cover is still a major component that affects the amount of incident radiation and the tracking system can only offset part of its effects by tracking the areas in the sky where the highest amounts of solar irradiance can be received.

2.2.2 Solar Receiver

In a CSP system, the receiver functions as an absorber which absorbs the solar radiation reflected onto it and converts it to heat energy. The heat energy is then transferred to the heat transfer fluid (HTF) which is in contact with the inner surface of the receiver. In a single-axis tracking reflector, the solar radiation reflected in a line across the receiver. Meanwhile, dual-axis or full tracking mechanisms focusses the solar radiation in a single spot. In the early days CSP receivers, emphasis was given to tubular designs. However, in recent times more attention is being placed on volumetric receiver designs (Ávila-Marín, 2011).

2.2.2.1 Tubular Receivers

The tubular receiver was designed and implemented during the preliminary period of CSP plants. Tubular receivers utilize tubular designs which functions by absorbing concentrated solar radiation through a collection of tubes. The heat energy is then transferred to the HTF within the tubes. A cross-section of the basic design and the temperature gradient is shown in Figure 2.6.

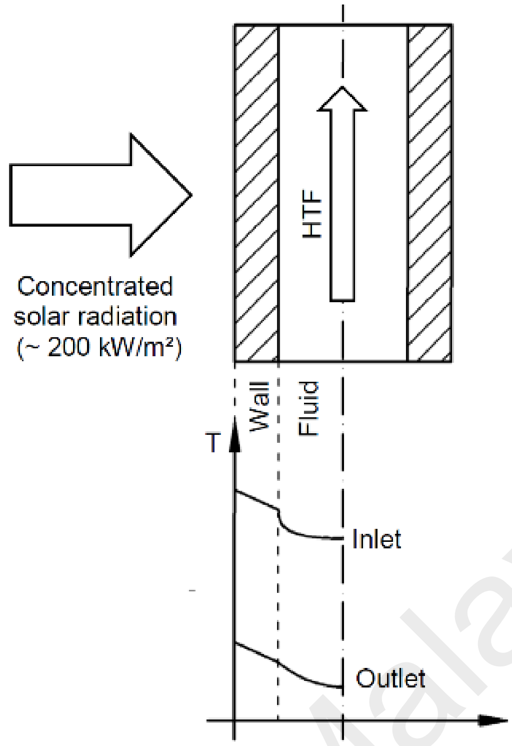

Figure 2.6: Cross-Section and temperature gradient of tubular receivers (Romero, Buck, & Pacheco, 2002)

Based on Figure 2.6, it can be seen that the temperature of the tube body remains higher than the HTF temperature across the inlet and outlet. This is a disadvantage as in limits the maximum operating temperature of the receivers due to which is based on the recommended operating temperature of the tube body material. This issue can be bypassed by pressurizing the HTF in the tube, in which the limiting factor becomes the yield strength of the tube body's material. Another issue faced when using tubular receivers is the ambient heat loss, which can be in the form of thermal convection, radiation, or reflective losses. In order to minimize such losses, tubular receivers are encased within a cavity with other receivers. Reflective losses can also be minimized by applying coatings, which are usually dark colored, to aid solar absorbance.

The Solar One project, which was the first large scale test for a solar power tower (SPT) plant, had a central tower with external tubular receivers as shown in Figure 2.7 below. The Solar One SPT plant was completed in 1981 and operated from 1982 to 1988 with a capacity of 10 MWe. and it was located in the Mojave Desert, USA. In the system, water is used as the HTF and is in direct contact with the inner area of the receiver. Water was converted to steam directly and power generation was done using the Rankine Cycle (NREL, 2001).

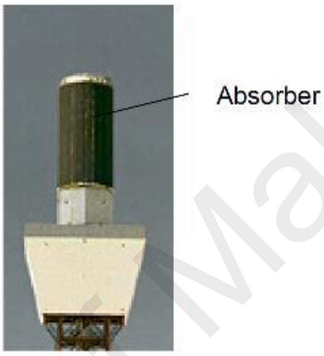

Figure 2.7: Solar One tubular receiver (Ctein, n.d.)

Different variations of the tubular receiver have been designed and implemented throughout the years. One such design is the SOLGATE low temperature receiver as shown in Figure 2.8. This receiver can accommodate liquids with outlet temperatures of approximately 550 °C ("SOLGATE Final Publishable Report," 2002).

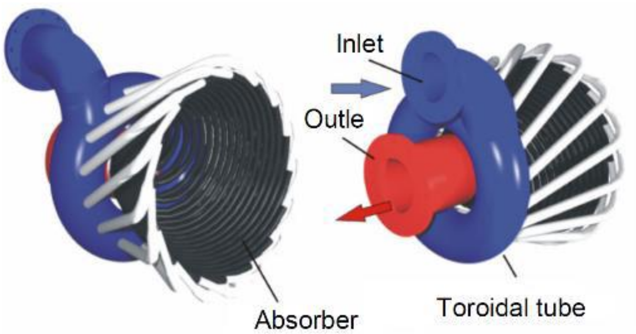

Figure 2.8: SOLGATE low temperature tubular receiver ("SOLGATE Final Publishable Report," 2002)

Another variation of the tubular receiver design is the Solar Hybrid Power and Cogeneration plants (SOLHYCO) tubular cavity design as shown in Figure 2.9. This tubular receiver was integrated into a system and combine with a 100kW micro turbine, with an outlet fluid temperature of approximately 800°C (Heller, 2011).

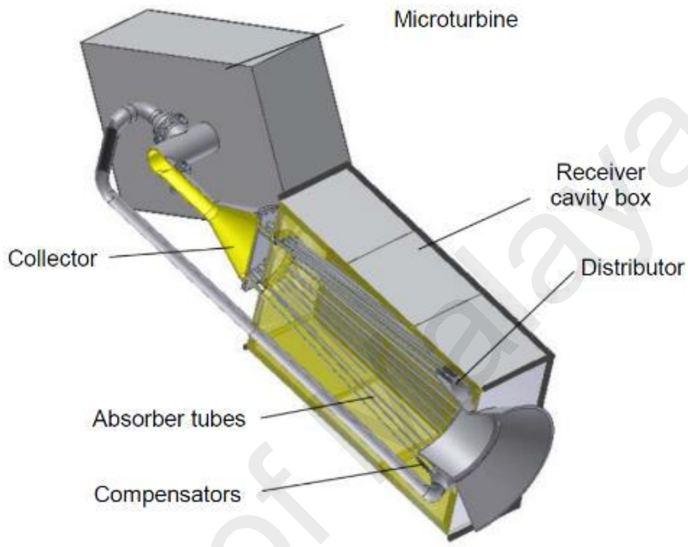

Figure 2.9: SOLHYCO tubular cavity receiver (Heller, 2011)

The difference between this receiver design and other designs is that this design is based on profiled multi-layer (PML) tubes which are tubes with three metallic layers. The outer layer is a nickel-based alloy that can withstand high temperatures, which is used to provide structural strength. The middle layer is copper, which is used to transfer heat from the receiver due to its excellent heat conductivity. The inner layer is also made using the same nickel-based alloy as the outer layer. The inner layer protects the copper layer from corrosion and oxidation at high temperatures (Heller, 2011).

Another tubular receiver design that is, in parts, similar to the SOLHYCO design, is the Solar Up-Scale GAS Turbine System (SOLUGAS) as shown in Figure 2.10. This system adopts a combined cycle with a solar pre-heated

Brayton topping cycle followed by a Rankine bottoming cycle (Korzynietz et al., 2016). The receiver houses rows of absorber tubes in a circular insulated chamber, which are used to pre-heat pressurized HTF, which was air in this case, up to a temperature of 800°C before the air enters the combustion chamber of a gas turbine with a capacity of 4.6 MWe.

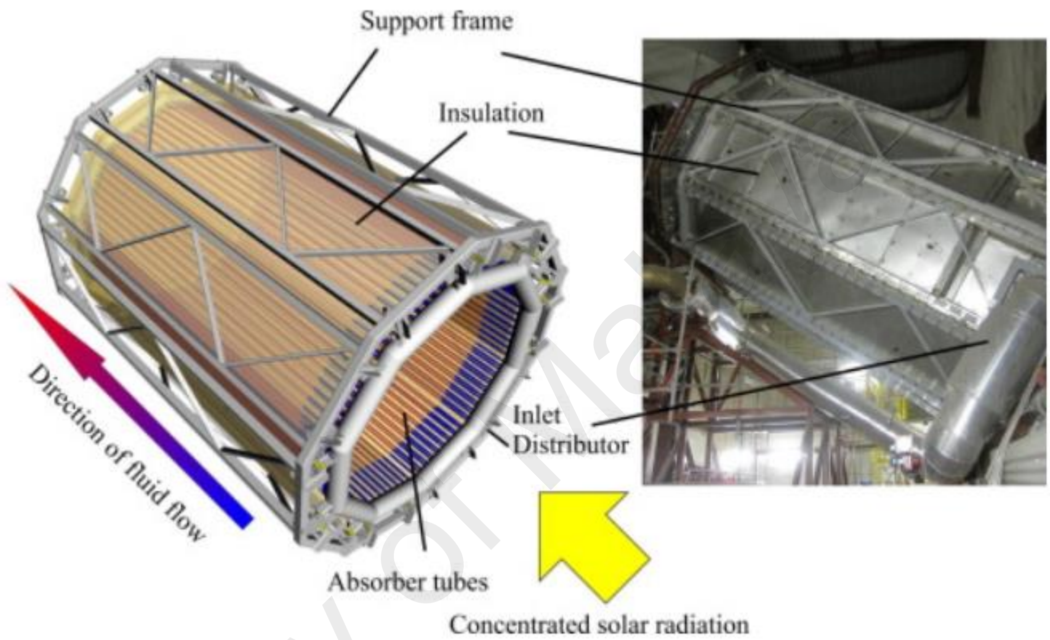

Figure 2.10: SOLUGAS tubular cavity receiver (Korzynietz et al., 2016)

2.2.2.2 Volumetric Receivers

Volumetric receivers, also known as absorption receivers, are designed in a way where the heat from concentrated solar radiation is absorbed directly by the working fluid which comes in contact with it. The design incorporates a receiver cavity fitted with absorbers, which are usually made of materials that comprise of porous interconnecting elements such as foam, honeycomb structures and others with specific porosity (Aichmayer, 2011). The benefit of a volumetric receiver design is the heat transfer area, which is much larger compared to the heat transfer area of the tubular receivers. This allows for the absorber material to absorb higher amounts of solar flux when in contact with concentrated solar radiation while keeping compact at high temperatures (Kami et al., 1997).

Another advantage of this design is that the temperature increases while having a lower solar flux density concentrated on the receiver when compared to the tubular receiver. This results in a irradiated surface temperature which is lower than the outlet temperature, thus reducing re-radiation losses (Ávila-Marín, 2011). The basic cross-section of a volumetric receiver is shown in Figure 2.11. The HTF, usually air, flows through the volume while solar or heat energy is transferred through forced convection from the absorber to the HTF.

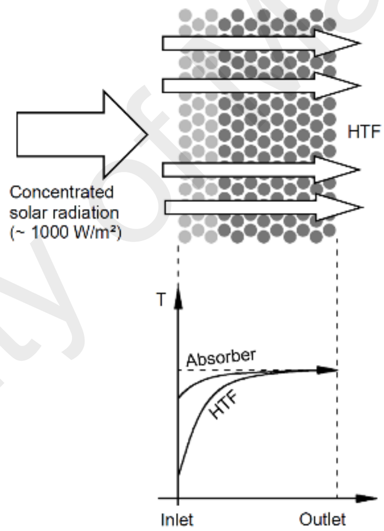

Figure 2.11: Cross-section of volumetric receivers (Romero et al., 2002)

The primary heat transfer mode involved in the transfer of heat from the absorber to the HTF in a volumetric receiver is convective heat transfer. The radiation induced heating of the HTF due to the effects of refraction and scattering is much lower compared to convective heat transfer and hence, it is usually negligible (Bergman, Lavine, Incropera, & Dewitt, 2011).

The most common materials used to manufacture the absorbers are metals and ceramics due to their ability to withstand high temperatures. The usage of metals for absorbers in volumetric receivers enables an outlet fluid temperature to reach t a temperature of 800°C to 1000°C. Receivers fabricated using siliconized silicon carbide (SiSiC) and silicon carbide (SiC) are able to achieve temperatures of up to 1200°C and 1500°C respectively (Ávila-Marín, 2011).

Volumetric receivers are functional in either atmospheric pressure or pressurized conditions. Designs that operates at atmospheric pressure are commonly known as open volumetric receivers while those that operate in pressurized conditions are commonly known as closed volumetric receivers.

2.2.2.3 Open Volumetric Receivers

The open volumetric receiver design functions by absorbing concentrated solar radiation through a honeycomb patterned ceramic absorber, which increases the temperature of the assembly. Then, ambient air, which is used as the HTF, is drawn into and through the receivers where it will absorb the heat energy from the receivers and exit as hot air. In order to increase the efficiency of the receiver, an air return system can be implemented. The air return system functions by using the cool air leaving the receiver system to cool the structure of the receiver. The cool air will then be heated to a certain temperature before entering the receiver again as the HTF, thus increasing the efficiency of the heating process. Early variations of the open volumetric receivers such as the HiTRec I was not equipped with the air return system. However, subsequent variations such as the SOLAIR 200, SOLAIR 3000 and HiTRec II were equipped with the system (Ávila-Marín, 2011). A cross-section of the HiTRec II receivers along with a basic illustration of the working principle and the individual components are shown in Figure 2.12.

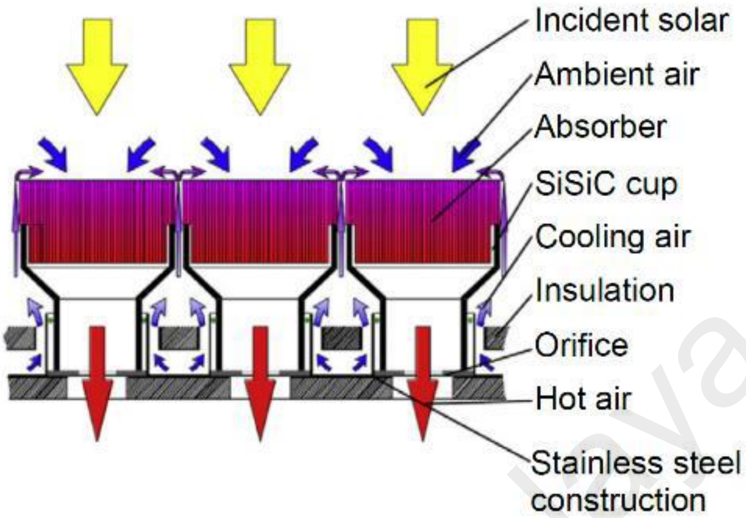

Figure 2.12: Cross-section of HiTRec II open volumetric receiver (Ávila-Marín, 2011)

Figure 2.13 shows the assembly of multiple open volumetric receivers which are connected together to form a large receiver structure which is installed on solar towers. The receiver structure is comprised of many individual absorbers that have an area of around 0.02 m^2 each.

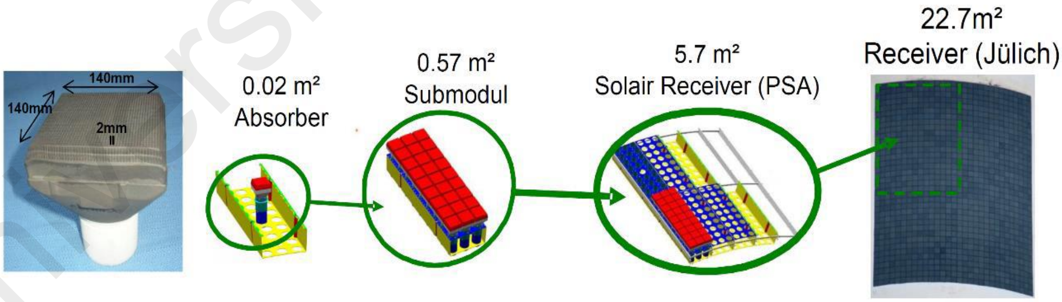

Figure 2.13: Open volumetric receiver assembly (Bernhard Hoffschmidt, 2014)

In most cases, the heated air from the receivers is used as the heat supply to produce superheated steam, which will then be used to generate electricity. An example of such a plant is the Jülich power plant in Germany, which draws in air at 120°C through the receivers and the air leaves the receivers at a temperature up to 680°C at atmospheric pressure (Bernhard Hoffschmidt, 2014).

2.2.2.4 Closed Volumetric Receivers

Closed volumetric receivers differ from the open volumetric receivers as they utilize pressurized air as the HTF. Due to it being a closed system to contain the higher air pressure, the closed volumetric receiver relies on a transparent window for concentrated solar radiation to enter. The window and the cavity within also helps reduce reflection, convection and re-radiation losses (Aichmayer, 2011). Closed volumetric receivers also incorporate secondary concentrators to enhance the solar concentration levels and to shield the receiver structure.

There are two types of closed volumetric receivers, namely, the Directly Irradiated Annular Pressurized Receiver (DIAPR) and the Receiver for Solar-Hybrid Gas Turbine and CC systems (REFOS). The DIAPR is designed with porcupine absorbers fabricated using ceramics rated for high temperatures. A cross-section of the DIAPR is shown in Figure 2.14.

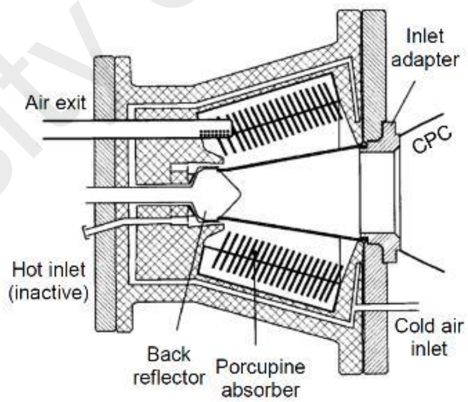

Figure 2.14: Cross-section of Directly Irradiated Annular Pressurized Receiver (DIAPR) (Kribus et al., 2001)

Pioneering research on closed volumetric receivers emphasized on the designing of the transparent window. This is due to the various difficulties associated with the window which includes size limitations, mechanical strength, cooling capability, high variable working temperatures and stress-free installation (Ávila-Marín, 2011).

Experiments done on project DIAPR have shown the capability of the receiver to function nominally at pressures up to 30 bars and solar radiation flux of up to 10 MW/m^2, with a outlet HTF temperatures of up to 1300°C (Kami et al., 1997). The efficiency of the receiver was estimated to be between 70 and 80 percent while having reflectivity losses of less than one percent for the transparent window. In 2009, Aora Solar, an Israeli CSP developer, constructed a solar power tower which utilizes the DIAPR technology in the Arava dessert. The plants has only a single receiver module coupled with gas micro-turbine to produce 100kWe and 170kWth of energy (Neiman, 2009).

The REFOS receiver was a modified closed volumetric receiver used in the REFOS project in 1996. It was also used in the SOLGATE project in 2001 (Aichmayer, 2011). During the REFOS project, the REFOS receiver was shown to be able to absorb 350kWth of thermal energy with a solar flux of 1 MW/m^2 per module, which resulted in an outlet HTF (air) temperature of 815°C at a pressure of 15 bar (Buck et al., 2002). However, the efficiency of the receiver was below expectations due to the poor performance of the secondary concentrator.

2.2.2.5 Solid Particle Receivers

Solid particle receivers also known as the direct absorbing particles is an alternate method used to absorb and transfer heat energy in CSP plants. The concept of this system involves a continuous flow of particles that absorbs the concentrated solar radiation directly. A diagram of the solid particle receiver concept is shown in Figure 2.15. The particles are made out of materials like ceramics which can absorb large amounts of heat without failing as the temperature of the particle curtain can increase to 1000°C (Kim, Siegel, Kolb, Rangaswamy, & Moujaes, 2009).

The solid particles do not have a flux density limit as they are used to absorb and transfer the heat (Bernhard Hoffschmidt, 2014). The solid particles are also used as the thermal energy storage (TES) medium.

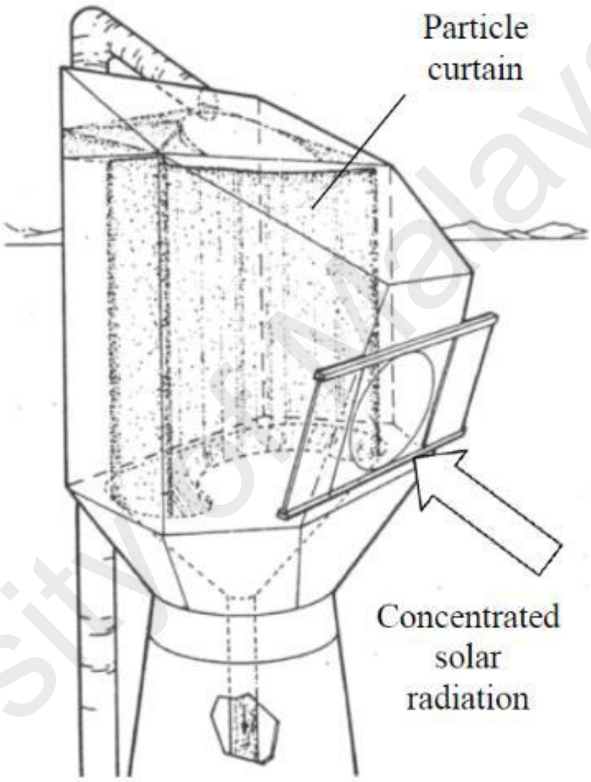

Figure 2.15: Solid particle receiver with particle curtain (Evans, Houf, Greif, & Crowe, 1987)

Solid particle receivers are commonly used as the heat source for processes such as the solar driven water-splitting thermo-chemical (WSTC) cycles for hydrogen production (Kim et al., 2009). For the case of electricity generation, the solid particle has similar functions as molten salt as a HTF and storage medium. The solid particles are pumped to the receiver for heat absorption. Then, the high temperature particles are either pumped through a heat exchanger to turn water into steam or stored in a storage block to be used at a later time. Once the heat has been transferred or used, the cooled particles are pumped back to the receivers to repeat the process. A schematic diagram of the solid particle receiver SPT plant is shown in Figure 2.16.

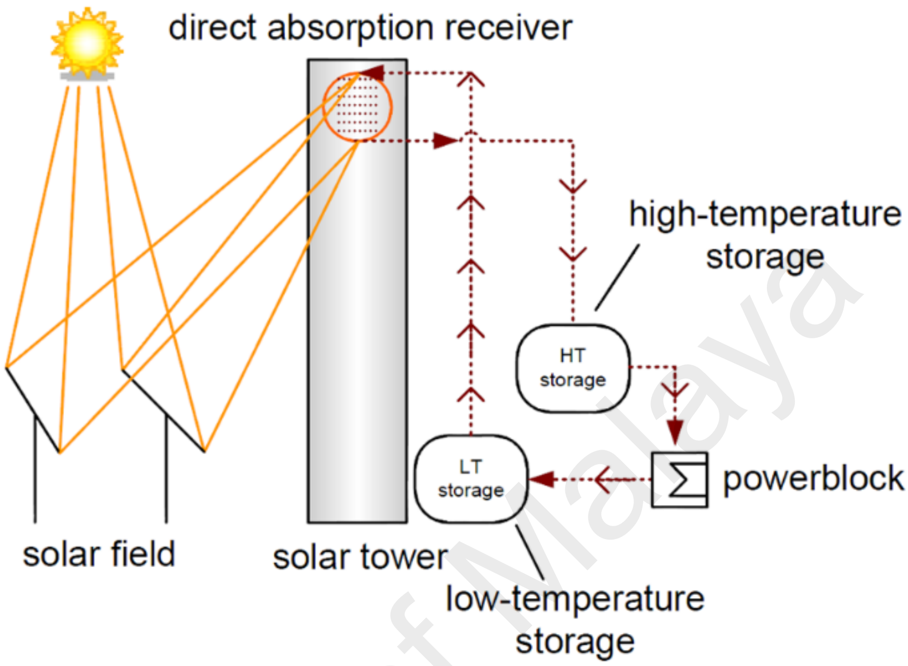

Figure 2.16: SPT plant with a solid particle receiver (Bernhard Hoffschmidt, 2014)

2.2.2.6 Heat Pipe Receivers

Heat pipe receivers are a type of receiver that function using metal vaporization and vapor transport (Obrey et al., 2015). This receiver design was initially used in aerospace applications before being adopted into CSP plant designs during the 1970s (Aichmayer, 2011). The heat pipe receiver has a versatile design that can incorporate the entire heating process which includes heat absorption, transfer and thermal storage into a single device (Xiaohong, Xiange, Miao, & Dawei, 2016). The concept of the heat pipe receiver is essentially a container that has a receiver end, also known as the evaporator, as well as the heat exchanger or output portion, also known as the condenser. A cross-section of the heat pipe receiver is as shown in Figure 2.17.

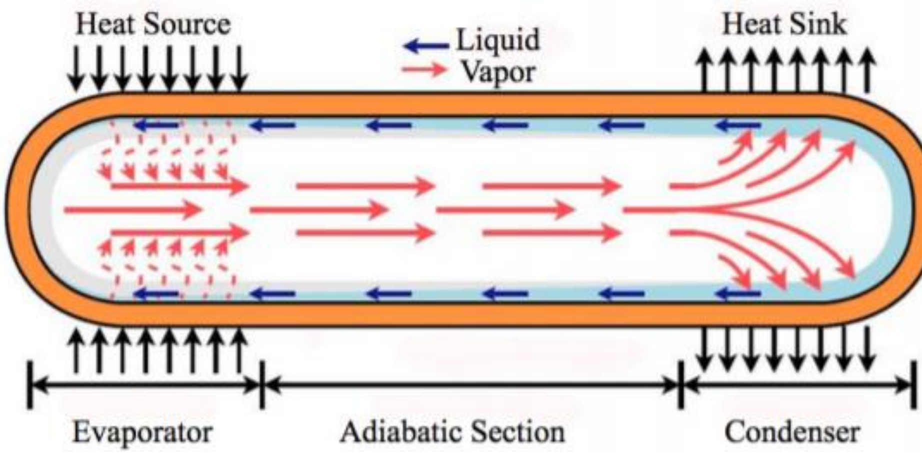

Figure 2.17: Cross-section of a heat pipe receiver (Obrey et al., 2015)

The cycle begins with the evaporator absorbing heat during periods where concentrated solar radiation is available. A portion of the heat absorbed is stored as latent energy while the remaining energy causes the temperature of the working fluid to increase and eventually evaporate. This causes an increase in vapor pressure at the evaporator end due to the saturation condition. The vapor pressure difference causes the vapor to flow to the condenser end where heat is released as latent heat, and the vapor turns into condensate. Capillary action then draws the condensate back to the evaporator. Some of the advantages of the heat pipe design include the high temperature capabilities, which are within the range of 500-1000°C, and the low pressure stresses in high temperature components due to operation at atmospheric pressure (Bienert, 1980). The operational limits for a heat pipe receiver varies according to its material, but the common benchmark is an outlet temperature upper limit of 900°C and a lower limit of 400°C in which the receiver will function below optimal values (ELBEH, 2017).

2.2.3 Heat Transfer Fluids

Heat transfer fluids (HTF) are an integral part of a CSP system as it is responsible for transporting heat energy from the absorbers to the heat exchangers where steam is generated. The heat transfer fluids can also be used for thermal storage for usage during poor weather conditions or during the night. It is important to optimize the cost and efficiency for the heat transfer fluids as a huge amount of these fluids are used during the operations of the CSP. The ideal characteristics for a heat transfer fluid are: high boiling point, high thermal stability, low melting point, low vapor pressure (below atmospheric pressure) at high temperature, low corrosion on the tubes containing the fluid, high thermal conductivity, low viscosity, high heat capacity for energy storage and low cost (Pacio & Wetzel, 2013). The operating temperatures for different types of HTFs are as shown in Figure 2.18 below.

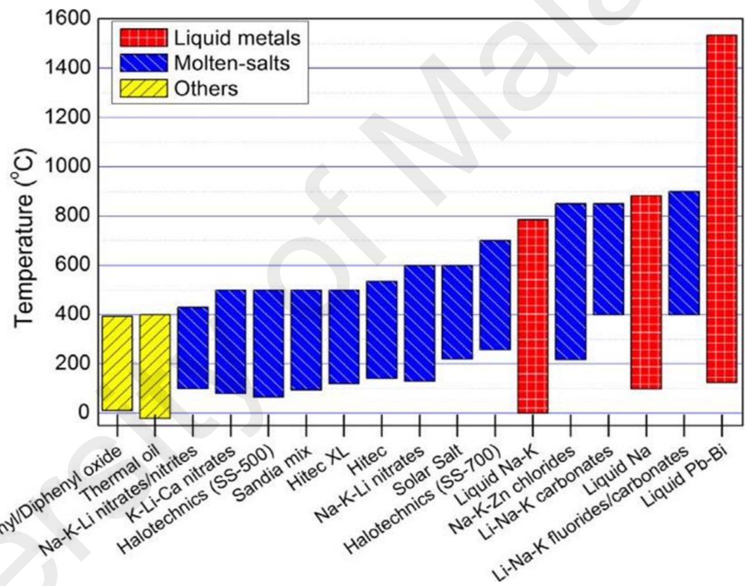

Figure 2.18: Operating temperature range for heat transfer fluids (Vignarooban, Xu, Arvay, Hsu, & Kannan, 2015)

The most common heat transfer fluid currently being used in CSPs is water/steam. However, the popularity of molten salts is rising, especially for new CSPs.

2.2.4 Power Cycle

There are mainly three different thermo-mechanical cycles involve in solar thermal power generation technologies, namely the Rankine Cycle, Stirling Cycle and

Brayton Cycle. These 3 cycles are widely used among the operational CSPs worldwide.

2.2.4.1 Rankine Cycle

The bulk of the electricity in the world is generated using steam turbines (Lovegrove & Stein, 2012b). In most power plants, steam is produced in the boiler through the combustion of fossil fuel. A CSP system does exactly what fuel combustion does and as such it can be applied to any dominant power generating technology involving heat energy to electrical energy conversion. The Rankine cycle begins by feeding pressurized water into the boiler with a feed-water pump. The boiler then superheats the water which turns into high pressure steam. The steam is fed to a steam turbined which generates electricity. The low-pressure steam exiting from the turbine will then be cooled at a cooling tower before being fed back to the feed-pump to repeat the process. In most cases, steam bleed from various stages of the process are used to pre-heat the feedwater before entering the boiler, which increases the efficiency of the overall system (Lovegrove & Stein, 2012b). This cycle is mainly used in CSPs with parabolic trough and solar tower (ELBEH, 2017).

2.2.4.2 Stirling Cycle

The Stirling cycle or Stirling Engines are externally heated engines with reciprocating pistons that operate on a gaseous liquid, usually hydrogen or helium, in a closed loop. The Stirling engines currently being integrated in CSP applications have mainly been small (in the tens of kWe range) (Lovegrove & Stein, 2012b). It is mainly used in Parabolic Dish systems which results in a high net solar to electricity conversion efficiencies (Luzzi & Lovegrove, 2004). Due to the high temperatures which can be achieved in the Stirling cycle, small scale applications have high efficiencies of up to 30% at design point DNI (Lovegrove & Stein, 2012a) (Pihl & Frescativägen, n.d.).

2.2.4.3 Brayton Cycle

The Brayton Cycle is the foundation for the operation of gas turbines (ELBEH, 2017). The process is similar to that of the Rankine cycle, but air is used instead of water/steam. The process begins with air being compressed adiabatically in a compressor. The air is then superheated at constant pressure to around 1000 degrees Celsius in a combustion chamber. The air is then expanded adiabatically at the turbine which generates electricity. CSP systems replaces the fossil fuel combustion process and currently the Brayton cycle is only implemented in solar tower and dish systems during to the high heat requirement (Lovegrove & Stein, 2012a).

2.2.5 Thermal Energy Storage

In most modern day CSP plants, thermal storage systems or thermal energy storage (TES) are implemented in order to enable constant power generation even during the night, or during cloudy and rainy days. There are two types of TES, i.e. the direct and indirect thermal storage. A diagram of both types of thermal storage and their basic function is shown in Figure 2.19.

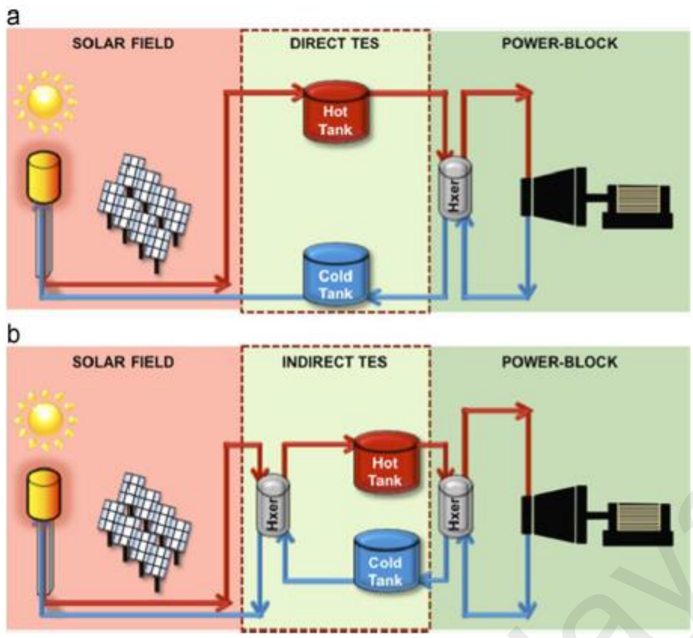

Figure 2.19: Direct (a) and Indirect (b) thermal storage systems in SPT plants (Stekli, Irwin, & Pitchumani, 2013)

Figure 2.19(a) shows the direct thermal storage process. In this process, the HTF and the thermal storage shares the same medium. Whereas in the indirect thermal storage process as shown in Figure 2.19(b), an exchanger is needed for heat to be transferred from the HTF to the thermal storage medium as both process do not share the same medium. At present, the more common thermal storage system implemented in parabolic troughs and SPT plants is the two-tank sensible energy storage which uses a form of molten salt that contains NaNO3 and KNO3 with a 60-40 weight percentage (Liu et al., 2016).

In both the direct and indirect thermal storage systems, the cold HTF, which could be water, molten salt or synthetic oil depending on the plant design, is pumped to the receiver where heat energy is absorbed. Then the hot HTF will either be directly stored in the hot tank or go through a heat exchanger to transfer heat to the thermal storage loop. Then, depending on the energy demand, the system will operate in reverse and the stored energy will be used to generate steam for power generation. During its testing phase, the Solar Two SPT plant was able to achieve an energy efficiency of up to 98% for the thermal energy storage (TES) system. (Pacheco, 2002).

The operating temperature limits or range of the TES depends on the type of CSP plant and solar field technology. SPT plants can generate HTF temperatures of up to 565°C which results in a TES temperature range of around 290 to 565°C while parabolic trough plants can generate HTF temperatures of up to 393°C which results in a TES temperature range of 292 to 393°C (Liu, Saman, & Bruno, 2012). It is important that the receiver, HTF and TES are able to withstand high temperatures. This is due to the fact that high operating temperatures can increase the overall solar-to-electricity efficiency, decrease the levelized cost of electricity (LCOE) and reduce the TES volume (Kutscher, Mehos, Turchi, Glatzmaier, & Moss, 2011).

Instead of the conventional molten salt TES system, there is also an alternative method known as the phase-change materials (PCM) currently still in development. Phase-change materials functions by absorbing or releasing large amounts of heat energy during phase change. Some of the advantages of PCM is that it has high energy density, which reduces the size of storage units, and also that it releases heat energy at a constant temperature during phase change (Deign, 2012). Two of the PCM TES technology that have been studied and are in development are the cascade type PCM storage system and the encapsulated PCM thermal storage. The cascade type PCM TES system functions by having different storages with a cascading melting point and latent energy of the materials (Prieto & Cabeza, 2019). This allows for constant heat transfer even as the temperature decreases. Encapsulated PCM is a technology used to overcome the problem of the increase in volume due to the melting of salt, by producing salt capsules to accommodate the change in volume (Mathur, 2013).

There are two important parameters for a power plant known as the capacity factor and the plant dispatchability. The capacity factor is the ratio between the number of hours the plant is generating electricity annually and the maximum possible power generation within the same period. The plant dispatchability is the ability for a power plant to generate power based on an operator's demand. The implementation of a TES in CSP plants will have increase both the capacity factor and plant dispatchability due to its ability to be used during peak periods or during poor weather conditions. The TES capacity is determined based on the load requirements and the SPT system are usually required to generate a higher amount of heat energy then the rate plant capacity in order to achieve optimal usage of the TES.

Another important parameter for TES is the solar multiple (SM) which is defined as the ratio between the thermal power produced by the solar field at the design point and the thermal power required by the power block at nominal conditions (Montes, Abánades, Martínez-Val, & Valdés, 2009). A CSP plant with a SM of 1 means that the solar field is producing the exact amount of energy needed to operate the power plant at the rated capacity under reference solar conditions. A SM larger than 1 indicates that the solar field is producing more energy than the rated capacity of the power plant, and hence, the excess energy can be stored in a TES system or used by other applications. CSP plants with no TES systems currently have SM values between 1.1 to 1.5 while plants with TES systems have SM values between 3 to 5 (IEA-ETSAP & IRENA, 2013).

2.3 Heliostat Cleaning

SPT power plants utilize large solar fields which contain a large number of heliostats, with numbers up to hundreds of thousands depending on the design and size of the power plant. The reflectivity of each heliostat is directly proportional to the efficiency of the heliostat. As mentioned previously, a reduction in reflectivity levels, which mainly occur due to the development of a layer of dust or dirt on the surface of mirrors of the heliostats. The reduction of reflectivity levels reduces the efficiency of each heliostats, which, in total, will have an extremely detrimental on the overall efficiency of the system. A reduce in efficiency will results in a lower energy output and a loss of revenue. As such, it is important to ensure the heliostats are cleaned regularly.

There are two cleaning methods currently in use in CSP plants around the world, namely, the wet brush cleaning and jet cleaning. Based on a test conducted in Spain, which involved exposing solar reflectors in outdoor locations and conducting different cleaning procedures, the most efficient method is based on wet brush cleaning, with an average efficiency of 98.8% during rainy seasons and 97.2% during dry seasons (Fernández-García, Álvarez-Rodrigo, Martínez-Arcos, Aguiar, & Márquez-Payés, 2014). As such, the wet brush cleaning method is the most ideal method with optimal water and fuel consumption.

The wet brush cleaning method can be executed using two different approach, namely, the conventional and automated approach. The conventional approach, also known as the semi -automatic process, involves a truck which cleans the mirrors using a cleaning arm fitted with brushes as shown in Figure 2.20. This method is mainly used in parabolic trough plants, but it can be customized for SPT plants as well. The automated method involves the Heliostat Cleaning Team Oriented Robot (HECTOR) which is patented technology currently being developed and tested by a company named SENER based in Spain. The HECTOR is an automated cleaning system which utilizes individual cleaner robots functioning in a fleet as shown in Figure 2.21.

Figure 2.20: Semi-automatic cleaning of heliostats in Noor III (Bouaddi et al., 2018)

Figure 2.21: HECTOR automated heliostat cleaning robot ("HECTOR successfully completes qualification tests," 2012)

Besides the two cleaning methods stated above, alternative cleaning methods are also available such as ultrasonic cleaning and automated wiper lip. Ultrasonic cleaning is a non-contact cleaning technique, also called acoustic cleaning, which uses ultrasonic waves that generate cavitation bubble into liquids (Bouaddi et al., 2018). This phenomenon is achieved through piezoelectric materials that change their form under the effect of electric charge (Kohli & Mittal, 2016). The cavitation bubbles implode when in contact with ultra-sonic waves, which then delivers microscopic high velocity jets that removes dirt from the heliostat surface. The automated wiper lip functions similar to a vehicle wiper. In order to further reduce water consumption, the wiper system operates after every dew formation or rain. The wiper moves from the top of the heliostat downwards, wiping off any dirt particles on the heliostat. The advantage of this system is the low water consumption and simple mechanism.

2.4 Water Demands for CSP plants

One of the main activity which require water in a CSP plant is heliostat washing. During operation, a layer of dust and dirt particles will form on the surface of the heliostats, which, if left unmonitored, will be detrimental to the efficiency of the heliostats due to decreased reflectivity. The reduction in heliostat efficiency will also reduce the electricity output and overall efficiency of the entire system. As such, heliostat washing activities are needed to be carried out periodically to maintain the efficiency of the heliostats. Based on the environment around East and West Malaysia, heliostat washing shall be conducted twice a week with a water consumption of 0.7 litre per m^2 for each heliostat.

Besides heliostat washing, steam cycle makeup also requires additional water supply. Although the water-steam loop for the SPT plant is a closed system, a portion of the water will be drained during operational boiler blow down. This is done to remove any suspended particles or solids from the steam boilers. It is also done to ensure the water properties are within the recommended limits to minimize scaling and corrosion. Additional water is fed into the system to make up for the water loss during boiler blow down. The water loss is estimated to be at 125,000 m^3/yr (ELBEH, 2017).

The hybrid cooling system which will is commonly integrated into SPT plants also requires a certain amount of water to make up for the water loss during the process. This is due to the evaporative cooling procedure (i.e. cooling tower) which is coupled with the air-cooling process to form the hybrid cooling system. The cooling system is set to function in hybrid mode only during the periods where peak electrical demands occur, which results in the SPT plant running at max capacity and thus, more cooling is needed to condense the exiting low pressure steam. This ensures that the temperature of the water entering the SPT and subsequently the efficiency of the system as a whole will be maintained at a desirable level. For the worst-case scenario, the hybrid cooling system will be operated with the cooling tower running constantly for 75% of the cooling load and the remainder of the cooling is done using air-coolers.

2.5 Maintenance activities for CSP plants

One of the main reoccurring cost for the operation of a powerplant include the scheduled maintenance and overhaul of components such as the steam turbine generator, various feedwater pumps, condenser, evaporative cooling equipment and piping according to the recommended maintenance schedule provided by the manufacturers. Moreover, periodic washing for the heliostats is needed using clean/distilled water to maintain the efficiency and reflectivity of the heliostats. Besides that, monthly inspections on transmission lines and substations required or as needed during emergency situations (ELBEH, 2017). Depending on the agreement, the routine inspection will either be done by a private firm or Tenaga National Berhad (TNB). Based on an interview with Fauzan Mohamad, the head of innovation at TNB, drones can be used to perform inspections (“Exclusive: Why Malaysia uses drones to monitor power lines | GovInsider,” n.d.). This helps reduce the cost and manpower needed for inspection activities. The frequency of inspection varies depending on multiple factors such as the age of the system and equipment life cycle. A report from the U.S. Energy Information Administration state that most of the solar thermal power plant operators fix the operation and maintenance cost at $67.26/kW-year (*Incorporating Renewables Into The Electric Grid: Expanding Opportunities For Smart Market and Energy Storage*, 2016).

2.7 Desalination of Sea Water

The desalination process of sea water is basically the process of extracting dissolved salt from saline water. There are multiple methods for the desalination process, but the methods most commonly used are a variation of the thermal process or the membrane process.

The thermal process is essentially the process of distillation for water. The process, which is similar to the water cycle in nature, involves the heating of saline water until it evaporates. Then the vapor is redirected to a separate container where it is cooled to form a low conductivity condensate. Three of the most common thermal processes used in sea water desalination are the Multi-effect distillation (MEF), Multi-stage flash (MSF) and Vapor compression (VC) processes. The drawback of the thermal process is the large energy consumption and water volume requirements compared to using membranes (Darwish, Hassabou, & Shomar, 2013)

Membrane technology uses electrical potential (electrolysis), mechanical pressure or a concentration gradient as the driving force to generate liquid flow across a semi-permeable membrane that separates the salt particles from water (Deng, Xie, Lin, Liu, & Han, 2010). The most commonly used membrane technology is the Reverse Osmosis (RO) process, followed by the Membrane Distillation (MD) process. The RO process is by far the most popular and commercialized process in the world with 65% of the world's desalination plants based on it, while the MD process is only present 2% of the world's desalination production due to the technology still being in its early stages (Gorjian & Ghobadian, 2015).

In a comparative study conducted by QEERI in Qatar on the desalination of sea water using RO and MSF system, it was found that for the production of 1.2 Mm^3/day of clean water, the MSF system requires three times more sea water while using around 75% more energy than the RO process (Darwish et al., 2013). Thus, is can be said that the MSF system is detrimental to the environment due to the use of fossil fuel unless an alternative heating method like solar energy is used.

The cost of desalination has significantly reduced in the last decade due to technological advances, especially in the RO process (Ghaffour, Missimer, & Amy, 2013). The standard installed cost for a desalination plant is approximately USD 1 million for every 1,000m^3/day (McGovern, n.d.), without taking into account the cost for constructing and maintaining the water distribution infrastructure. The operational cost of large-scale Sea and Brackish Water Reverse Osmosis (SWRO) plants has dropped below USD 0.5/m^3 at certain locations and conditions while the cost increases by 50% (USD 1.00/m^3) at other locations (Ghaffour et al., 2013).

In recent years, more research has been done on the solar still as an alternative and more environmentally friendly method of desalinating water. In a recent study, a solar still was combined with a Fresnel lens, which has a dimension of 400 mm x 300 mm with a focal length of 510 mm and light intensity of 92%. With the CSP modification in place and at an optimum tilt angle of 45 degrees, results show that an average increment of 92% in water yield was achieved compared to a solar still without a CSP modification (Ho & Bahar, 2018).

2.8 CSP Solar to Electricity Efficiency

Solar to electricity efficiency is the efficiency of a CSP system in converting solar radiation to electricity. Any efficiency improvements will result in a cost reduction. The approximate efficiency for different CSP technologies and the maturity level of each technology is shown in Figure 2.22. Based on the data in Figure 2.22, it can be seen that solar tower systems with molten salt as the heat transfer fluid and the heat storage medium have the highest efficiency with an annual efficiency of 17-18%. On the other hand, the CSP system that has the lowest efficiency is the Linear Fresnel system with saturated/superheated steam as the heat transfer fluid. The efficiency of the Linear Fresnel system is only around 9-13% (Brussels & Ce, 2011).

However, solar tower systems can achieve higher efficiency and an increase from the current 18% to at least 23% is to be expected (ELBEH, 2017). This increase can be achieved by primarily using supercritical steam or carbon dioxide as the heat transfer fluid. The heat from the primary heat transfer fluid is then transferred to a secondary heat transfer fluid, which can be either air or steam to drive a cogeneration plant with an upper Brayton cycle and a lower Rankine cycle.(Liu et al., 2016). The current available technology for SPT systems utilizes superheated steam, saturated steam, or molten salt (with storage) as the heat transfer fluid. Superheated steam HTFs have the highest annual efficiency compared to molten salt and saturated steam. It is worth noting that saturated steam is no longer common as the other HTFs have superior annual efficiencies (ELBEH, 2017).

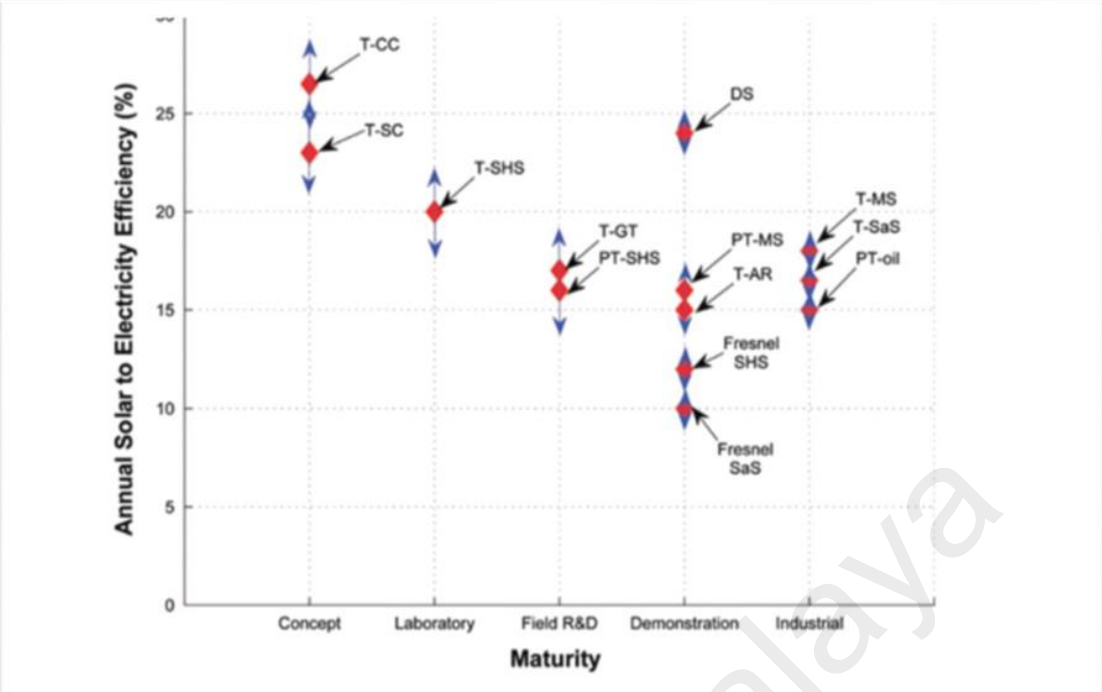

CSP technology	Technical options
Parabolic troughs (PT)	PT-oil: oil as HTF and molten salt storage PT-SHS: superheated steam as HTF PT-MS: molten salt as HTF and storage
Linear Fresnel systems (F)	Fresnel SaS: saturated steam as HTF Fresnel SHS: superheated steam as HTF
Towers (T)	T-SaS: saturated steam as HTF T-SHS: superheated steam as HTF T-MS: molten salt as HTF and storage T-AR: ambient pressure air as HTF and Rankine cycle T-GT: pressurised air as HTF and Brayton cycle T-SC: supercritical cycle T-CC: pressurised air as HTF and combined cycle
Parabolic dishes (DS)	DS: helium Stirling cycle

Figure 2.22: Annual solar-to-electricity efficiency as a function of development maturity (Brussels & Ce, 2011)

2.9 Simulation Software Validation

Most simulation software undergo a validation phase before being commercialized and used in research. This applies to both the SolarPILOT and SAM software as well. In a study done by Qatar University, the SolarPILOT and SAM software were validated by simulating an actual SPT plant and then comparing the results to the actual values of the plant. The SPT plant in question is the Crescent Dune Solar Energy Project which is situated in the USA. It started operation in 2015 and has a capacity of 110MW with 10 hours of thermal storage.

SolarPILOT was used to generate the solar field and to perform optimization for the heliostat arrangment, tower height and receiver size. Parameters such as the climate, layout setup, land boundary, plant size, heliostat and receiver size were obtained based on the official technical data available on SolarPACES as well as weather data available in SolarPILOT and Google Earth Pro. Based on the results, it was found that the number of heliostats in the solar field simulated using SolarPILOT is 10,216 heliostats, which is 1.3% lesser than the exact number of heliostats present at Crescent Dunes's solar field, which is 10,347 heliostats (ELBEH, 2017). The solar field layout is also almost identical to the actual Crescent Dunes solar field layout.

SAM was used to model the performance and finances of the SPT plant. The data previously obtained from SolarPILOT was imported into SAM. The technical data the project available to the public was obtained from SolarPACES and the remaining input was based on SAM's default values. Based on the results, it was found that the annual energy produced by the SPT plant is approximately 430,000 MWh and the capacity factor is 49.6% (ELBEH, 2017). Since the actual Crescent Dunes SPT plant is expected to generate around 500,000 MWh annually, the difference between the simulated and actual result is 14%. However, based on the lack of precise information for certain inputs in SAM, it can be said that SAM is considerably accurate and suitable for approximated results.

In another study conducted by researchers at Stellenbosch University in South Africa, SolarPILOT was used to generate heliostat field layouts and optimizing the field layout using power delivered to the receiver or time-of-use (TOU) weighted power (Pidaparthi, Landman, Hoffmann, & Dinter, 2017). The solar field data was then used to compare the optical efficiency using analytical method and Monte-Carlo Raytracing (MCRT) technique.

Based on the validation as well as their usage in multiple research, it can be deduced that both the simulation software are capable of producing reliable results that provides a good representation of the real world performance of CSP plants.

2.10 Prospective of CSP in Malaysia

Initial research on CSP have been done by previous researches in Malaysia in the past. However, the researchers mainly focused on the sub-system levels with no substantial findings on the feasibility of CSP implementation with reference to the DNI in Malaysia (Affandi, Gan, & Ab Ghani, 2014). In 1997, researchers at University Putra Malaysia carried out pioneering work on CSP using a solar bowl as the CSP system (Li et al., 2009). It was found that the annual energy collection and the efficiencies of a solar bowl is lower than other collector optics and it has no other advantages to compensate for it (Ng, Adam, & Azmi, 2012).

In a recent research by Y Rafeeua and M.Z.A. Ab Kadir from University Putra Malaysia in 2012, they mentioned about a significant variation in the efficiency of the concentrator based on the use of different reflective materials (Rafeeu & Ab Kadir, 2012). Reflectors or concentrators are key components of any CSP system as they are used to reflect and focus sun rays onto the heat receiver. As such, it is important that the materials used to fabricate the concentrator have sufficient reflectance. The materials selection also needs to take into account the requirements for low costs and a long lifespan, as well as durability. This is due to the fact that the reflecting surface will deteriorate faster as it is exposed to the Malaysian tropical environment with copious rainfall and high levels of humidity (Affandi et al., 2014).

The main CSP technology that has been researched in Malaysia is the Parabolic Dish (PD) system. The pioneer work for this system is done using the solar bowl in UPM as stated previously. The performance of a reflector is influenced by the quality of the reflector, sun shape, solar tracking accuracy and the location of a CSP plant (Noor & Muneer, 2009). The most common material used for concentrators are silver or aluminium, which amounts to about 80% to 90% total reflectance of the DNI at the surface (William & Richard, 1994)(Yang, Yao, Liu, Ni, & Tong, 2007). It was also found that under a tropical environment, mirror reflectors with a silver back surface have improved reflectance and had the capability to achieve higher temperature (Yousif, Al-Shalabi, & Rilling, 2010)(Singh, Tan, Ezriq, & Narayana, 2012).

Besides the reflector or concentrator, the tracking technology of a PD system is also vital in the optimization and maximization of the power output and efficiencies. A tracking system is able to vary the position of the dish to follow the position of the sun throughout the day and the absorber to be as close as the reflected sun beam as possible (Yousif et al., 2010).

Another key factor that affects the output of a CSP is the Direct Normal Irradiance (DNI). A knowledge on the quality and reliability of sunlight is essential to get an accurate analysis of the performance of a CSP system (Azhari, Sopian, Zaharim, & Al Ghoul, 2008). DNI is the direct radiation from the sun that did not undergo reflection or refraction. In order to be economically feasible, a CSP system requires an average DNI of 1900-2000kWh/m /year or daily solar radiation value 2 of at least 5kWh/m /day (Hwang, 2010). Although the DNI in Malaysia is only around 1,401-1,600 kWh/m /year (Stoffel et al., 2012), there is no technical reason as to why CSP plants are unable to run at DNI lower than the stated average. Previous studies have revealed that most parts of the world except Canada, Japan, Russia and South Korea have high potential areas for CSP (Affandi et al., 2014).

Another useful parameter than can be used to gauge the performance of a CSP plant is the optical efficiency of the plant. A preliminary study on field optical efficiency of CSP in Malaysia found that the calculated average cosine efficiency and total optical efficiency of a CSP plant in Melaka is 63% and 52% respectively. A comparison of the calculated results and the values from Aswan are shown in Figure 2.23 below.

Heliostat position	(Malaysia) Average	(Aswan) Average
Atmospheric Transmittance efficiency (%)	0.94	0.95
Cosine Efficiency (%)	0.63	0.85
Mirror Reflectivity efficiency (%)	0.88	0.88
Total Optical Efficiency (%)	0.52	0.70

Figure 2.23: Efficiency of CST in Malaysia vs Aswan (Rafeq et al., 2013)

One of the studies on SPT in Malaysia was done by researchers at University Technology Petronas (UTP), where the design of a SPT heliostat field of 3 dual-axis heliostat units located in Ipoh, Malaysia was introduced (Ali et al., 2013). The study includes calculating the incident solar power to a fixed target on the tower by analyzing the tower height and ground distance between the heliostat and the tower base (Ali et al., 2013). The heliostat positions were calculated based on the sun position values obtained using a mathematical model. It was found that the heliostat field produces 7.5kW during its peak value in day 361, which is December 27.

In 2018, a research was done on the feasibility of a 25kW parabolic dish CSP technology with a Stirling engine in Malaysian environment. It was found that the 25kW PD system is technically feasible in Malaysian environment, but not economically feasible. The main constraints are due to meteorological factors such as rain and clouds which affect the output, except for certain times of the year (Omar et al., 2018). The limited effective operation time along with the high initial cost for the PD system largely affect the economic feasibility due to the long ROI. However, as the technology matures, the cost to erect such systems will be reduced similar to the current wind and photovoltaic (PV) technologies.

2.11 Cost of Solar Photovoltaic (PV) Farms

The cost of solar PV has reduced over the years due to developments and improvements in manufacturing process and materials. The efficiency and power output per square meter of a solar panel has also increased. The combination of both factors resulted in the reduction of investment cost and the resulting cost of electricity for a solar farm. The Malaysia Airports Holdings Berhad solar PV system in KLIA, which is provided and maintained by SunEdison Inc., is a RM 200 million project that has a capacity of 26 GWh per year and will be functional for 21 years ("MAHB goes for renewable energy at KLIA," 2014). Given a maintenance cost of RM 33.75/kW per year (USD 7.5/kW per year) based on reports from the National Renewable Energy Laboratory (NREL) and a discount rate of 8%, the calculated levelized cost of electricity (LCOE) was found to be approximately RM 0.10/kWh and the NPV was found to be RM 2,249,885 based on an online excel template ("Levelized Cost of Electricity (LCOE) - Overview, How To Calculate," n.d.).

Based on a report by pv-magazine, the large scale solar (LSS) program introduced by the government has attracted bids for LSS2 with 1.6 GW of capacity at prices between RM 0.33/kWh to RM 0.53/kWh as well as bids for LSS3 with 6.7 GW of capacity at prices between RM 0.24/kWh to RM 0.32/kWh (Bellini, 2020; Hall, 2019).

In another study, a numeric analysis was done for large scale solar PV in the KLIA area. It was found that a solar PV system with a capacity of 1MW generates approximately 1.293MWh of energy annually. With an initial investment of RM 8,174,863.75, the NPV was found to be RM 1,300,196.97 with an IRR of 11.59% (Jali et al., 2015).

2.12 Gaps in Knowledge and Future Growth

There are a few gaps in knowledge with regards to CSP technologies in Malaysia. Previous studies are mainly conducted on Parabolic Dish (PD) systems and little emphasis were given for the other CSP technologies. The feasibility studies are also mostly conducted based on analysis of meteorological data as well as solar irradiation data and comparing them with the operating requirements of CSP plants. The functionalities of both the SolarPILOT and SAM software are also based on its usage in 2017 and there might me new features and calculation models for both software which can be explored and used. As such, more research can be done on other CSP technologies such as the solar power tower (SPT) through simulation using updated versions of the software developed to perform the said tasks.

2.13 Significance of Study

Over the last century, the burning of fossil fuels like coal and oil has increased the concentration of atmospheric carbon dioxide (CO_2) (Causes | Facts – Climate Change: Vital Signs of the Planet, n.d.), which causes an increased in greenhouse effect and global warming. The rapidly increasing energy demand is also a concern as fossil fuel alone is not a sustainable option to handle the demand. The Malaysian government also has a target of 20 percent electricity generation from renewable energy (RE) sources by 2025 (The Star Newspaper, 2019). This project would result in an increase in knowledge regarding the feasibility of implementing the concentrated solar power plant in Malaysia.

2.14 Summary of Literature Review

As global warming worsens and climate change is becoming a significantly critical issue, renewable energy technologies such as Concentrated Solar Power (CSP) are fast becoming a global trend.

There are four main types of CSP technology, namely, parabolic trough, solar power tower, parabolic dish, and linear Fresnel. The basic concept of CSP is to concentrate solar radiation onto a specific area where heat absorption will take place. The heat is then transferred using a heat transfer fluid to a heat exchanger to generate steam for power generation. The parabolic trough and parabolic dish use parabolically curved reflectors which are either shaped in a trough or a dish, to concentrate solar radiation on a single point. Linear Fresnel technology uses flat mirror reflectors which are specifically positioned to reflect sunlight onto an absorber tube. Lastly, the solar power tower uses large amounts of heliostats which reflects the sunlight onto a receiver on top of a tower.

There are 5 main components or process involved in a CSP plant, namely, the solar reflector, solar receiver, heat transfer fluids, thermal energy storage and power cycle. Usually, solar-tracking systems, either single axis or double axis, are implemented into the reflectors to improve efficiency and power output. Solar receivers are essentially the component that absorbs the concentrated solar radiation reflected by the solar reflectors, there are various designs for the receiver, most notably the tubular and volumetric receivers along with their variants. Tubular receivers used to be the emphasis of researchers in the past, but currently volumetric receivers are more popular due to the increased temperature headroom and efficiency. Currently, there are five types of heat transfer fluid in use or under development, namely air, water/steam, thermal oils, organics, molten salt, and liquid metals. The efficiency of these HTF vary according to the applications. The two main types of thermal energy storage (TES) in CSP plants today are the direct and indirect storage arrangements. Direct storage utilizes the same medium for the HTF and TES while indirect storage has a separate loop and possibly medium for the HTF and TES. Lastly, the power cycle of the plant which determines the process involved in power generation are the Rankine cycle (steam), Brayton cycle (air) and Sterling cycle (air or other gases). The process most commonly used in power plants are the Brayton cycle and Rankine cycle.

The desalination process of sea water can be done using either the thermal process or the membrane technology. The types of thermal process are the Multi-effect distillation (MEF), Multi-stage flash (MSF) and Vapor compression (VC) processes. The drawback of the thermal process is the large energy consumption and water volume requirements compared to using membranes. The most commonly used membrane technology is the Reverse Osmosis (RO) process, followed by the Membrane Distillation (MD) process, with RO being the most matured and commercialized process with 65% of usage in desalination plants around the world. RO is also one of the most efficient desalination process in the world.

Solar to electricity efficiency is a good measure of the performance of a CSP system. SPT systems with molten salt as the HTF and the heat storage medium have the highest efficiency with an annual efficiency of 17-18%. Meanwhile, the Linear Fresnel system with saturated/superheated steam as the HTF has an efficiency of only around 9-13% which is the lowest among all technologies. Currently the most commonly used HTF with the highest annual efficiency are superheated steam and molten salt.

Studies on CSP systems done in Malaysia are largely focused on Parabolic dishes. According to research data, Malaysia does not have enough solar irradiation to meet the average requirements to run a CSP plant. However, there is no technical reason as to why CSP plants are unable to run at irradiation level below the average. It was found that Solar Tower systems has the highest annual solar-to-electricity efficiency when compared to the other available technical options.

There is a lack of research done on other CSP technologies and simulation-based research on the topic. As such, more research can be done on other CSP technologies through simulation using updated versions of the software, namely SolarPILOT and SAM, which were developed to do perform the said task. Validation was done on both software by comparing the simulated data with the actual specifications of the Crescent Dunes Energy Project. It was found that both software produce accurate results and any discrepancies are due to the lack of certain input information. As such, it can be said that the software are reliable and suitable for the feasibility study.

CHAPTER 3: Methodology

3.1 Introduction

In this study, the research is simulation based and the simulation software used are SolarPILOT and SAM. The study will only be conducted on Solar Power Tower (SPT) models on two suitable locations selected in Malaysia. The locations in Malaysia were evaluated and the weather data file for both selected locations will be obtained and formatted accordingly. Next, the weather data file will be fed into SolarPILOT for the generation and optimization of the solar/heliostat field. The solar filed layout data is then fed into SAM for performance and financial simulation and the results of SAM were used for the feasibility analysis.

3.2 Selection of Concentrated Solar Power Plant Locations

The location of a CSP plant is one of the most important factors that determine the performance and feasibility of a CSP plant. Parameters such as climate, seasons, solar irradiance, sun hour and precipitation for any given location need to be evaluated before the design and modeling of a CSP plant can commence. In this paper, two locations were selected for the design and modelling of a CSP plant. Preliminary selection of the optimal location for CSP plants is based on two main criteria, namely is the order of,

1) Climate conditions
2) Proven success for solar power generation

The first criterion can be broken down into 3 main parameters, namely, annual average sun hours, annual average solar irradiance, and annual average rainfall. These parameters are shown in Figure 3.1, Figure 3.2, and Figure 3.3 below

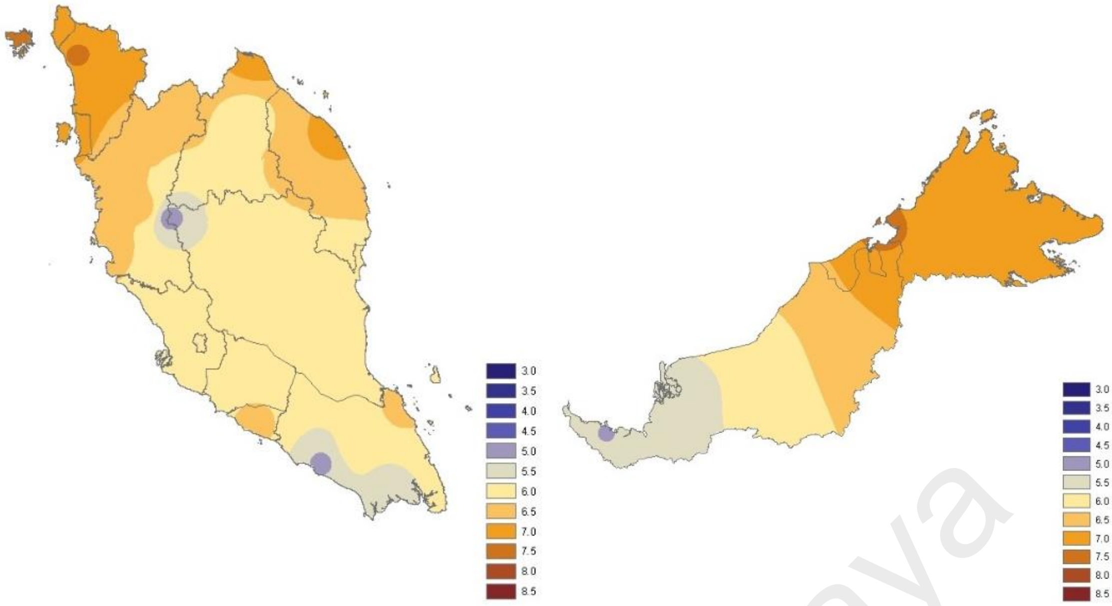

Figure 3.1: Annual Average Sun Hour (hrs/day) (“MetMalaysia: Iklim Malaysia,” n.d.)

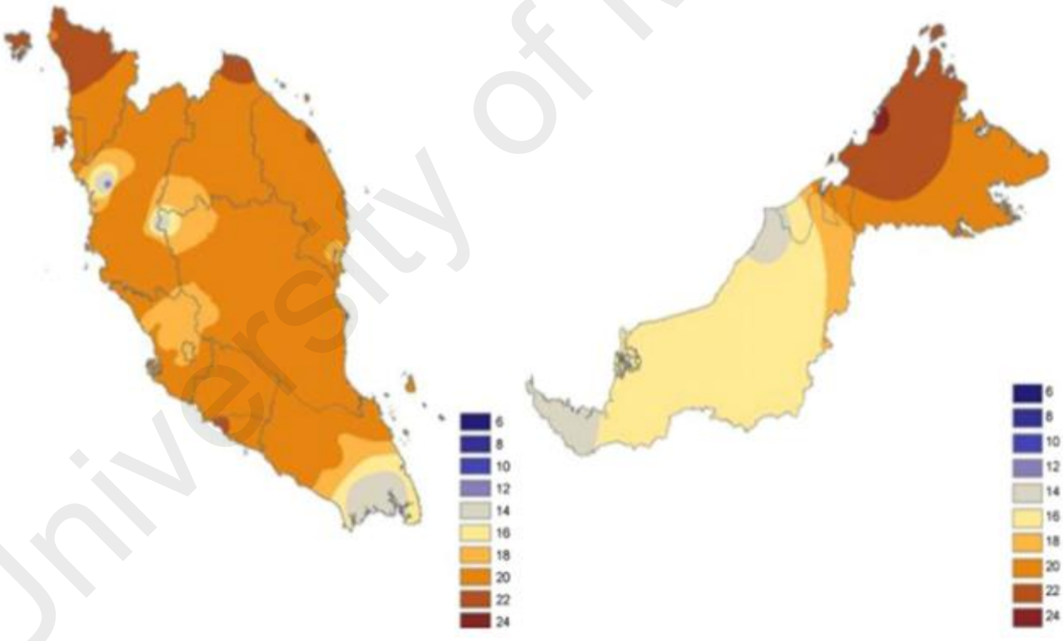

Figure 3.2: Annual Average Solar Irradiance (MJ/m^2/day) (Petinrin & Shaaban, 2015)

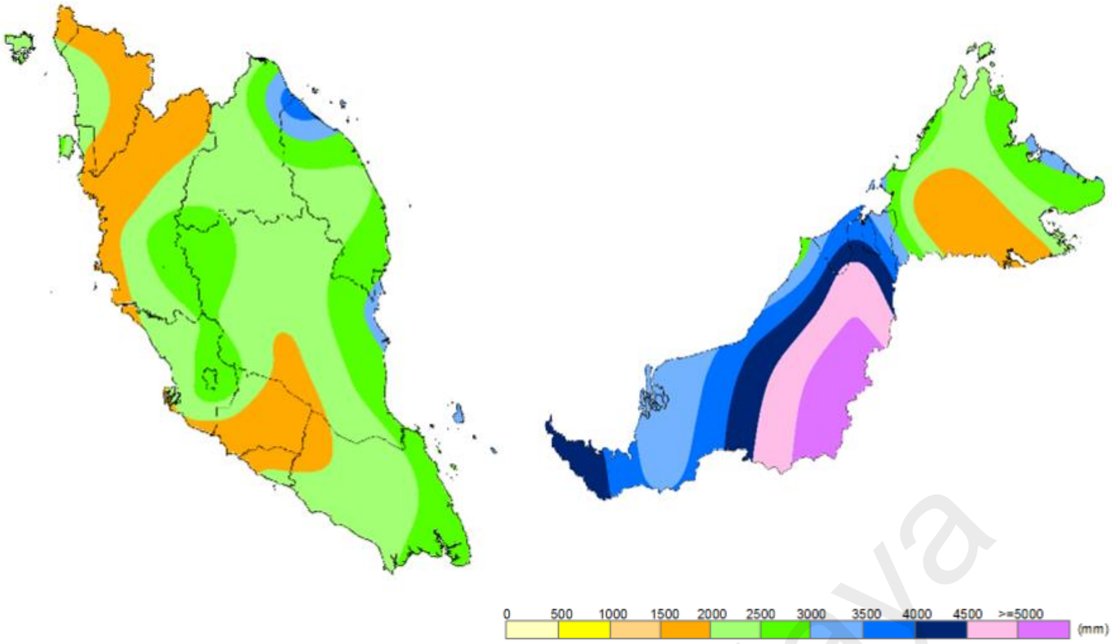

Figure 3.3: Annual Average Monthly Rainfall (mm/month) (“MetMalaysia: Iklim Malaysia,” n.d.)

In Figure 3.1, it can be seen that the northern states of the Malaysian Peninsula, e.g. Perlis, Kedah, Penang, and parts of Kelantan and Terengganu as well as Malacca, East Sarawak and Sabah in East Malaysia receive an average of 6.5 to 7 sun hours a day, while the other states mostly receive an average of 6 sun hours a day. In Figure 3.2, it is clear that the Malaysian Peninsula receives a higher value of annual average solar irradiance, with most states having an average value of 20 $MJ/m^2/day$. In East Malaysia, Sabah averages between 20 to 22 $MJ/m^2/day$ while Sarawak only average between 14 to 16 $MJ/m^2/day$. In Figure 3.3, in can be seen that most states in the Malaysian Peninsula, as well as Sabah from East Malaysia have an average rainfall between 2000 to 2500mm a month, with certain areas averaging higher at 3000mm and lower at 1500mm. Sarawak receives a much larger amount of rainfall upwards of 3000mm a month. Based on all these parameters, the northern states of the Malaysian Peninsula as well as Sabah are the most optimum areas for the design and modelling of a CSP plant.

For the second criterion, two large scale solar projects, namely the first airport solar system in Malaysia with a capacity of 19 MW, commissioned in Kuala Lumpur International Airport (KLIA) by SunEdison in 2014 as well as the largest solar farm in Malaysia with a capacity of 50 MW, commissioned by Tenaga National Berhad in 2018 could be used as examples of proven success in solar power generation technology ("KLIA installs RM200mil solar power system | The Star," n.d.; "Largest solar park in Malaysia starts operation | The Star," n.d.). The solar power system installed in KLIA saves the airport about RM2.1mil annually based on its current energy costs ("KLIA installs RM200mil solar power system | The Star," n.d.). Both solar projects are located in Sepang, Selangor. As such, the locations selected for the study are,

1) KLIA (the oil palm plantation in between KLIA and KLIA 2) due to a suitable climate and proven solar power systems in the area
2) Kota Kinabalu (Gaya Island) due to the fact that it had the most optimal climate conditions for a CSP in Malaysia.

A satellite image for both locations were obtained from Google Earth Pro and are shown in Figure 3.4 and Figure 3.5, respectively.

Figure 3.4: Oil palm plantation in between KLIA and KLIA 2 (Indicated with blue outline)

Figure 3.5: Kota Kinabalu (Gaya Island)

The designated areas for the CSP plants were marked using the “polygon” tool and the initial position of the central receiver towers were marked using the “placemark” tool in Google Earth Pro. The locations were then saved as .kml files.

3.3 Climate Data for Selected Locations

The detailed climate data of a location is needed for accurate calculations and approximation of the energy output by solar or wind power generation systems. Both, SolarPILOT and SAM require a specific set of climate parameters for the simulation and modelling of a CSP plant, as shown below.

1. Total global horizontal irradiance (GHI)
2. Total direct normal irradiance (DNI)
3. Total diffused horizontal irradiance (DHI)
4. Normal and dewpoint temperature
5. Relative humidity
6. Atmospheric pressure

7. Wind speed and direction
8. Albedo

A complete set of hourly (60 minutes intervals) values for each parameter, from 1.1.2019 to 31.12.2019 (1 year), for both locations, were obtained using the Solcast API toolkit with free credits provided by registering an account as a researcher. The data obtained were arranged into the format specified by SolarPILOT or SAM and saved in a .csv format.

3.4 SolarPILOT

In this paper, the SolarPILOT software was used to perform the following tasks,

1) Generate the solar field/heliostat layout
2) Run a performance simulation based on a specified sun position
3) Optimize specific parameters and apply the values to inputs
4) Repeat step 1 to 3 three times and select the parameter values which yielded the best results.

Since the climate data folder that came with the software does not include Malaysia's climate data, the climate data files for both locations are prepared individually as stated before and transferred to the climate data folder. The climate data file for KLIA or Gaya Island were then selected in SolarPILOT's "climate" tab. Then, the .kml files saved from Google Earth Pro were uploaded into SolarPILOT using the "use land boundary array" option in the "layout setup" tab. The solar field design power is set to 100 MWt. All other settings were based on the recommended values and remain unchanged. Step 2 and Step 3 were executed, with the optimized parameters as follows,

	Variable	Lower Bound	Upper Bound	Initial Step
Tower location offset - X	land.0.tower_o	-200	200	30
Tower location offset - Y	land.0.tower_o	-200	200	30
Tower optical height	solarfield.0.tht	none	none	11.7
Structure height	heliostat.0.hei	none	none	0.732
Structure width	heliostat.0.wid	none	none	0.732
Receiver diameter	receiver.0.rec_	none	none	1.059
Receiver height	receiver.0.rec_I	none	none	1.296

Figure 3.6: Optimized Parameters in SolarPILOT

The lower bound and upper bound for the tower location offset X and Y were manually set to -200 and 200m respectively, with an optimization step size of 30m to ensure the optimization of the tower position is centralized and does not deviate away from an acceptable range. The lower and upper bounds as well as the step size remain unchanged for the other parameters.

After repeating step 1 to 4 three times to obtain the results for 3 cycles of optimization, the results are compared and the parameter values which yielded the best performance was selected.

3.5 System Advisor Model (SAM)

The SAM software is mainly used to simulate and analyze the annual energy production, annual water usage as well as the financial impact or requirements of the CSP plants. Similar to SolarPILOT, the climate file for either KLIA or Gaya island were selected in the “location and resource” tab. All the optimized parameter values from SolarPILOT were transferred to the inputs in SAM manually, and the heliostat/solar field layout was imported from SolarPILOT in a .csv file. The other parameters were mostly left unchanged, with a few exceptions related to the power cycle, heliostat washing and financial calculations that were set with a designated value based on preference and/or common practices. SAM was also used to find the design-point DNI value using the PDF/CDF graphical approximation method which was needed for both SolarPILOT and SAM. The financial parameters that were evaluated are Power Purchase Agreement (PPA), Levelized Cost of Electricity (LCOE), Net Present Value (NPV) and Internal Rate of Return (IRR).

3.6 Additional Costs

As SAM only calculates the water consumption of a CSP plant and does not consider the cost to obtain it, additional costs were calculated individually and factored into the total overall cost of the system. The KLIA CSP plant uses the water supplied by Air Selangor Sdn, Bhd., which is the sole water provider for Selangor, Kuala Lumpur, and Putrajaya. As such, the cost of water was calculated using the provided water tariffs. The Gaya Island CSP plant uses sea water as the water supply, through the process of desalination. As such, the cost of construction, operation and maintenance of a desalination facility and the power consumption by said facility were calculated and factored into the respective total values for the plant.

CHAPTER 4: RESULTS

4.1 Land Boundary and Climate Data for KLIA and Gaya Island

Figure 4.1 and Figure 4.2 below shows the land boundary for the CSP solar field for KLIA and Gaya Island, respectively.

Figure 4.1: KLIA land boundary and initial tower position

Figure 4.2: Gaya Island land boundary and initial tower position

Both land boundaries have a total perimeter of 3150 m and a total area of 620,156 m^2. The size of the boundaries was made the same for a more accurate comparison.

The climate data for both location was obtained from the Solcast API toolkit using free credits for a researcher account as mentioned previously. A request was sent individually for each location by inputting the latitude and longitude and then selecting the required parameters and the logging resolution, which was 60 minutes. The following figure shows an example of the .csv climate data file obtained for Gaya Island.

PeriodEnd	PeriodStart	Period	AirTemp	Azimuth	CloudOpac	Dewpoint1	Dhi	Dni	Ebh	Ghi	Precipitabl	RelativeHu	SnowDept	SurfacePre	WindDirec	WindSpee	Zenith
2018-12-3	2018-12-31	PT60M	26.5	-127	33.3	23.3	321	166	111	431	51.3	82.6	0	977.3	127	2.3	50
2018-12-3	2018-12-31	PT60M	26.9	-139	8.6	22.9	257	609	473	730	51.4	78.5	0	977.4	114	2.1	39
2018-12-3	2018-12-31	PT60M	27.2	-159	0.7	22.6	182	828	705	886	51.5	76.1	0	976.9	101	1.8	32
2018-12-3	2018-12-31	PT60M	27.4	174	2.9	22.6	210	781	678	888	51.7	75	0	975.9	86	1.4	30
2018-12-3	2018-12-31	PT60M	27.6	150	6.9	22.5	246	674	557	803	51.9	73.9	0	974.9	62	1.1	34
2018-12-3	2018-12-31	PT60M	27.5	134	5.7	22.6	207	679	489	695	52.3	74.5	0	974.5	52	1.3	44
2018-12-3	2018-12-31	PT60M	27.2	124	3.7	22.8	150	674	387	538	53	76.7	0	974.6	58	1.9	55
2018-12-3	2018-12-31	PT60M	26.9	118	17.5	23	149	335	133	282	53.6	79	0	974.7	61	2.4	68
2018-12-3	2018-12-31	PT60M	26.7	115	49.8	23.3	48	17	3	52	54.5	81.5	0	975.1	67	2.4	82
2018-12-3	2018-12-31	PT60M	26.5	113	44.4	23.6	1	1	0	1	55.5	84.2	0	975.8	82	2.1	95
2018-12-3	2018-12-31	PT60M	26.4	113	55.8	24	0	0	0	0	56.6	87	0	976.5	99	2	109
2018-12-3	2018-12-31	PT60M	26.1	114	52.4	24.1	0	0	0	0	57.4	88.9	0	976.9	107	2	123
2018-12-3	2018-12-31	PT60M	25.8	118	57.5	24	0	0	0	0	58	89.8	0	977.2	104	2	136
2018-12-3	2018-12-31	PT60M	25.5	127	52.3	23.9	0	0	0	0	58.5	90.8	0	977.5	101	2	149
2018-12-3	2018-12-31	PT60M	25.3	148	52	23.8	0	0	0	0	58.9	91.9	0	977.4	99	2	159
2018-12-3	2018-12-31	PT60M	25	-171	45.1	23.8	0	0	0	0	59	93	0	977	98	2	162
2018-12-3	2018-12-31	PT60M	24.8	-137	37.8	23.8	0	0	0	0	59.1	94.2	0	976.6	96	2	155
2018-12-3	2018-12-31	PT60M	24.6	-122	36.9	23.7	0	0	0	0	59.4	95	0	976.4	93	2.1	144
2018-12-3	2018-12-31	PT60M	24.5	-116	18.5	23.7	0	0	0	0	59.9	95.6	0	976.5	89	2.3	131

Figure 4.3: Solcast .csv climate data format

The format shown in Figure 4.3 above differs from the format used by SolarPILOT and SAM. Thus, the data from Solcast was manually transferred to another .csv file with the right format and naming scheme. There was an error in the system which cause the DHI, DNI, and GHI values to be logged at the wrong hours of the day where it is at night and there was no sunlight (between 11pm and 6am). After consulting with Solcast support, they advised to transpose the data to begin at 6am for the KLIA data and 7am for the Gaya Island data. The reason for the difference between KLIA and Gaya Island is because Sabah is supposedly in a different time zone as compared to Peninsula Malaysia, but the time zone was made the same to allow for better syncing and administrative purposes in 1982 (Aziz et al., 2017). Figure 4.4 below shows an example of the finalized data and format for the climate data files.

Location ID	City	State	Country	Latitude	Longitude	Time Zone	Elevation	Source					
-	Gaya Islan	Sabah	Malaysia	6.008066	116.0436	8	5	Solcast					
Year	Month	Day	Hour	GHI	DNI	DHI	Tdry	Tdew	RH	Pres	Wspd	Wdir	Albedo
2019	1	1	0	0	0	0	25.5	23.9	90.8	977.5	2	101	0
2019	1	1	1	0	0	0	25.3	23.8	91.9	977.4	2	99	0
2019	1	1	2	0	0	0	25	23.8	93	977	2	98	0
2019	1	1	3	0	0	0	24.8	23.8	94.2	976.6	2	96	0
2019	1	1	4	0	0	0	24.6	23.7	95	976.4	2.1	93	0
2019	1	1	5	0	0	0	24.5	23.7	95.6	976.5	2.3	89	0
2019	1	1	6	0	0	0	24.3	23.7	96.2	976.5	2.6	85	0
2019	1	1	7	0	0	0	24.3	23.7	96.5	976.7	2.9	88	0
2019	1	1	8	15	14	12	24.3	23.8	96.6	977.1	3.2	95	0
2019	1	1	9	93	18	88	24.4	23.8	96.7	977.5	3.6	101	0
2019	1	1	10	306	180	220	24.9	23.7	93	977.6	3.8	102	0
2019	1	1	11	445	184	328	25.9	23.4	86	977.5	3.7	98	0
2019	1	1	12	539	191	388	26.9	23.1	79.5	977.4	3.6	95	0
2019	1	1	13	859	748	221	27.5	23	76.7	976.9	3.5	91	0
2019	1	1	14	903	821	190	27.5	23.1	77.1	976.1	3.5	86	0
2019	1	1	15	861	842	165	27.6	23.3	77.5	975.2	3.5	81	0
2019	1	1	16	736	807	151	27.4	23.4	78.8	974.8	3.7	80	0
2019	1	1	17	447	354	235	27	23.5	81.2	974.8	4.1	82	0
2019	1	1	18	200	104	156	26.6	23.6	83.7	974.8	4.5	83	0
2019	1	1	19	54	18	50	26.2	23.8	86.5	975.1	4.4	88	0
2019	1	1	20	1	1	1	25.9	24	89.5	975.7	4	96	0
2019	1	1	21	0	0	0	25.6	24.3	92.6	976.2	3.7	106	0
2019	1	1	22	0	0	0	25.4	24.4	93.8	976.7	3.5	114	0
2019	1	1	23	0	0	0	25.5	24.3	93.1	977.1	3.1	119	0

Figure 4.4: Climate file sample for Gaya Island

4.2 SolarPILOT SPT Modelling

4.2.1 Initial Setup for CSP Modelling and Performance Simulation

A new project was created in SolarPILOT for each location individually. After the climate file was selected for the respective locations, the design-point DNI value for each location was found using the PDF/CDF graphical method. The threshold value is as shown below.

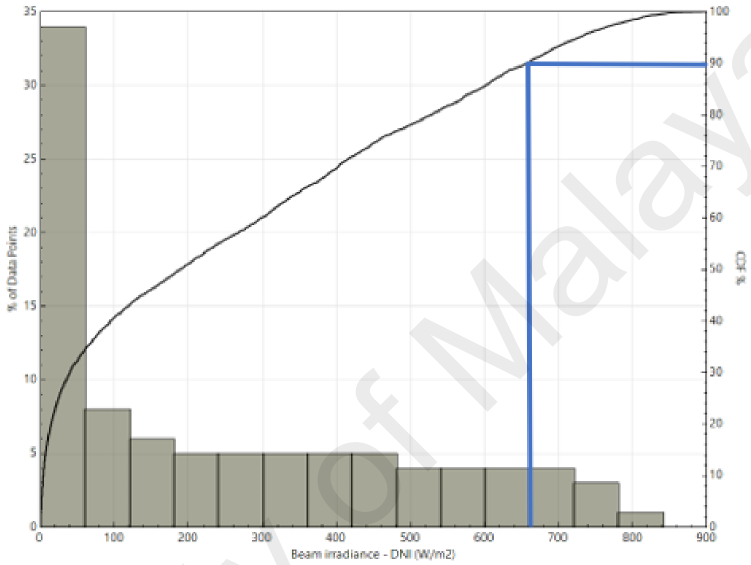

Figure 4.5: Design-point DNI value for KLIA CSP at 90% CDF value

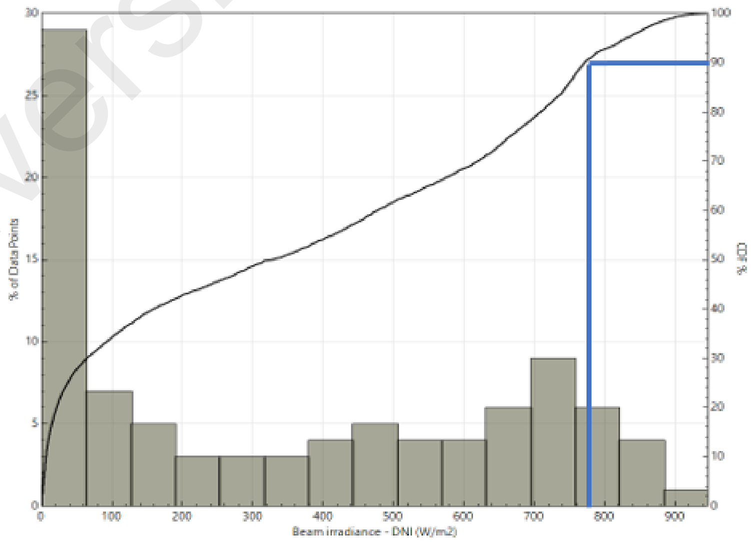

Figure 4.6: Design-Point DNI value for Gaya Island CSP at 90% CDF value

The recommended CDF threshold value by NREL is 95% (“System Advisor Model (SAM),” n.d.). However, it can be seen that majority of the DNI values throughout the year are below 200, so a large capacity CSP plant with high receiver thermal power rating is not necessary. As such, a 90% threshold was selected to allow for a better balance between the solar thermal rating of the plant and the cost of constructing and operating the plant. The design-point DNI values for KLIA and Gaya Island were found to be 660 W/m2 and 780 W/m^2 respectively. These values were inputted in the initial layout setup as shown in Figure 4.7 and Figure 4.8 below. The heliostat vertical and horizontal panels were also set to 5 and 4 respectively.

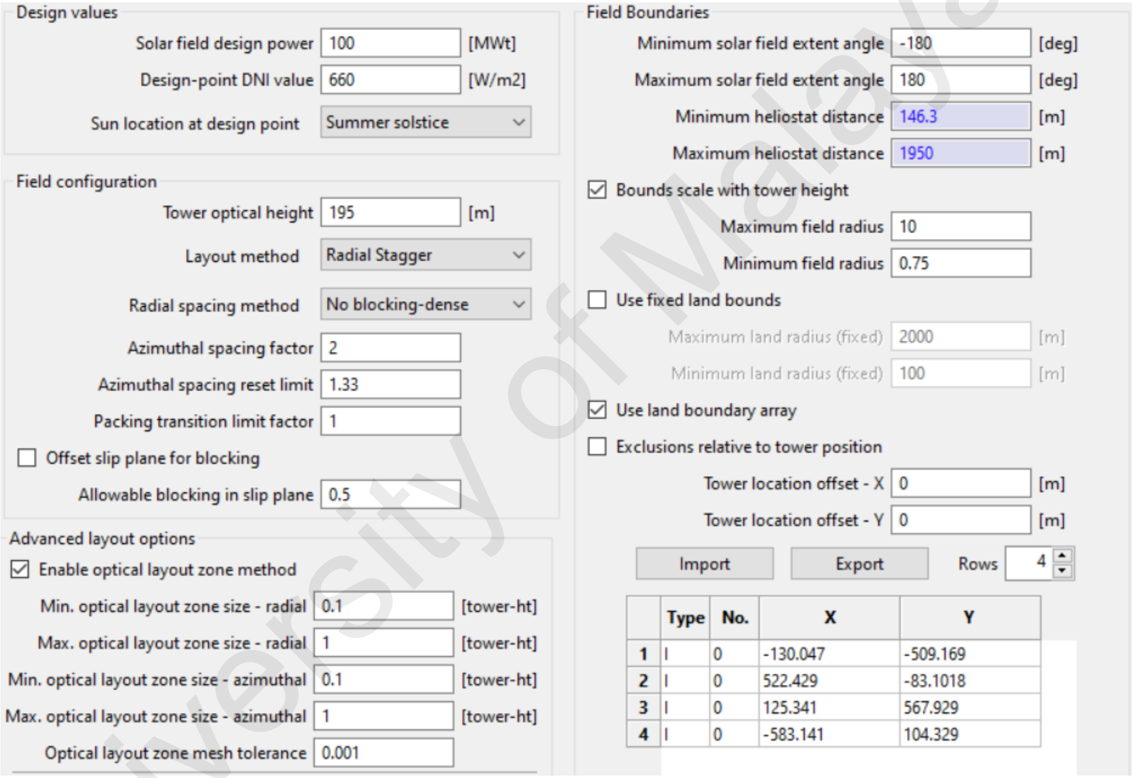

Figure 4.7: Initial layout setup for KLIA CSP plant

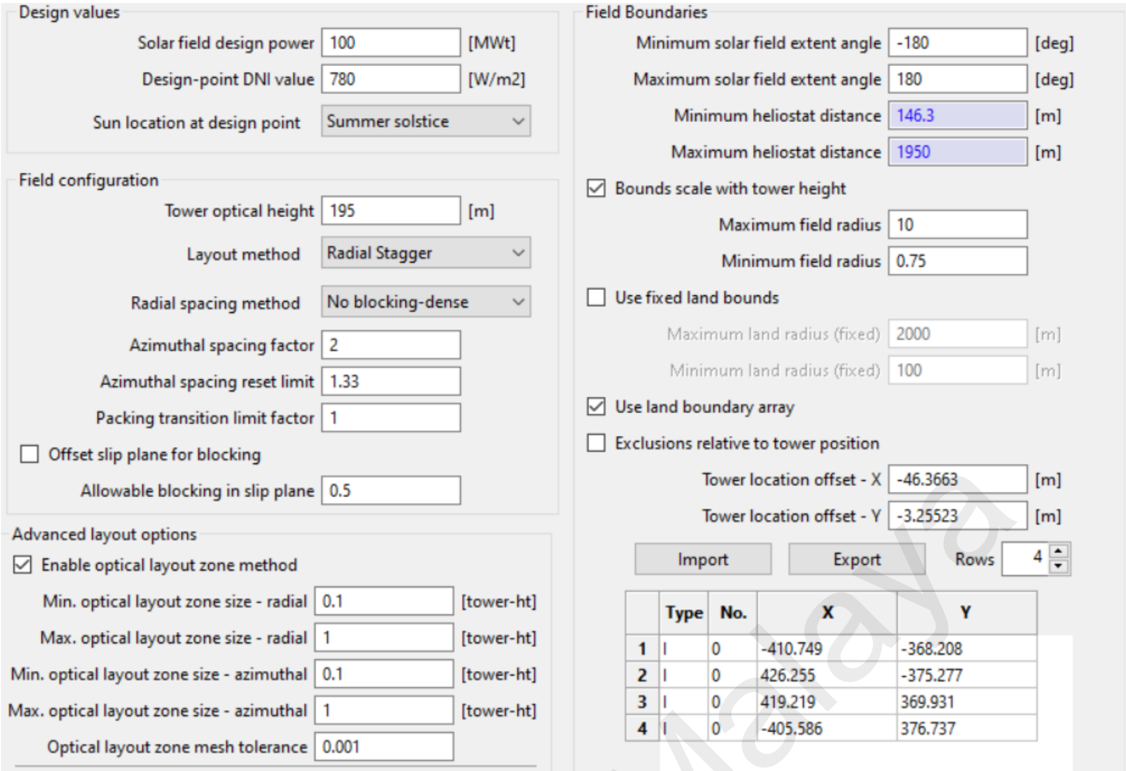

Figure 4.8: Initial layout setup for Gaya Island CSP plant

The table below shows the initial values for the parameters for both CSP plants which were selected to be optimized.

Table 4.1: Initial values for pre-optimized parameters

Parameter	Value (m)
Tower height	195
Tower location offset - X	0
Tower location offset - Y	0
Heliostat height	12.2
Heliostat width	12.2
Receiver diameter	21.6
Receiver height	17.65

The performance simulation was executed using the sun positions in Figure 4.9 for KLIA and Figure 4.10 for Gaya Island, respectively. These value remained unchanged for all simulations.

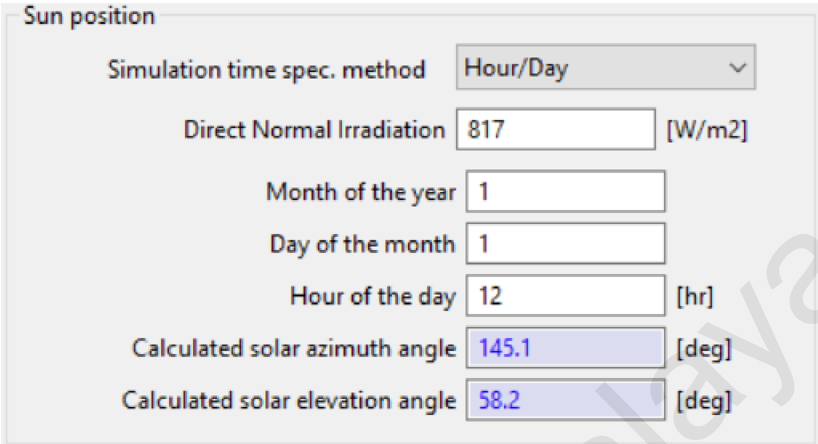

Figure 4.9: Sun position for the KLIA CSP plant performance simulation

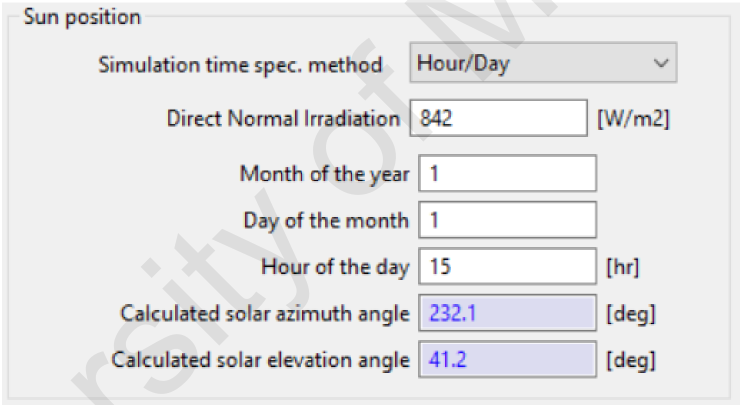

Figure 4.10: Sun position for the Gaya Island CSP plant performance simulation

There are no restrictions on the selection of sun positions. However, it is good practice to select a position where there is a high DNI value to enable the simulation to test the CSP plant at high or max capacity and give a more accurate estimation on the performance of the system.

4.2.2 Performance Simulation and Layout Selection for KLIA CSP Plant

Figure 4.11 and Figure 4.12 below show the performance simulation summary and field layout with the initial pre-optimized parameters for the KLIA CSP plant.

	Units	Value	Mean	Minimum	Maximum	Std. dev
Total plant cost	$	161,175,906.87				
Simulated heliostat area	m^2	208910				
Simulated heliostat count	-	1447				
Power incident on field	kW	170680				
Power absorbed by the receiver	kW	118106				
Power absorbed by HTF	kW	80186				
Cloudiness efficiency	%	100.00	100.00	100.00	100.00	0.0000
Shading efficiency	%	100.00	100.00	100.00	100.00	0.0000
Cosine efficiency	%	86.34	86.34	69.08	99.95	8.9439
Reflection efficiency	%	90.25	90.25	90.25	90.25	0.0000
Blocking efficiency	%	99.13	99.14	62.23	100.00	3.2610
Attenuation efficiency	%	95.73	95.71	93.59	96.92	0.7322
Image intercept efficiency	%	99.55	99.56	97.41	100.00	0.6725
Absorption efficiency	%	94.00				
Solar field optical efficiency	%	73.61		47.41	87.43	8.0984
Optical efficiency incl. receiver	%	69.20		44.56	82.18	7.6125
Annualized heliostat efficiency	%	0.00		44.74	74.35	3.8026
Incident flux	kW/m2	104.90		5.22	186.02	47.5905

Figure 4.11: Simulation summary with pre-optimized value for KLIA CSP plant

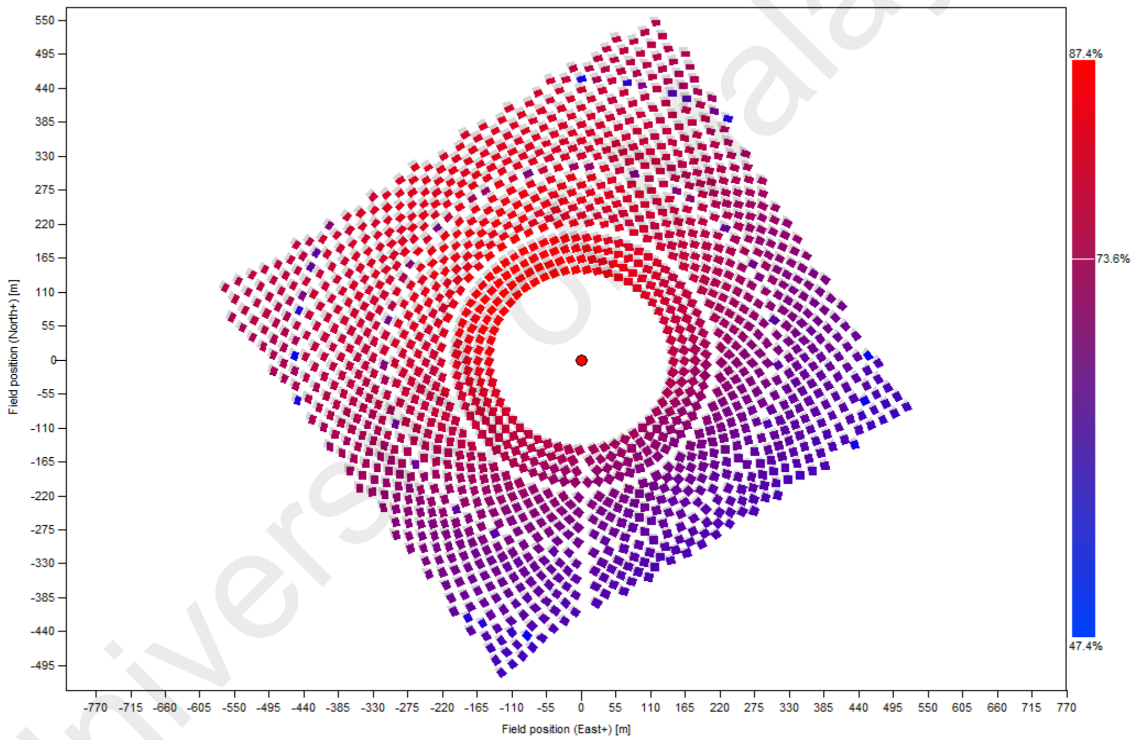

Figure 4.12: Field layout with pre-optimized value for KLIA CSP plant

Table 4.2 below shows the initial value and the optimized values for each parameter for the KLIA CSP plant.

Table 4.2: Initial and optimized values for selected parameters for KLIA CSP plant

Parameter	Initial Value (m)	Optimized Value 1 (m)	Optimized Value 2 (m)	Optimized Value 3 (m)
Tower height	195	177.976	177.973	177.942

Tower location offset - X	0	- 4.02855	-4.27012	-4.29678
Tower location offset - Y	0	31.4578	30.1282	30.1504
Heliostat height	12.2	14.4292	14.4618	14.4618
Heliostat width	12.2	15.7088	15.7161	15.7162
Receiver diameter	21.6	7.41294	7.3826	7.38079
Receiver height	17.65	10.4301	10.4162	10.4145

Figure 4.13, 4.14 and 4.15 below show the system performance summary for optimized values 1, 2 and 3 respectively.

	Units	Value	Mean	Minimum	Maximum	Std. dev
Total plant cost	$	92,857,393.40				
Simulated heliostat area	m^2	213489				
Simulated heliostat count	-	971				
Power incident on field	kW	174421				
Power absorbed by the receiver	kW	115070				
Power absorbed by HTF	kW	105967				
Cloudiness efficiency	%	100.00	100.00	100.00	100.00	0.0000
Shading efficiency	%	100.00	100.00	100.00	100.00	0.0000
Cosine efficiency	%	84.62	84.62	66.47	99.92	9.7306
Reflection efficiency	%	90.25	90.25	90.25	90.25	0.0000
Blocking efficiency	%	98.84	98.86	60.35	100.00	3.7942
Attenuation efficiency	%	95.84	95.80	93.83	97.10	0.7628
Image intercept efficiency	%	97.02	96.83	84.86	99.90	2.5485
Absorption efficiency	%	94.00				
Solar field optical efficiency	%	70.18		42.28	86.67	9.7587
Optical efficiency incl. receiver	%	65.97		39.75	81.47	9.1732
Annualized heliostat efficiency	%	0.00		39.80	73.82	5.3601
Incident flux	kW/m2	503.97		46.81	977.54	292.3456

Figure 4.13: System summary for optimized values 1 (KLIA)

	Units	Value	Mean	Minimum	Maximum	Std. dev
Total plant cost	$	92,797,035.44				
Simulated heliostat area	m^2	213851				
Simulated heliostat count	-	970				
Power incident on field	kW	174716				
Power absorbed by the receiver	kW	115203				
Power absorbed by HTF	kW	106140				
Cloudiness efficiency	%	100.00	100.00	100.00	100.00	0.0000
Shading efficiency	%	100.00	100.00	100.00	100.00	0.0000
Cosine efficiency	%	84.63	84.63	66.50	99.92	9.7186
Reflection efficiency	%	90.25	90.25	90.25	90.25	0.0000
Blocking efficiency	%	98.84	98.85	59.67	100.00	3.8083
Attenuation efficiency	%	95.84	95.80	93.82	97.10	0.7650
Image intercept efficiency	%	96.96	96.76	84.58	99.90	2.6026
Absorption efficiency	%	94.00				
Solar field optical efficiency	%	70.15		42.08	86.66	9.7737
Optical efficiency incl. receiver	%	65.94		39.55	81.46	9.1873
Annualized heliostat efficiency	%	0.00		39.79	73.81	5.3925
Incident flux	kW/m2	507.30		47.25	979.86	294.1448

Figure 4.14: System summary for optimized values 2 (KLIA)

	Units	Value	Mean	Minimum	Maximum	Std. dev
Total plant cost	$	92,744,110.19				
Simulated heliostat area	m^2	213632				
Simulated heliostat count	-	969				
Power incident on field	kW	174537				
Power absorbed by the receiver	kW	115067				
Power absorbed by HTF	kW	106008				
Cloudiness efficiency	%	100.00	100.00	100.00	100.00	0.0000
Shading efficiency	%	100.00	100.00	100.00	100.00	0.0000
Cosine efficiency	%	84.62	84.62	66.50	99.92	9.7239
Reflection efficiency	%	90.25	90.25	90.25	90.25	0.0000
Blocking efficiency	%	98.84	98.85	59.62	100.00	3.8107
Attenuation efficiency	%	95.84	95.80	93.82	97.10	0.7643
Image intercept efficiency	%	96.95	96.76	84.57	99.90	2.6043
Absorption efficiency	%	94.00				
Solar field optical efficiency	%	70.14		42.07	86.66	9.7780
Optical efficiency incl. receiver	%	65.93		39.54	81.46	9.1913
Annualized heliostat efficiency	%	0.00		39.80	73.81	5.3893
Incident flux	kW/m2	506.91		47.28	980.18	293.8501

Figure 4.15: System summary for optimized values 3 (KLIA)

Figure 4.16, 4.17 and 4.18 below show the solar field layout for optimized values 1, 2 and 3, respectively. The layouts were obtained after the performance simulation was executed in order to obtain the correct orientation of the heliostats.

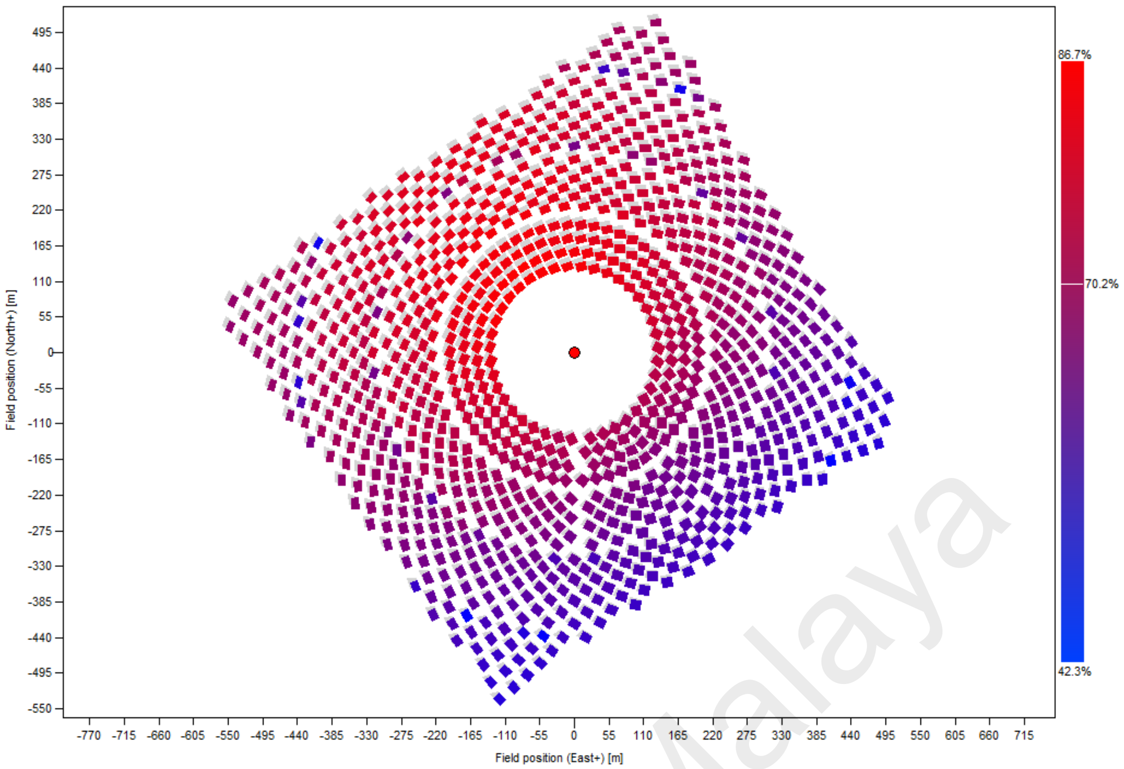

Figure 4.16: Field layout for optimized values 1 (KLIA)

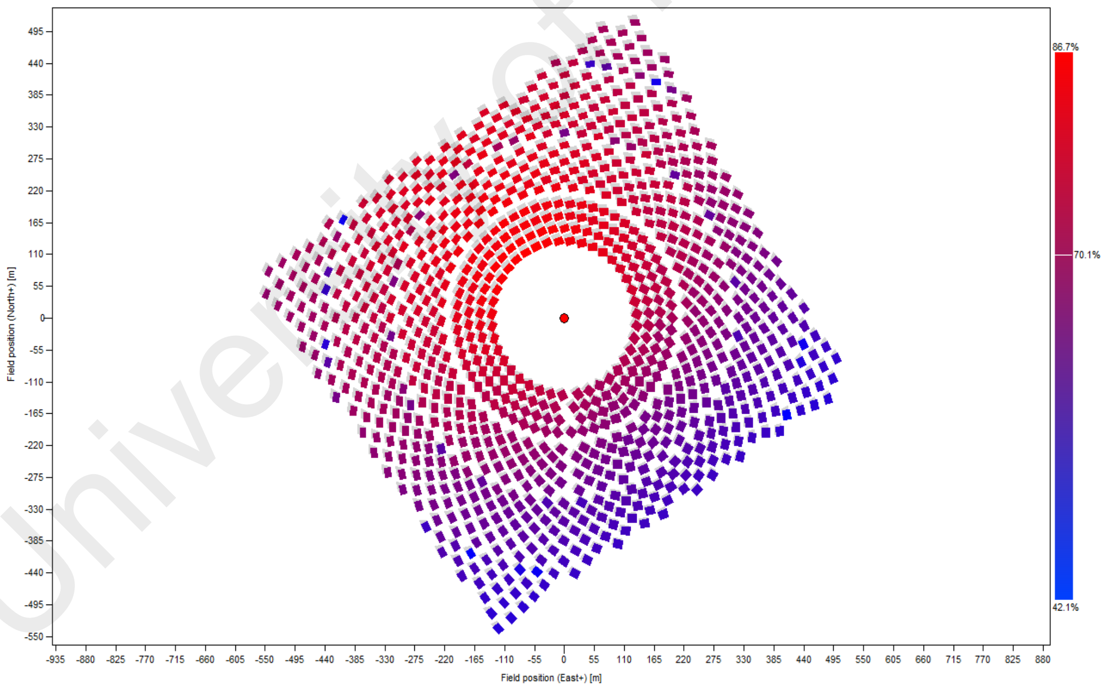

Figure 4.17: Field layout for optimized values 2 (KLIA)

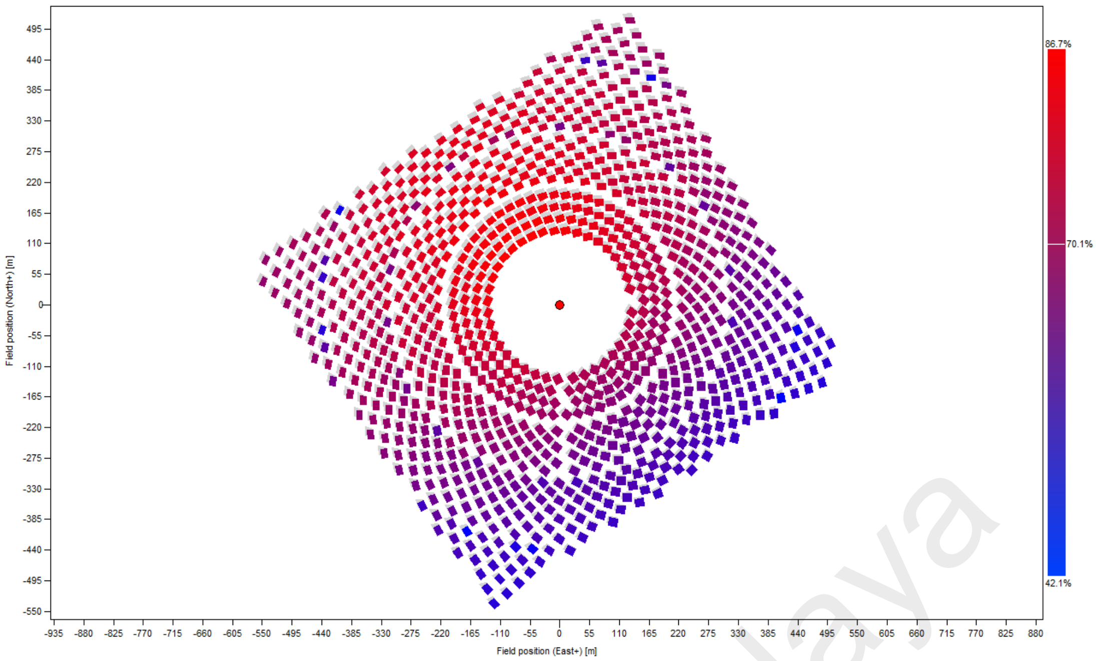

Figure 4.18: Field layout for optimized values 3 (KLIA)

By comparing between Figure 4.11, 4.13, 4.14 and 4.15, it can be seen that the unoptimized system layout resulted the highest cost and the lowest power absorbed by the heat transfer fluid (HTF) followed by the system layout with the value from optimization 1. Between the system performance with the values from optimization 2 and optimization 3, the difference in power absorbed by the receiver and HTF were both 0.12% while the difference in approximate cost was only 0.057%. As such, the parameter values in optimization 2 were selected as input value for the generation of solar field layout and the simulation of the CSP plant.

4.2.3 Performance Simulation and Layout Selection for Gaya Island CSP Plant

Figure 4.19 and Figure 4.20 below shows the performance simulation summary and field layout with the initial pre-optimized parameters for the Gaya Island CSP plant. There was a software error which prevented the saved image from displaying the total solar field optical efficiency (the red and blue shadings). As such, the regular field layout was used instead.

	Units	Value	Mean	Minimum	Maximum	Std. dev
Total plant cost	$	161,361,449.23				
Simulated heliostat area	m^2	210065				
Simulated heliostat count	-	1455				
Power incident on field	kW	176875				
Power absorbed by the receiver	kW	115100				
Power absorbed by HTF	kW	77180				
Cloudiness efficiency	%	100.00	100.00	100.00	100.00	0.0000
Shading efficiency	%	99.32	99.32	91.51	100.00	1.8390
Cosine efficiency	%	81.67	81.76	51.03	99.99	14.0420
Reflection efficiency	%	90.25	90.25	90.25	90.25	0.0000
Blocking efficiency	%	99.26	99.32	58.45	100.00	3.3229
Attenuation efficiency	%	95.73	95.71	93.90	96.92	0.7261
Image intercept efficiency	%	99.52	99.50	97.40	100.00	0.6966
Absorption efficiency	%	94.00				
Solar field optical efficiency	%	69.23		42.79	87.10	11.7924
Optical efficiency incl. receiver	%	65.07		40.22	81.87	11.0849
Annualized heliostat efficiency	%	0.00		44.99	74.58	3.7855
Incident flux	kW/m2	102.24		5.83	189.28	47.2298

Figure 4.19: Simulation summary with pre-optimized value for Gaya Island CSP plant

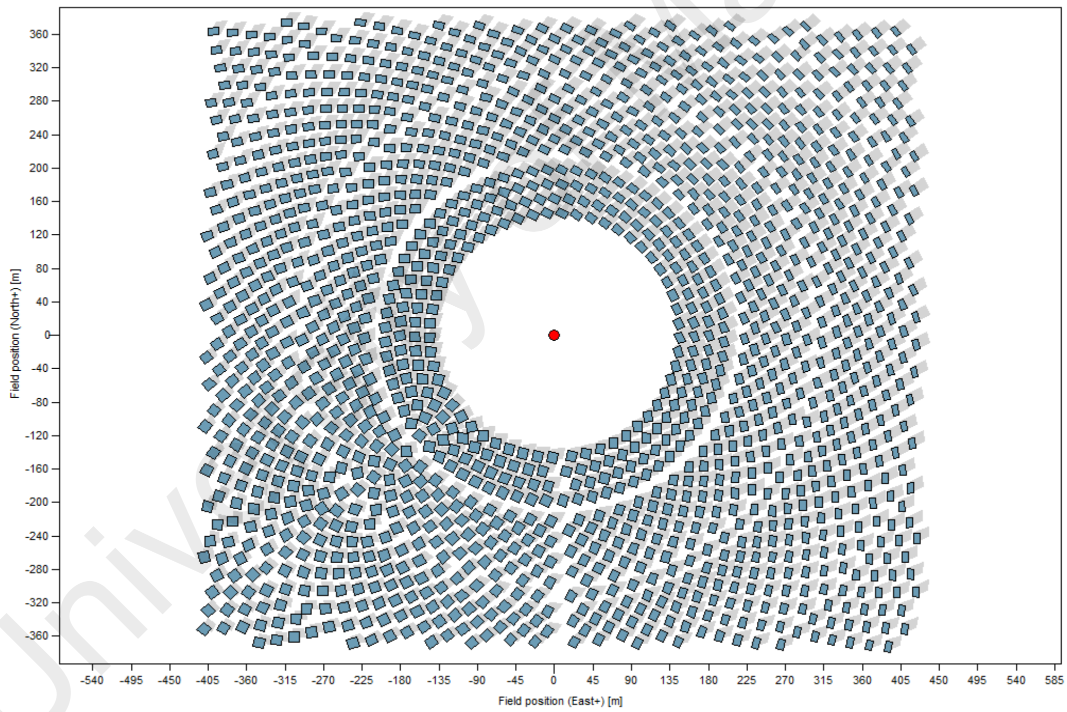

Figure 4.20: Field layout with pre-optimized value for Gaya Island CSP plant

Table 4.3 shows the initial value and the optimized values for each parameter for the Gaya Island CSP plant.

Table 4.3: Initial and optimized values for selected parameters for Gaya Island CSP plant

Parameter	Initial Value (m)	Optimized Value 1 (m)	Optimized Value 2 (m)	Optimized Value 3 (m)
Tower height	195	169.473	167.242	167.194
Tower location offset - X	0	-46.3663	-15.6523	-13.0559
Tower location offset - Y	0	-3.25523	-2.28183	27.6901
Heliostat height	12.2	10.7821	10.8313	10.6552
Heliostat width	12.2	16.4751	16.4723	16.5577
Receiver diameter	21.6	5.88539	5.97641	5.93652
Receiver height	17.65	11.942	12.0875	11.9923

Figure 4.21, 4.22 and 4.23 below shows the system performance summary for optimized values 1, 2 and 3, respectively.

	Units	Value	Mean	Minimum	Maximum	Std. dev
Total plant cost	$	88,344,823.34				
Simulated heliostat area	m^2	212110				
Simulated heliostat count	-	1231				
Power incident on field	kW	178597				
Power absorbed by the receiver	kW	110910				
Power absorbed by HTF	kW	102557				
Cloudiness efficiency	%	100.00	100.00	100.00	100.00	0.0000
Shading efficiency	%	100.00	100.00	100.00	100.00	0.0000
Cosine efficiency	%	82.38	82.38	50.34	99.99	14.0733
Reflection efficiency	%	90.25	90.25	90.25	90.25	0.0000
Blocking efficiency	%	99.30	99.37	57.25	100.00	2.8112
Attenuation efficiency	%	95.85	95.85	93.52	97.20	0.8056
Image intercept efficiency	%	93.36	92.88	68.37	99.98	5.4974
Absorption efficiency	%	94.00				
Solar field optical efficiency	%	66.06		29.58	87.31	13.2157
Optical efficiency incl. receiver	%	62.10		27.80	82.07	12.4227
Annualized heliostat efficiency	%	0.00		33.45	73.58	6.0089
Incident flux	kW/m2	534.37		40.67	1082.66	301.4440

Figure 4.21: System summary for optimized values 1 (Gaya island)

	Units	Value	Mean	Minimum	Maximum	Std. dev
Total plant cost	$	88,270,874.48				
Simulated heliostat area	m^2	211657				
Simulated heliostat count	-	1223				
Power incident on field	kW	178215				
Power absorbed by the receiver	kW	109840				
Power absorbed by HTF	kW	101325				
Cloudiness efficiency	%	100.00	100.00	100.00	100.00	0.0000
Shading efficiency	%	100.00	100.00	100.00	100.00	0.0000
Cosine efficiency	%	81.35	81.35	49.57	99.99	14.5055
Reflection efficiency	%	90.25	90.25	90.25	90.25	0.0000
Blocking efficiency	%	99.33	99.40	61.58	100.00	2.7526
Attenuation efficiency	%	95.90	95.88	93.83	97.22	0.7821
Image intercept efficiency	%	93.76	93.18	67.39	99.98	5.5403
Absorption efficiency	%	94.00				
Solar field optical efficiency	%	65.57		28.39	87.35	13.7843
Optical efficiency incl. receiver	%	61.63		26.69	82.11	12.9573
Annualized heliostat efficiency	%	0.00		33.93	73.71	5.7859
Incident flux	kW/m2	514.88		38.45	974.93	275.0561

Figure 4.22: System summary for optimized values 2 (Gaya Island)

	Units	Value	Mean	Minimum	Maximum	Std. dev
Total plant cost	$	87,549,294.29				
Simulated heliostat area	m^2	209124				
Simulated heliostat count	-	1222				
Power incident on field	kW	176083				
Power absorbed by the receiver	kW	106934				
Power absorbed by HTF	kW	98519				
Cloudiness efficiency	%	100.00	100.00	100.00	100.00	0.0000
Shading efficiency	%	100.00	100.00	100.00	100.00	0.0000
Cosine efficiency	%	80.28	80.28	48.97	99.99	14.8233
Reflection efficiency	%	90.25	90.25	90.25	90.25	0.0000
Blocking efficiency	%	99.43	99.50	72.59	100.00	2.3785
Attenuation efficiency	%	95.90	95.87	93.56	97.22	0.7791
Image intercept efficiency	%	93.52	92.82	66.59	99.99	5.9577
Absorption efficiency	%	94.00				
Solar field optical efficiency	%	64.61		27.98	87.34	14.3415
Optical efficiency incl. receiver	%	60.73		26.30	82.10	13.4810
Annualized heliostat efficiency	%	0.00		38.91	73.48	5.7454
Incident flux	kW/m2	508.63		46.21	949.24	267.0772

Figure 4.23: System summary for optimized values 3 (Gaya Island)

Figure 4.24, 4.25 and 4.26 below show the solar field layout for optimized values 1, 2 and 3, respectively. The layouts were obtained after the performance simulation was executed in order to obtain the correct orientation of the heliostats.

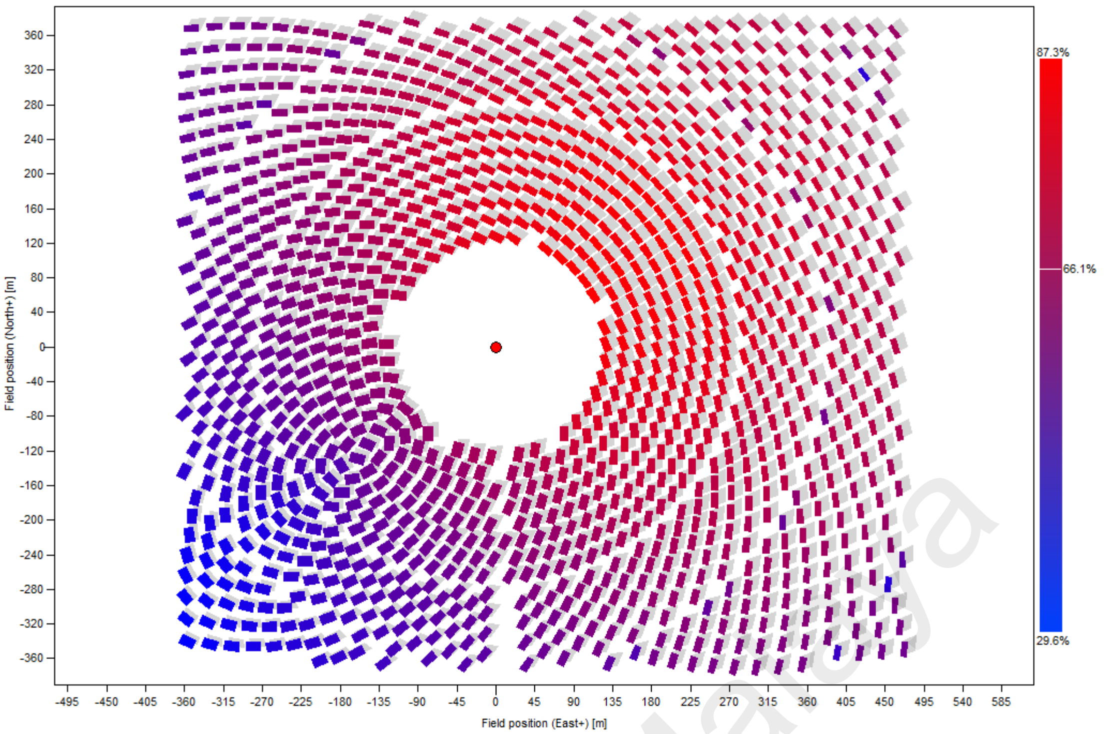

Figure 4.24: Field layout for optimized values 1 (Gaya Island)

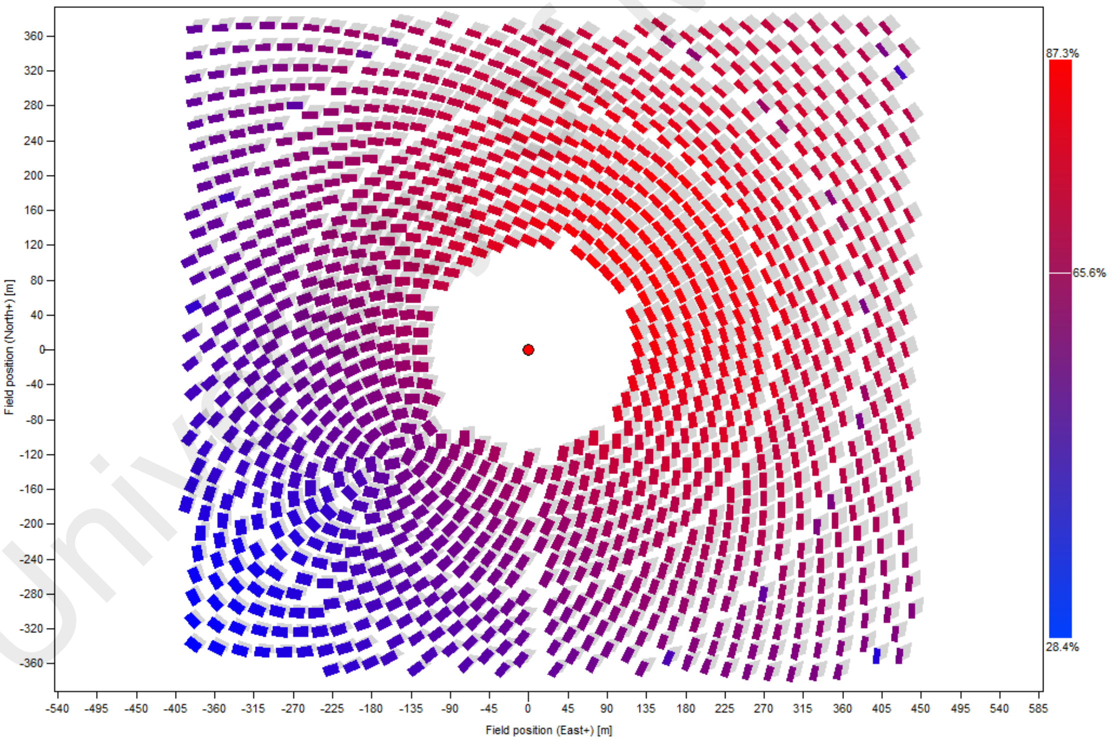

Figure 4.25: Field layout for optimized values 2 (Gaya Island)

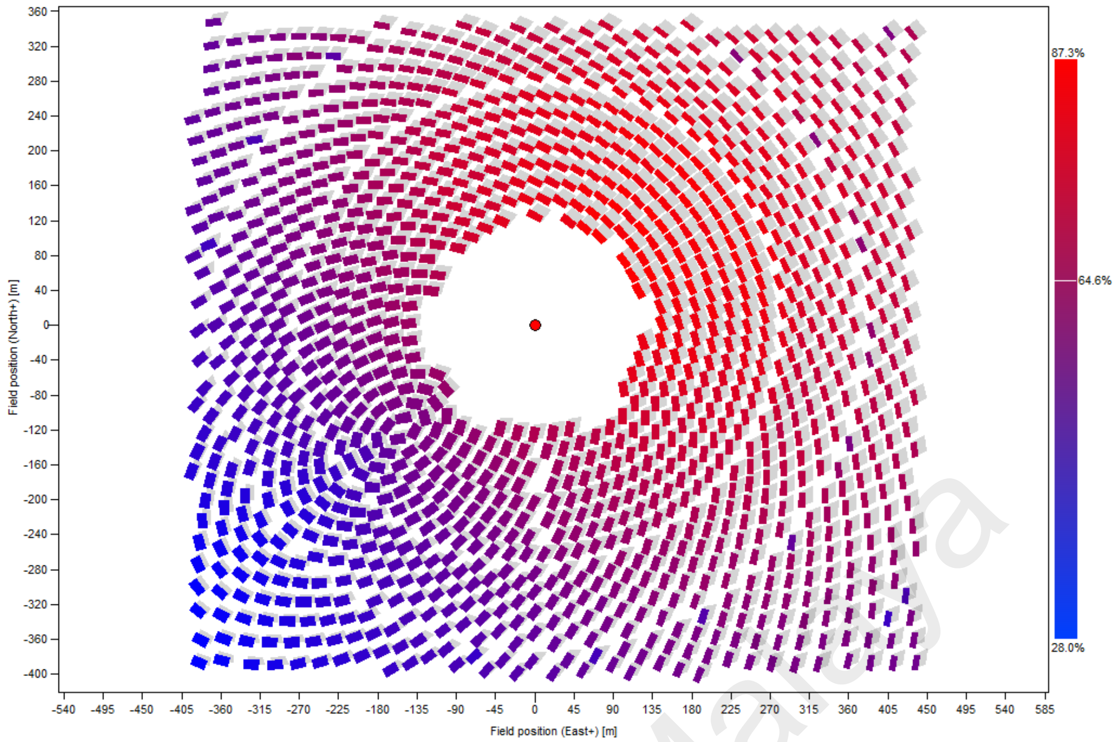

Figure 4.26: Field layout for optimized values 3 (Gaya Island)

By comparing between Figure 4.19, 4.21, 4.22 and 4.23, it can be seen that the unoptimized system layout resulted the highest cost and the lowest power absorbed by the heat transfer fluid (HTF) followed by the system layout with the value from optimization 3. Between the system performance with the values from optimization 1 and optimization 2, the difference in power absorbed by the receiver and HTF were 0.96% and 1.2% while the difference in approximate cost was only 0.084%. As such, the parameter values in optimization 1 were selected as input value for the generation of solar field layout and the simulation of the CSP plant.

4.3 SAM Annual Performance and Financials Simulation

The results from SolarPILOT regarding the solar field parameters and the climate data file prepared for each location were fed into SAM for performance and cost simulation of the CSP plants. The system design, solar field, tower, and receiver parameters are discussed. Furthermore, the water demand for both plants, the desalination capacity and cost for the Gaya plant, along with the thermal storage parameter are shown. Lastly, the annual and monthly expected electrical production and the resulting CO_2 emissions reduction are shown with the breakdown of the approximated total cost.

4.3.1 SAM Simulation for KLIA CSP Plant

In this section, the results obtained from SAM will be briefly described.

4.3.1.1 KLIA CSP Performance Simulation Results

Figure 4.27 below shows the design parameters for the KLIA CSP plant in SAM. The design point DNI is set to 660 W/m^2 with the other parameters remain unchanged. The receiver thermal power of 100 MWt was found to have a design turbine gross output of 13.7 MWe.

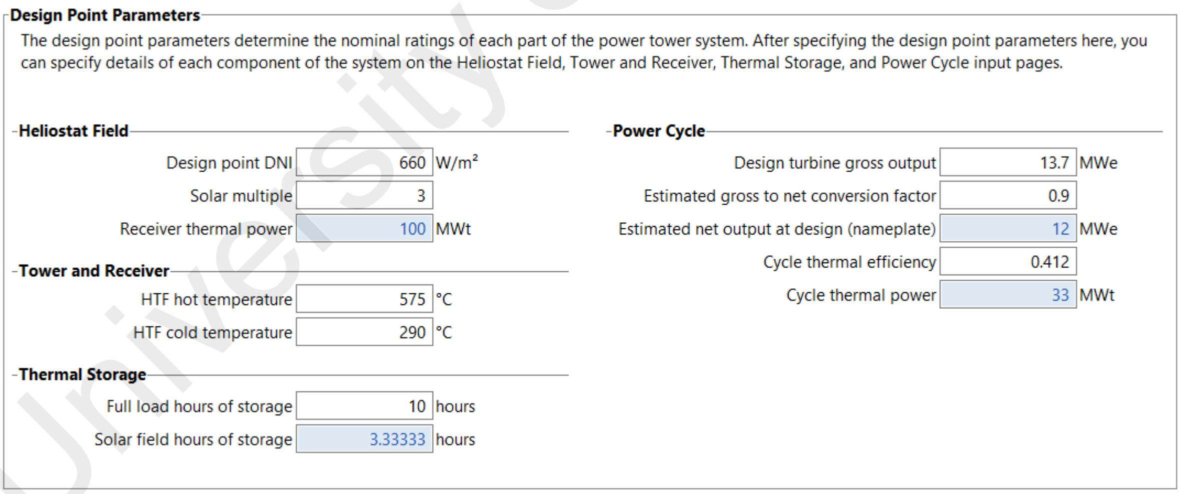

Figure 4.27: SAM design parameters for KLIA CSP plant

Figure 4.28 shows the general arrangement of a CSP plant as shown in SAM. The arrangement includes the heliostat field, thermal storage, tower, and receiver as well as the power cycle which is almost identical to that of a conventional fossil fuel power plant. Figure 4.29 shows the overlay of the KLIA CSP plant on the image of the actual location.

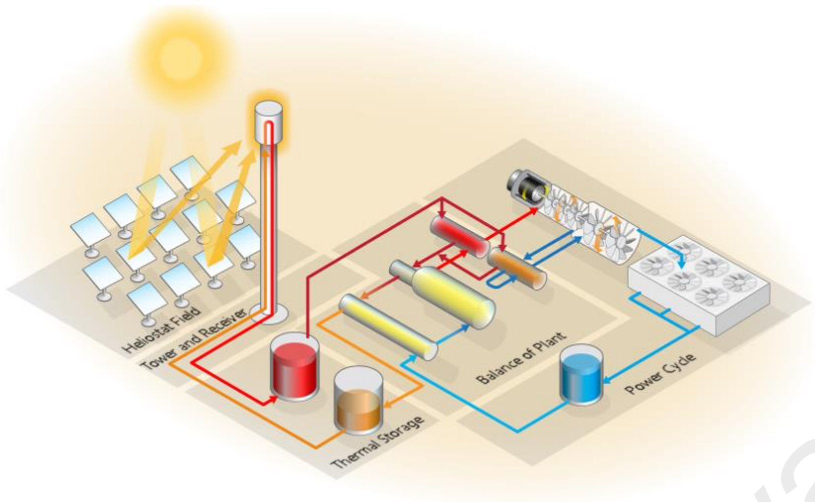

Figure 4.28: CSP plant arrangement

Figure 4.29: KLIA CSP plant overlay on the CSP location

Figure 4.30 shows the heliostat layout generated by SAM based on the imported heliostat positions from SolarPILOT. The optimization settings were not used as the optimization was already done in SolarPILOT.

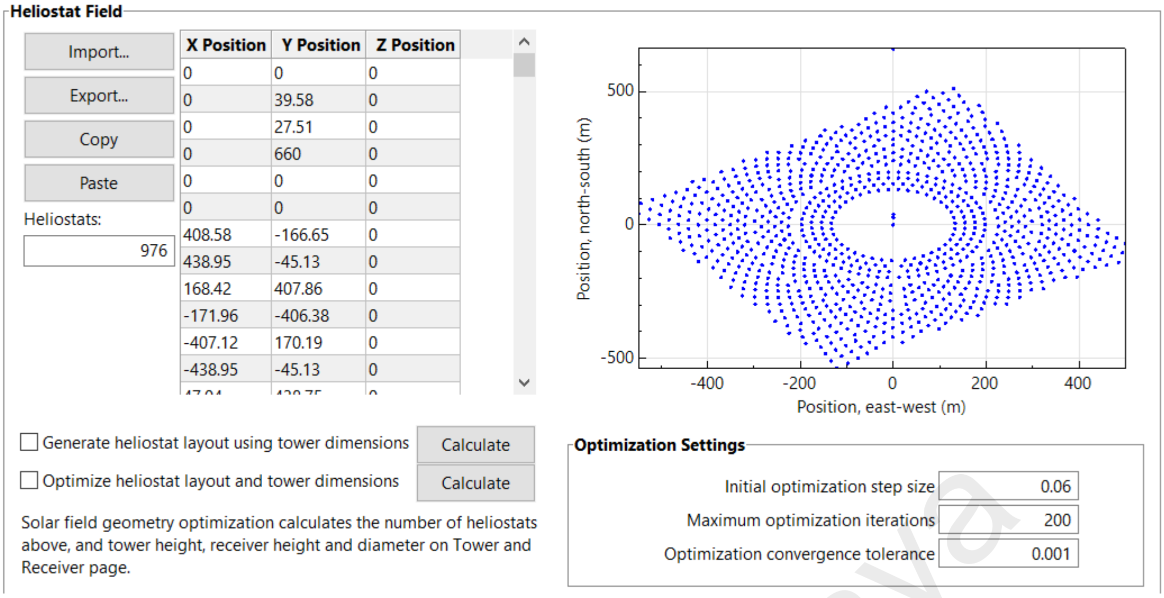

Figure 4.30: SAM heliostat layout for KLIA CSP plant

Figure 4.31 shows the heliostat operation parameters and properties. Dimensions for the heliostats are identical to the optimized values from SolarPILOT. The atmospheric attenuation values are the default values recommended by SAM.

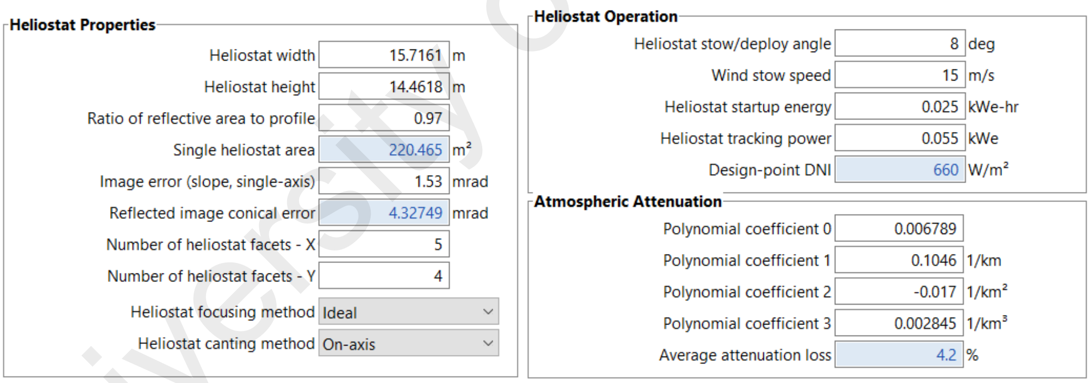

Figure 4.31: SAM heliostat properties, heliostat operation and atmospheric attenuation for KLIA CSP plant

Figure 4.32 shows the land area, layout constraints, heliostat field availability and washing frequency for the heliostats. The non-solar field land area was set at 35 acres which brought the total land area to 203 acres. The total heliostat reflective area was found to be 215,173 m^2. The solar field layout constraints and heliostat field availability were identical to the values in SolarPILOT. It is expected that heliostat mirror washing occur twice a week, which totals up to 104 times a year.

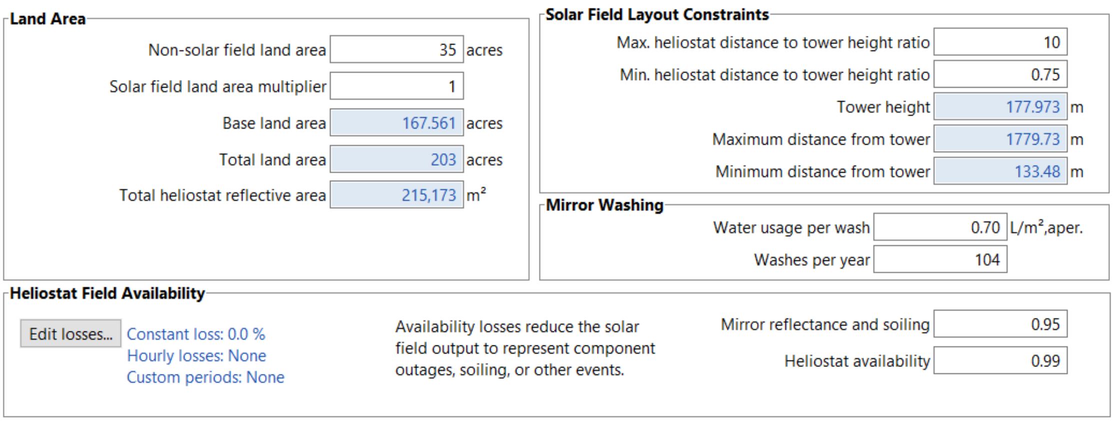

Figure 4.32: SAM land area, field layout constraints, washing frequency and heliostat availability for KLIA CSP plant

Figure 4.33 shows the tower and receiver parameters and dimensions which are identical to the optimized values in SolarPILOT. The receiver heat transfer properties, design, and operation, HTF type, flow type, piping loses, and receiver flux modelling parameters were selected based on the recommended values and selections by SAM.

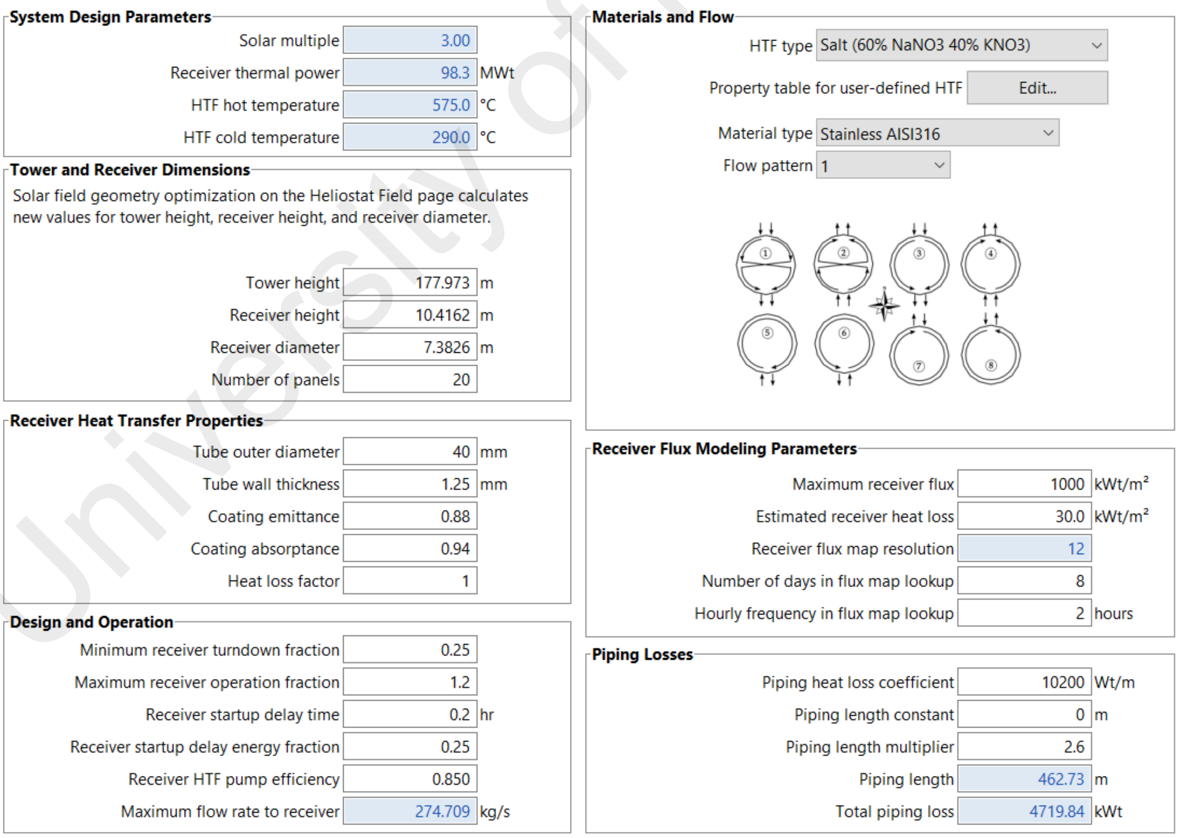

Figure 4.33: SAM tower, receiver and HTF properties and parameters for KLIA CSP plant

Figure 4.34 shows the power cycle design parameters. Rankine cycle was selected for the operation of the power cycle. A hybrid condenser operation was selected which allows for a cooling combination between a cooling tower and the conventional air-cooling method. In actual operation, air-cooling will be used full time while the cooling tower will be used during peak operations which generate high heat and high temperatures. Hybrid cooling operation also provides the best efficiency which reduces the water usage during cooling procedures. All other parameter values were in accordance with the recommended SAM values.

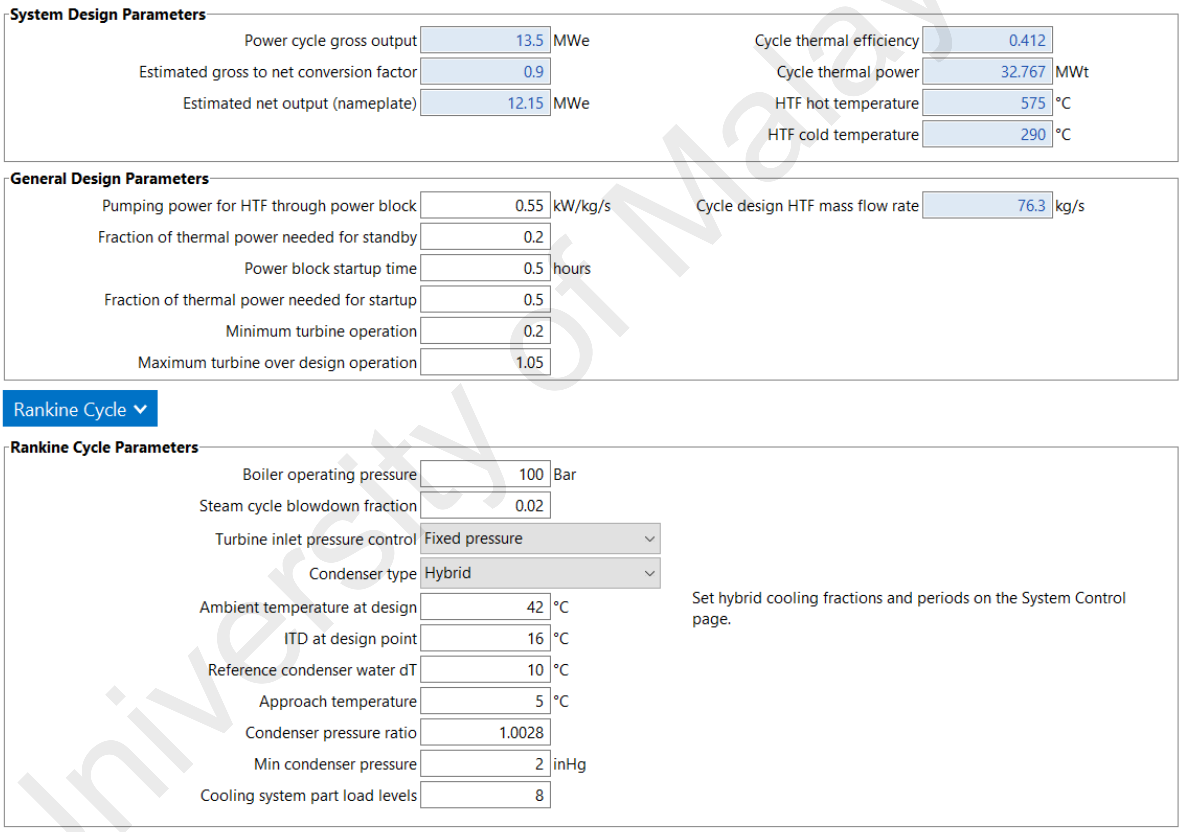

Figure 4.34: Power cycle parameters for KLIA CSP plant

Figure 4.35 shows the thermal storage parameters for the CSP plant. All parameters were set in accordance with the recommended values by SAM.

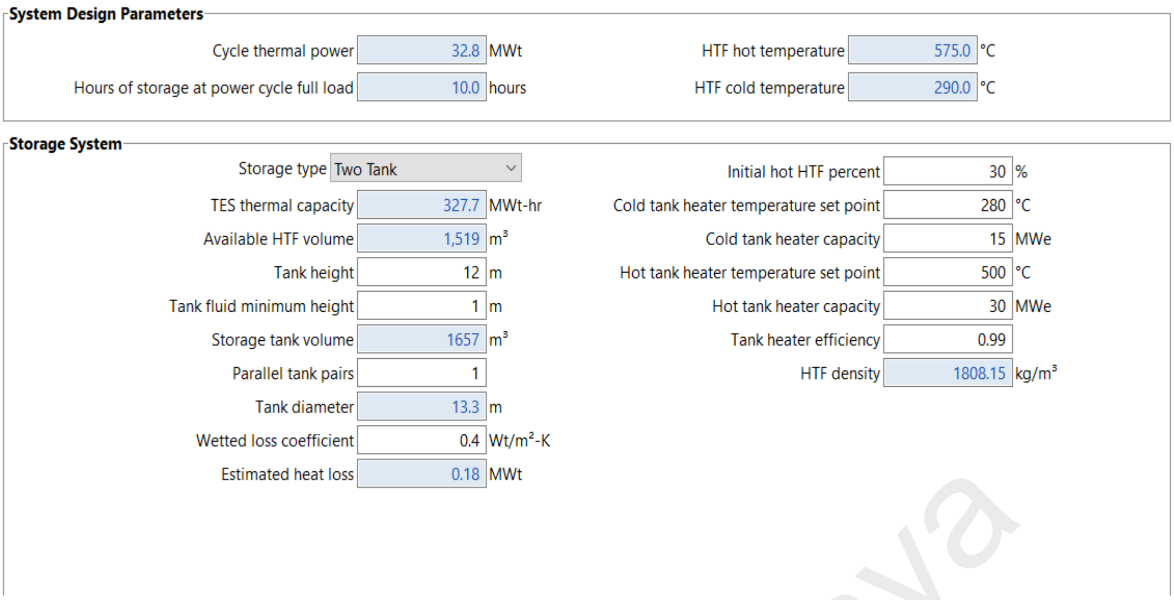

Figure 4.35: Thermal storage parameters for KLIA CSP plant

The plant energy consumption was set to 0.0055 MWe/MWcap which was the default value recommended by SAM.

There are three primary uses for water in a CSP plant, namely, heliostat washing activities, steam cycle makeup and hybrid cooling system augmentation. As stated previously, heliostat mirror washing was expected to occur twice a month. The total heliostat reflective area is 215,173 m^2 which requires approximately 151 m^3, based on 0.7 litre per m^2 of water usage. Table 4.4 below shows the breakdown of the monthly water consumption based on the number of washes for each month and the total water consumption for each month.

Table 4.4: Monthly water consumption for heliostat mirror washing for KLIA CSP plant

Month	Number of washes	Total water consumption (m^3)
January	8	1208
February	8	1208
March	8	1208
April	10	1510

May	8	1208
June	8	1208
July	10	1510
August	8	1208
September	8	1208
October	10	1510
November	8	1208
December	10	1510
TOTAL	104	15,704

The water consumption related to the steam cycle makeup and hybrid cooling was simulated by SAM on an hourly basis for the whole year in kg/s, which were manually converted to kg/h for easier conversion and calculations. The weight of 1 m^3 of water volume was assumed to be 1000 kg. Thus, the monthly water consumption was calculated and tabulated in Table 4.5 below.

Table 4.5: Monthly water consumption for steam cycle makeup and hybrid cooling for KLIA CSP plant

Month	Total water consumption (kg/h)	Total water consumption (m^3)
January	357,060	357
February	388,289	388
March	340,885	341
April	265,858	266
May	267,454	267
June	191,753	192
July	243,775	244

August	192,924	193
September	142,433	142
October	182,733	183
November	170,007	170
December	238,867	239
TOTAL	2,984,198	2984

The total water consumption for the heliostat washing activities, steam makeup and hybrid cooling for the CSP plant is as shown in Table 4.6 and Figure 4.36.

Table 4.6: Total combined monthly water consumption for KLIA CSP plant

Month	Heliostat washing (m^3)	Steam makeup and cooling (m^3)	Total water consumption (m^3)
January	1208	357	1565
February	1208	388	1596
March	1208	341	1549
April	1510	266	1776
May	1208	267	1475
June	1208	192	1400
July	1510	244	1754
August	1208	193	1401
September	1208	142	1350
October	1510	183	1693
November	1208	170	1378
December	1510	239	1749
TOTAL	15,704	2984	18,688

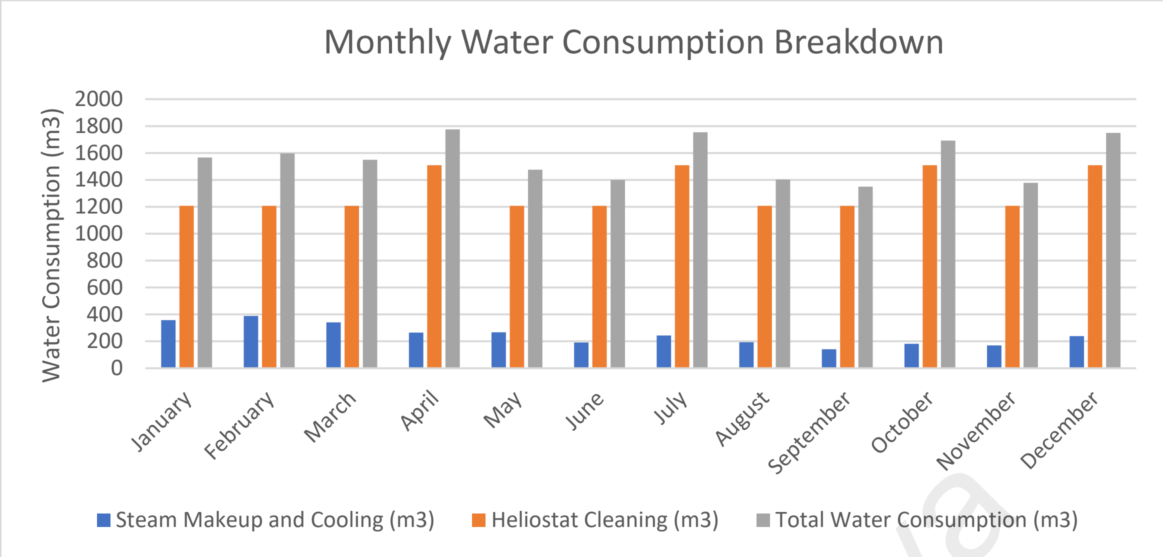

Figure 4.36: Monthly water consumption breakdown for KLIA CSP plant

Based on Table 4.6 and Figure 4.36, it can be seen that the steam makeup and cooling water consumption is normally distributed with its peak occurring in February whereas April has the highest total monthly water consumption. The annual water consumption from heliostat cleaning is 84% of the total annual water consumption which is significantly higher than the water consumption by steam makeup and cooling.

The energy production during the 1st year of operation are shown in Table 4.7 below. February has the highest energy production with 5,426,070 kWh. A performance degradation of 1% a year was selected to better model the performance characteristics of the CSP plant over the years. Based on the available experience with CSP plants, the lifetime of a CSP plant could be more than 30 years (Pihl & Frescativägen, n.d.). In this paper, the lifetime for a CSP plant was selected to be 35 years. Figure 4.37 below shows the annual energy production considering the 1% annual performance degradation.

Table 4.7: Energy production during 1st year of operation for KLIA CSP plant

Month	Energy Production (kWh)
January	4,981,690
February	5,426,070

March	4,738,030
April	3,683,950
May	3,689,210
June	2,621,450
July	3,347,530
August	2,657,740
September	1,903,600
October	2,493,300
November	2,311,930
December	3,291,460
TOTAL	41,145,964

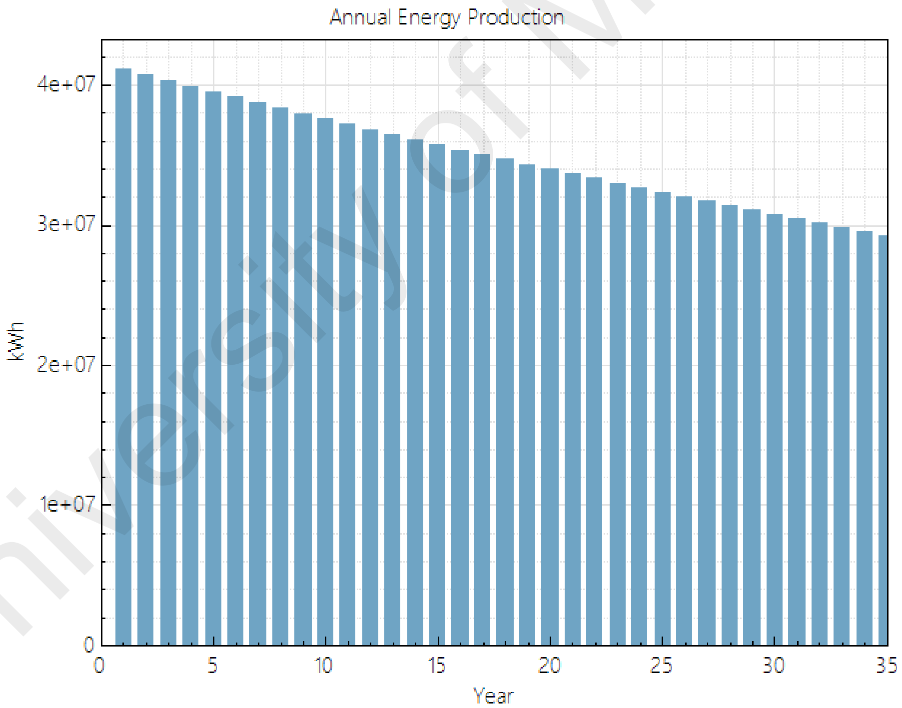

Figure 4.37: Annual Energy Production with 1% degradation for KLIA CSP plant

In year 35, the CSP plant experiences a production loss of approximately 1,000,000 kWh every month due to degradation.

Based on a study by The Parliamentary Office of Science and Technology in London, the CO_2 gas emissions of some of the most efficient combined cycle gas turbine process is estimated to be around 140 gCO2eq/kWh in a German study and around 200 gCO2eq/kWh in a UK study (*Carbon Footprint of Electricity Generation*, n.d.). Thus, the mid-point between both values, which is 170 gCO2eq/kWh, was taken. By multiplying this number with the energy produced by the CSP plant, the reduction in CO2 gas emissions was found. The approximated reduction in emission by utilizing the designed CSP plant in the first year instead of combined cycle gas turbine process is shown in Table 4.8. The total amount of CO_2 emissions reduced is 6994.81 tonne CO_2.

Table 4.8: Monthly CO_2 emission reduction for KLIA CSP plant

Month	Energy production (kWh)	CO_2 emission reduction (tonCO_2)
January	4,981,690	846.89
February	5,426,070	922.43
March	4,738,030	805.47
April	3,683,950	626.27
May	3,689,210	627.17
June	2,621,450	445.65
July	3,347,530	569.08
August	2,657,740	451.82
September	1,903,600	323.61
October	2,493,300	423.86
November	2,311,930	393.03
December	3,291,460	559.55
TOTAL	41,145,964	6994.81

4.3.1.2 KLIA CSP Financial Simulation Results

The total system installed cost consists of the direct capital costs, indirect capital costs and operation and maintenance costs. The costs of each plant components were determined as per the recommended values by SAM. In this paper, tax is not considered in the cost calculations. This is due to the fact that the Green Investment Tax Allowance provides a tax allowance of 100% of qualifying capital expenditure incurred on green technology assets and projects ("Guidelines on GITA Assets," 2019; "Guidelines on GITA Projects," 2019). The usual operating and maintenance costs for a CSP plant include mirror washing, repair, and replacement as well as major equipment maintenance activities (based on the equipment manufacturer's recommendations) that are approximately done every 5 to 7 years (ELBEH, 2017). According to an article by IRENA, the fixed O&M costs are estimated to be USD 65/kW-yr (Renewable Energy Agency, 2012). Based on the yearly inflation rate of the US currency from 2010 to 2020, the current O&M was estimated to be USD 77.44/kW-yr. The contingency cost is set to 7% of the subtotal cost, which is USD 5,284,501.50. The total direct cost totaled up to USD 80,777,384.00. The indirect capital cost was not considered as it was assumed that Malaysia Airport Holdings Bhd (MAHB) would lease the land the to the operator similar to the SunEdison Solar PV project ("KLIA installs RM200mil solar power system | The Star," n.d.). Since the details for the leasing and royalty agreement is unknown, it was not included in the cost calculations. As SAM did not have the option to include the cost of water usage, the cost was calculated separately and factored into the total installed cost. Based on the Selangor state water tariff as shown in Table 4.9 below, the total cost for water usage was calculated and tabulated in Table 4.10 as shown below.

Table 4.9: Air Selangor water tariff for commercial usage

Usage	Tariff Code	Rate (RM)	Min. Payment (RM)
Commercial	11	-	36.00
35m^3		2.07	
35m^3 and above		2.28	

Table 4.10: Monthly water usage cost for KLIA CSP plant

Month	Water consumption (m^3)	Cost (RM)
January	1565	3560.99
February	1596	3632.19
March	1549	3524.11
April	1776	4041.61
May	1475	3356.69
June	1400	3184.09
July	1754	3991.26
August	1401	3186.76
September	1350	3071.64
October	1693	3852.08
November	1378	3134.51
December	1749	3980.07
Total	18,688	42,601.74

The total cost for water usage over 35 years of operation, assuming the water tariff remains unchanged, was found to be RM 1,491,060.90. Using the conversion rate of I USD = 4.35 RM, the total cost for water usage was found to be RM 342,646.69. As there were no options to include additional cost in SAM, the water usage cost was added to the "Heliostat cost fixed" column instead, which does not alter the value of the other parameters and costs. By adding the direct capital costs and water usage cost, the total installed cost was found to be USD 80,777,384. The estimated total installed cost per net capacity was found to be USD 6,551.29. Figure 4.38 below shows the breakdown for the direct capital costs and the total installed cost for the CSP plant. Figure 4.39 shows the operation and maintenance cost for the CSP plant.

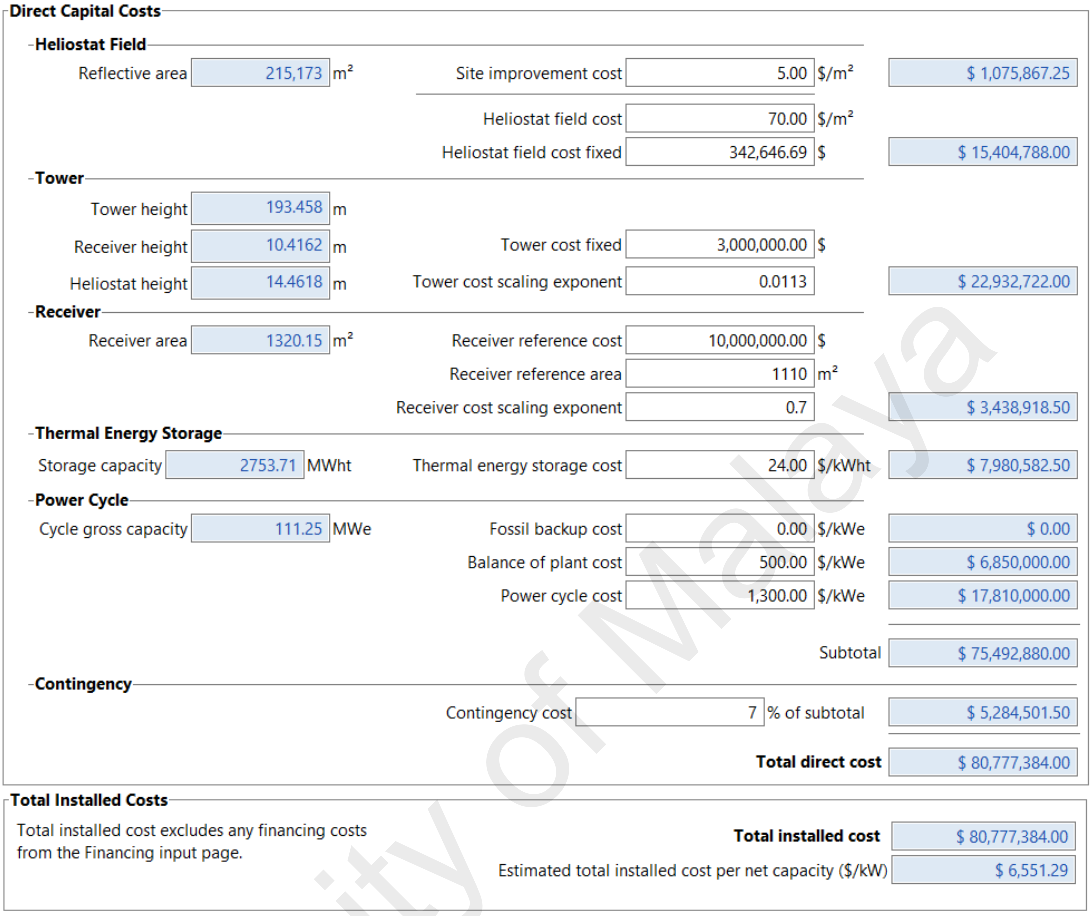

Figure 4.38: Direct capital costs and total installed cost for KLIA CSP plant

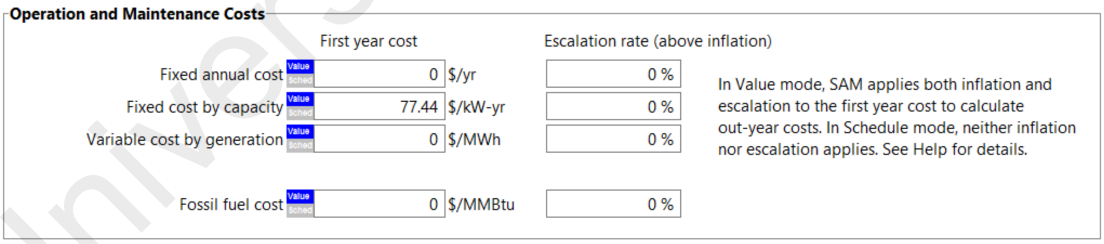

Figure 4.39: Operation and maintenance cost for KLIA CSP plant

SAM provides two solution modes to calculate the revenue of the project, namely the IRR target or PPA price. The internal rate of return (IRR) of the project is a measure of the profit margin of a project, and it is defined as the rate that leads to a net present value of zero. The PPA price in SAM is the bid price in a power purchase agreement (PPA), and it can be defined as the price that a project gains for each unit of electricity that the system generates. In this paper, an IRR target was chosen as the solution mode instead of a fixed PPA price. The IRR target year is the year at which the IRR target specified is achieved with a net present value of zero. An IRR target of 11% and a target year of year 20 was selected for this CSP project. At year 20, it is expected that the total installed cost has been paid and the CSP plant will start making a profit.

The analysis period of the project is identical to the estimated lifetime of the project which is 35 years. The inflation rate was set at 2.5% per year and the real discount rate to be 8% per year. The annual insurance rate was set at 0.5% of the installed cost. Lastly, the net salvage value of the plant when decommissioned was set at 10% of the installed cost with the end of analysis period value of $ 8,077,739. Project and property tax are not included in this paper. Figure 4.40 shows the financial parameters for the CSP plant excluding taxes and insurance.

Figure 4.40: Financial parameters for KLIA CSP plant

Figure 4.41 shows the project term debt for the CSP plant. The debt was set to be equal to 30% of total capital cost and equal payment was selected for the debt payback. The tenor was set at 18 years with an annual interest rate of 7%. The debt closing costs and up-front fee remained the default value recommended by SAM.

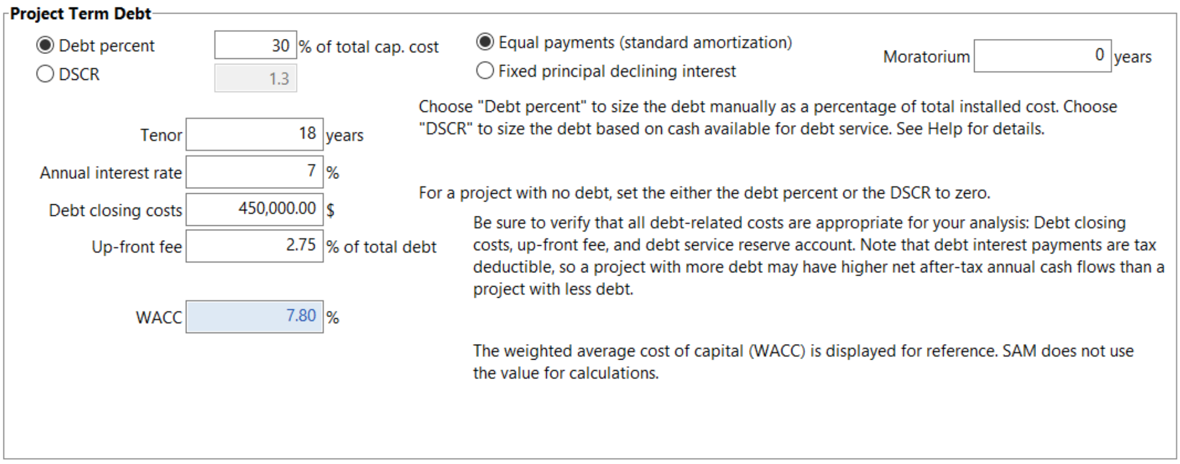

Figure 4.41: Project term debt for KLIA CSP plant

Figure 4.42 shows the solution mode for revenue calculations. Other parameters such as capacity and curtailed payments are not considered. The time of delivery settings were based on the default values by SAM and remain unchanged.

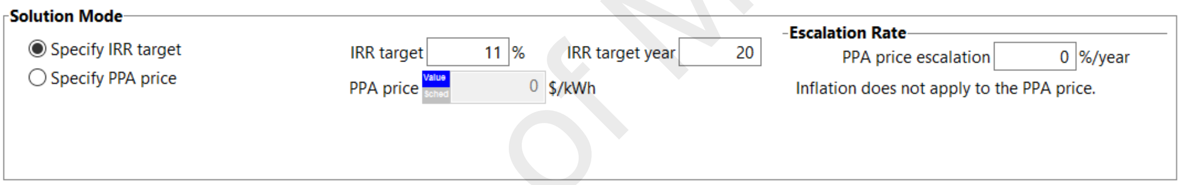

Figure 4.42: Solution mode for revenue calculations for KLIA CSP plant

4.3.1.3 Summary of Results and Cash Flow for KLIA CSP Plant

Table 4.11 shows the summary of results which includes both the performance and financial metrics. The capacity factor of the plant in year 1 was found to be 38.1%. The nominal levelized cost of energy (LCOE) and real LCOE was found to be 26.61 cents/kWh and 21.06 cents/kWh respectively. The net present value of the project was found to be a positive value of USD 7,701,224.

Table 4.11: Summary of results for KLIA CSP plant

Metric	Value
Annual energy (year 1)	41,145,964 kWh

Capacity factor (year 1)	38.1%
Annual water usage	18,649 m^3
PPA price (year 1)	26.31 cents/kWh
Levelized COE (nominal)	26.61 cents/kWh
Levelized COE (real)	21.06 cents/kWh
Net present value	USD 7,701,224
Internal rate of return (IRR)	11.00%
Year IRR is achieved	20
IRR at end of project	12.37%
Net capital cost	USD 81,903,032
Equity	USD 57,333,784
Size of Debt	USD 24,659,252

The project after-tax cash flow is shown in Figure 4.43. Year 0 is the year the CSP plant is installed, hence it has a negative cash flow. The remaining years show a gradual decline in revenue which is synchronous with the decline in energy production. In year 35, the salvage value was added to the revenue. The details of the project cash flow were tabulated in Table 4.12 for the project's lifetime revenue and Table 4.13 for the project's lifetime O&M costs.

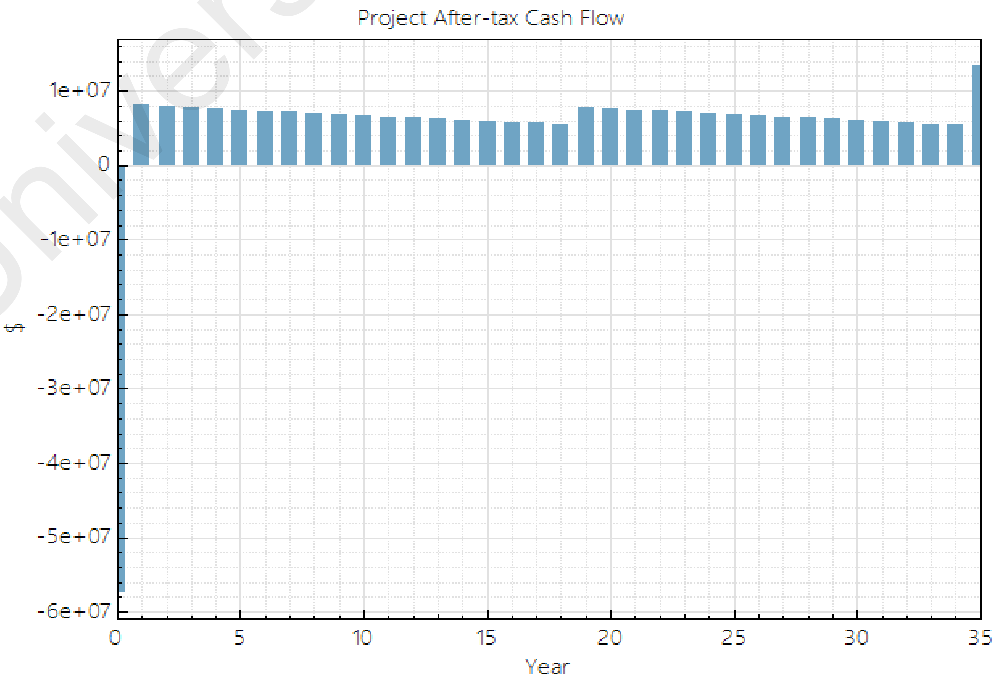

Figure 4.43: Project after-tax cash flow for KLIA CSP plant

Table 4.12: KLIA CSP plant lifetime revenue

Year	Energy production (kWh)	PPA price (cents/kWh)	PPA revenue (USD)	Salvage value (USD)	Total gross revenue (USD)
0	0	0	0	0	0
1	41,145,964	26.3103	11,869,906	0	11,869,906
2	40,734,504	26.3103	11,751,207	0	11,751,207
3	40,327,156	26.3103	11,633,695	0	11,633,695
4	39,923,888	26.3103	11,517,358	0	11,517,358
5	39,524,648	26.3103	11,402,185	0	11,402,185
6	39,129,400	26.3103	11,288,163	0	11,288,163
7	38,738,108	26.3103	11,175,281	0	11,175,281
8	38,350,724	26.3103	11,063,528	0	11,063,528
9	37,967,220	26.3103	10,952,893	0	10,952,893
10	37,587,548	26.3103	10,843,364	0	10,843,364
11	37,211,672	26.3103	10,734,930	0	10,734,930
12	36,839,556	26.3103	10,627,581	0	10,627,581
13	36,471,160	26.3103	10,521,305	0	10,521,305
14	36,106,448	26.3103	10,416,092	0	10,416,092
15	35,745,384	26.3103	10,311,931	0	10,311,931
16	35,387,928	26.3103	10,208,812	0	10,208,812
17	35,034,048	26.3103	10,106,724	0	10,106,724
18	34,683,708	26.3103	10,005,657	0	10,005,657
19	34,336,872	26.3103	9,905,600	0	9,905,600
20	33,993,504	26.3103	9,806,544	0	9,806,544
21	33,653,568	26.3103	9,708,479	0	9,708,479
22	33,317,032	26.3103	9,611,394	0	9,611,394
23	32,983,862	26.3103	9,515,280	0	9,515,280
24	32,654,024	26.3103	9,420,127	0	9,420,127
25	32,327,484	26.3103	9,325,926	0	9,325,926
26	32,004,208	26.3103	9,232,667	0	9,232,667
27	31,684,166	26.3103	9,140,340	0	9,140,340
28	31,367,324	26.3103	9,048,937	0	9,048,937
29	31,053,652	26.3103	8,958,447	0	8,958,447
30	30,743,114	26.3103	8,868,863	0	8,868,863
31	30,435,684	26.3103	8,780,174	0	8,780,174
32	30,131,328	26.3103	8,692,372	0	8,692,372
33	29,830,014	26.3103	8,605,449	0	8,605,449
34	29,531,714	26.3103	8,519,394	0	8,519,394

35	29,236,396	26.3103	8,434,200	8,077,738	16,511,938

Table 4.13: KLIA CSP plant lifetime O&M costs

Year	O&M expenses (USD)	Insurance expenses (USD)	Total operating expenditure (USD)	Net capital cost/debt related costs (USD)	Total net revenue (USD)
0	0	0	0	-81,903,032	0
1	954,835	403,887	1,358,722	-1,719,848	8,791,336
2	978,706	413,984	1,392,690	-1,669,263	8,689,255
3	1,003,174	424,334	1,427,507	-1,615,136	8,591,051
4	1,028,253	434,942	1,463,195	-1,557,221	8,496,942
5	1,053,959	445,816	1,499,775	-1,495,252	8,407,157
6	1,080,308	456,961	1,537,269	-1,428,945	8,321,948
7	1,107,316	468,385	1,575,701	-1,357,997	8,241,583
8	1,134,999	480,095	1,615,094	-1,282,082	8,166,353
9	1,163,374	492,097	1,655,471	-1,200,854	8,096,569
10	1,192,458	504,399	1,696,858	-1,113,939	8,032,568
11	1,222,270	517,009	1,739,279	-1,020,940	7,974,712
12	1,252,827	529,935	1,782,761	-921,431	7,923,389
13	1,284,147	543,183	1,827,330	-814,957	7,879,019
14	1,316,251	556,763	1,873,013	-701,029	7,842,050
15	1,349,157	570,682	1,919,839	-579,127	7,812,966
16	1,382,886	584,949	1,967,835	-448,691	7,792,286
17	1,417,458	599,572	2,017,031	-309,125	7,780,568
18	1,452,895	614,562	2,067,456	-159,789	7,778,411
19	1,489,217	629,926	2,119,143	0	7,786,458
20	1,526,448	645,674	2,172,121	0	7,634,423
21	1,564,609	661,816	2,226,425	0	7,482,055
22	1,603,724	678,361	2,282,085	0	7,329,309
23	1,643,817	695,320	2,339,137	0	7,176,143
24	1,684,912	712,703	2,397,616	0	7,022,512
25	1,727,035	730,521	2,457,556	0	6,868,370
26	1,770,211	748,784	2,518,995	0	6,713,672
27	1,814,466	767,503	2,581,970	0	6,558,370
28	1,859,828	786,691	2,646,519	0	6,402,418
29	1,906,324	806,358	2,712,682	0	6,245,765
30	1,953,982	826,517	2,780,499	0	6,088,364

31	2,002,831	847,180	2,850,012	0	5,930,163
32	2,052,902	868,360	2,921,262	0	5,771,111
33	2,104,225	890,069	2,994,293	0	5,611,156
34	2,156,830	912,320	3,069,151	0	5,450,244
35	2,210,751	935,128	3,145,879	0	13,366,059

The calculations for the net capital cost in Table 4.13 include the total installed cost, debt closing costs and debt upfront fee only. The value does not take into account the cost of acquiring financing, construction financing and reserve accounts; All the parameters and values for these factors were set to zero.

4.3.2 SAM Simulation for Gaya Island CSP Plant

The SAM performance and financials simulation for the Gaya Island CSP plant is mostly similar to the simulation for the KLIA CSP plant, with the exception of the DNI values, the imported optimized values from SolarPILOT and the water source/cost.

4.3.2.1 Gaya CSP Performance Simulation Results

Figure 4.44 below shows the design parameters for the Gaya Island CSP plant in SAM. The design point DNI is set to 780 W/m^2 with the other parameters remain unchanged. The receiver thermal power of 100 MWt was found to have a design turbine gross output of 13.7 MWe.

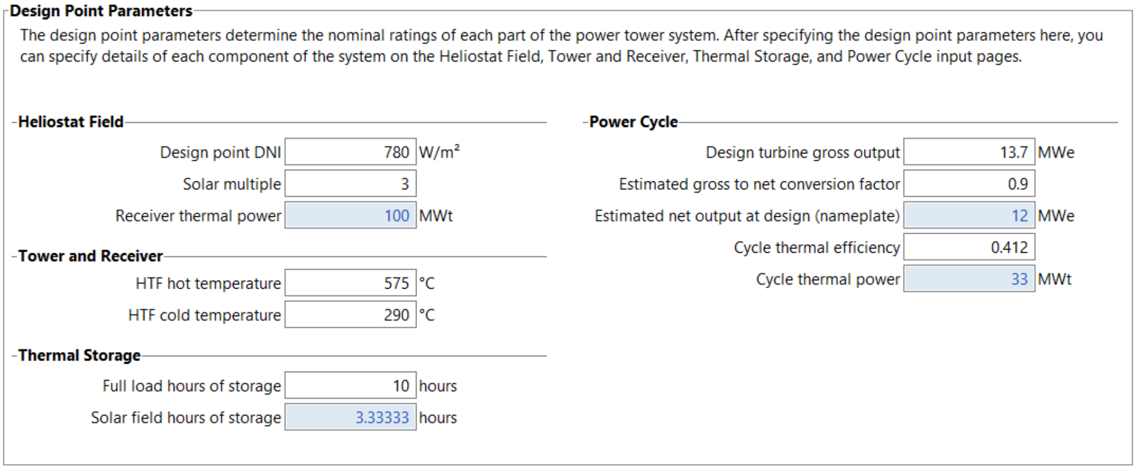

Figure 4.44: SAM design parameters for Gaya Island CSP plant

Figure 4.45 shows the overlay of the Gaya Island CSP plant on the image of the actual location. The plant arrangement as well as the position of each components at the center of the solar field is identical to the KLIA CSP plant.

Figure 4.45: Gaya Island CSP plant overlay on the CSP location

Figure 4.46 shows the heliostat layout generated by SAM based on the imported heliostat positions from SolarPILOT. The optimization settings were not used as the optimization was already done in SolarPILOT.

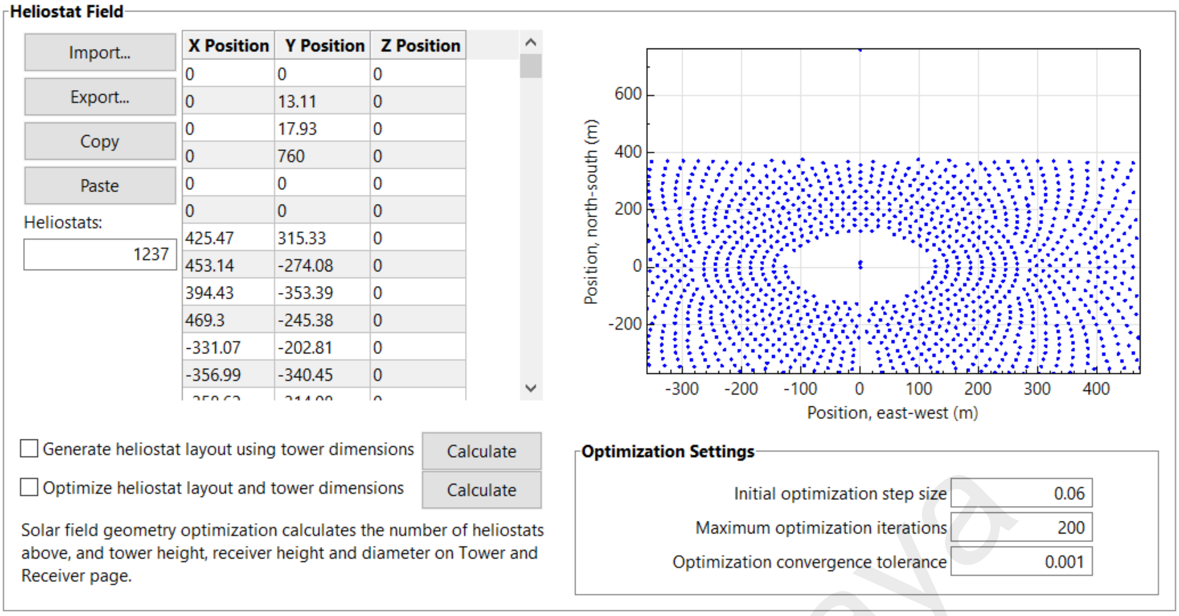

Figure 4.46: SAM heliostat layout for Gaya Island CSP plant

Figure 4.47 shows the heliostat operation parameters and properties. Dimensions for the heliostats are identical to the optimized values from SolarPILOT. The atmospheric attenuation values are the default values recommended by SAM.

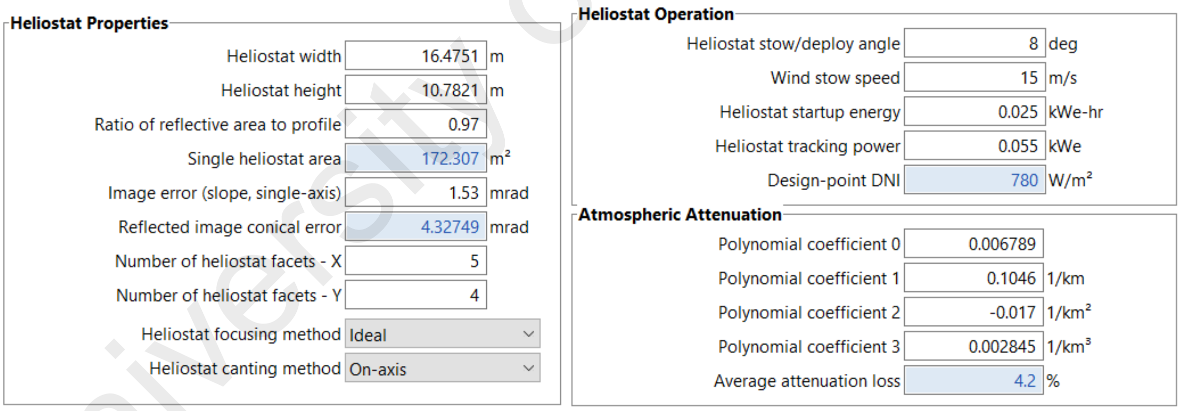

Figure 4.47: SAM heliostat properties, heliostat operation and atmospheric attenuation for Gaya Island CSP plant

Figure 4.48 shows the land area, layout constraints, heliostat field availability and washing frequency for the heliostats. The non-solar field land area was set at 35 acres which brought the total land area to 223 acres. The total heliostat reflective area was found to be 213,144 m^2. The solar field layout constraints and heliostat field availability were identical to the values in SolarPILOT. It is expected that heliostat mirror washing occur twice a week, which totals up to 104 times a year.

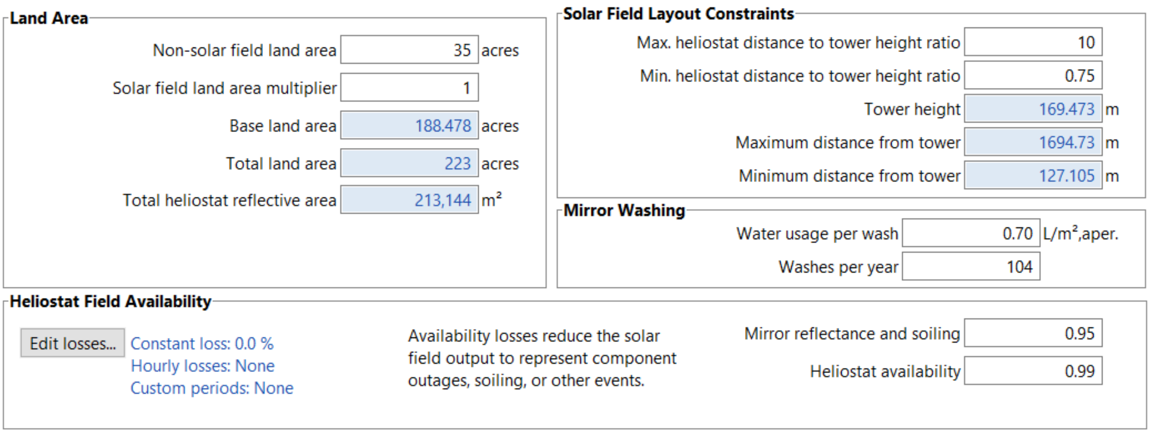

Figure 4.48: SAM land area, field layout constraints, washing frequency and heliostat availability for Gaya Island CSP plant

Figure 4.49 shows the tower and receiver parameters and dimensions which are identical to the optimized values in SolarPILOT. The receiver heat transfer properties, design, and operation, HTF type, flow type, piping loses, and receiver flux modelling parameters were selected based on the recommended values and selections by SAM.

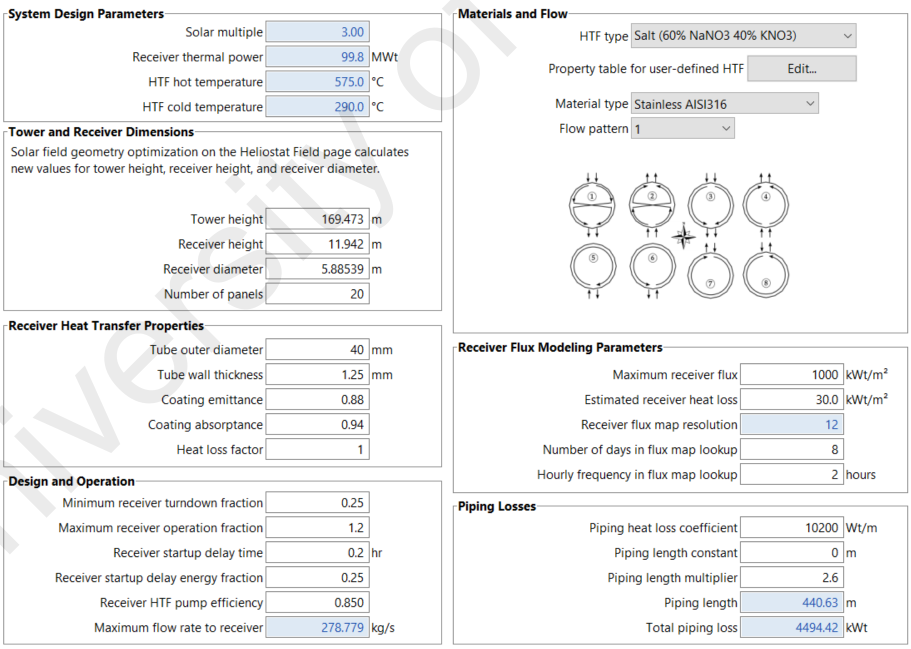

Figure 4.49: SAM tower, receiver and HTF properties and parameters for Gaya Island CSP plant

Figure 4.50 shows the power cycle design parameters. Similar to the KLIA CSP plant, Rankine cycle was selected for the operation of the power cycle. The hybrid condenser operation was also selected which allows for a cooling combination between a cooling tower and the conventional air-cooling method. During actual operation, air-cooling will be used full time while the cooling tower will be used during peak operations which generate high heat and high temperatures. All other parameter values were in accordance with the recommended SAM values.

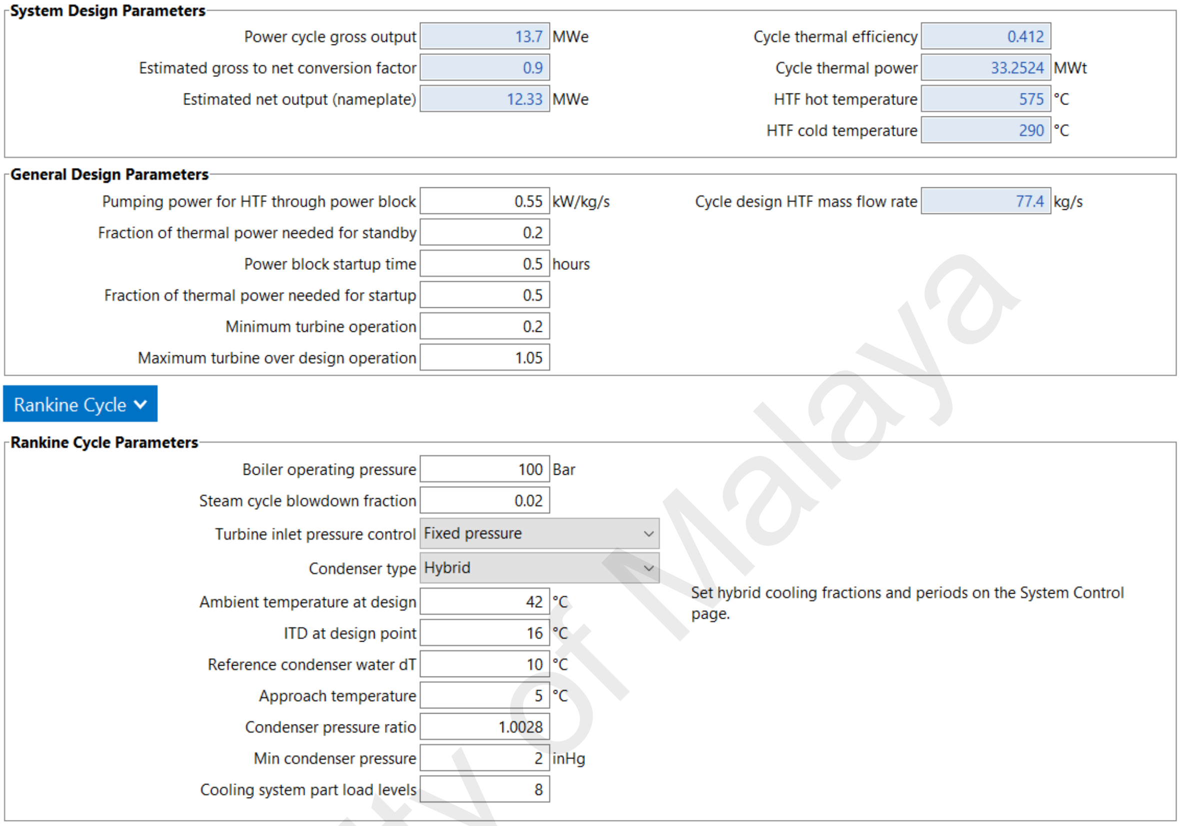

Figure 4.50: Power cycle parameters for Gaya Island CSP plant

The thermal storage parameters for the Gaya Island CSP plant is identical to the KLIA CSP plant. All parameters were set in accordance with the recommended values by SAM. The plant energy consumption was set to 0.0055 MWe/MWcap which was the default value recommended by SAM.

Similar to the KLIA CSP plant, heliostat mirror washing was expected to occur twice a month. The total heliostat reflective area is 213,144 m^2 which requires approximately 149 m^3, based on 0.7 litre per m^2 of water usage. Table 4.14 below shows the breakdown of the monthly water consumption based on the number of washes for each month and the total water consumption for each month.

Table 4.14: Monthly water consumption for heliostat mirror washing for Gaya Island CSP Plant

Month	Number of washes	Total water consumption (m^3)
January	8	1192
February	8	1192
March	8	1192
April	10	1490
May	8	1192
June	8	1192
July	10	1490
August	8	1192
September	8	1192
October	10	1490
November	8	1192
December	10	1490
TOTAL	104	15,496

The water consumption related to the steam cycle makeup and hybrid cooling was simulated by SAM on an hourly basis for the whole year in kg/s, which were manually converted to kg/h for easier conversion and calculations. The weight of 1 m^3 of water volume was assumed to be 1000 kg. Thus, the monthly water consumption was calculated and tabulated in Table 4.15 below.

Table 4.15: Monthly water consumption for steam cycle makeup and hybrid cooling for Gaya Island CSP Plant

Month	Total water consumption (kg/h)	Total water consumption (m^3)
January	334059	334
February	432912	433
March	442938	443
April	388752	389
May	428753	429
June	270604	271
July	308904	309
August	324773	325
September	321849	322
October	360919	361
November	300073	300
December	256115	256
TOTAL	4170651	4171

The total water consumption for the heliostat washing activities, steam makeup and hybrid cooling for the CSP plant is as shown in Table 4.16 and Figure 4.51.

Table 4.16: Total combined monthly water consumption for Gaya Island CSP plant

Month	Heliostat washing (m^3)	Steam makeup and cooling (m^3)	Total water consumption (m^3)
January	1192	334	1526
February	1192	433	1625
March	1192	443	1635
April	1490	389	1879
May	1192	429	1621

June	1192	271	1463
July	1490	309	1799
August	1192	325	1517
September	1192	322	1514
October	1490	361	1851
November	1192	300	1492
December	1490	256	1746
TOTAL	15,496	4171	19,667

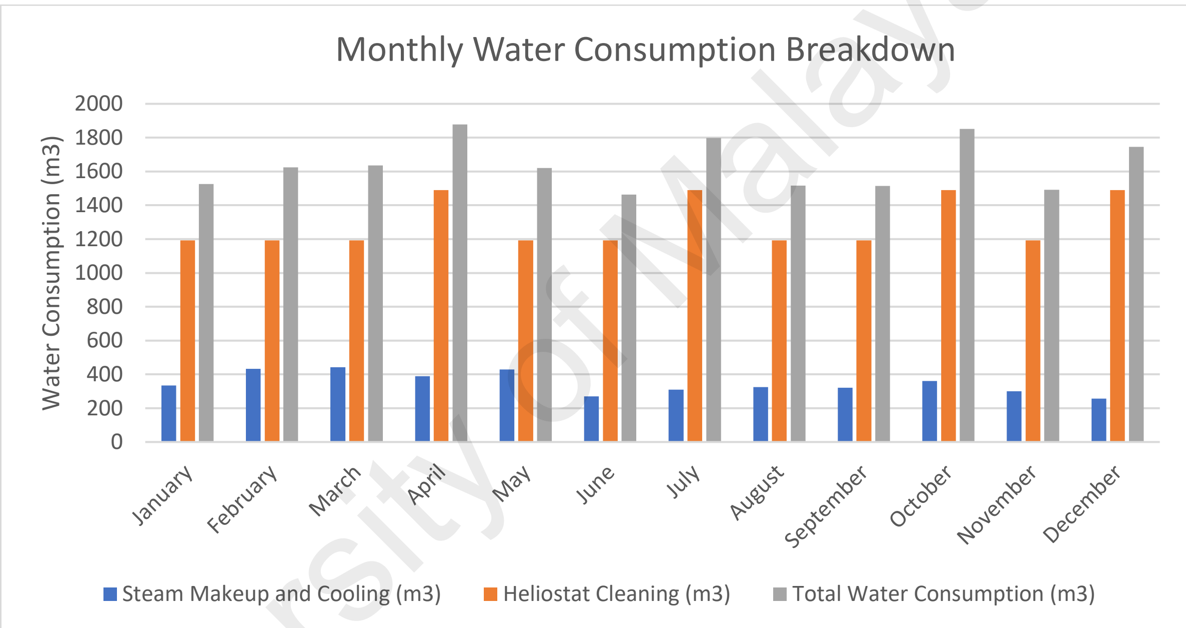

Figure 4.51: Monthly water consumption breakdown for Gaya Island CSP plant

Based on Table 4.16 and Figure 4.51, it can be seen that the steam makeup and cooling water consumption is normally distributed with its peak occurring in March whereas April has the highest total monthly water consumption. The annual water consumption from heliostat cleaning is 79% of the total annual water consumption which is significantly higher than the water consumption by steam makeup and cooling.

The energy production during the 1st year of operation are shown in Table 4.17 below. March has the highest energy production with 6,204,530 kWh. Similar to the KLIA CSP plant, a performance degradation of 1% a year was selected and the lifetime for a CSP plant was selected to be 35 years. Figure 4.52 below shows the annual energy production considering the 1% annual performance degradation.

Table 4.17: Energy production during 1st year of operation for Gaya Island CSP plant

Month	Energy Production (kWh)
January	4,654,170
February	6,072,200
March	6,204,530
April	5,425,670
May	5,990,430
June	3,720,820
July	4,271,910
August	4,4951,70
September	4,447,540
October	5,024,900
November	4,165,770
December	3,526,630
TOTAL	57,999,736

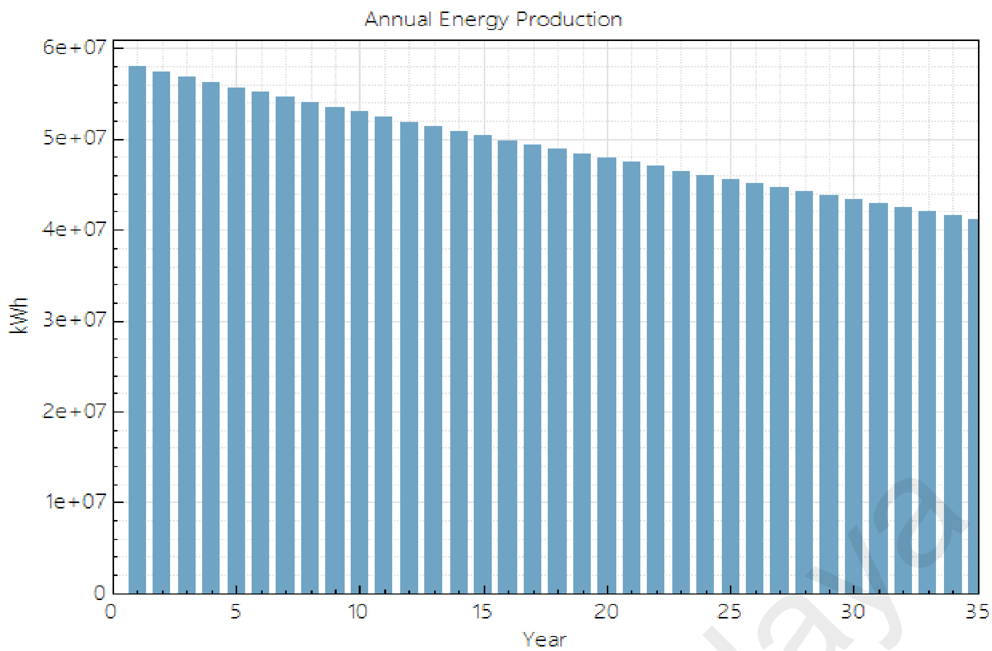

Figure 4.52: Annual Energy Production with 1% degradation for Gaya Island CSP plant

In year 35, the CSP plant experiences a production loss of approximately 1,000,000 kWh every month due to degradation.

For the Gaya Island CSP plant, water is obtained through the desalination of sea water instead. As mentioned previously, desalination of water through reverse osmosis consumes 4 kWh/m^3. Based on the total water consumption tabulated in Table 4.16, the monthly power consumption of the desalination facility was calculated and shown in Table 4.18.

Table 4.18: Desalination facility power consumption

Month	Water consumption (m^3)	Power consumption (kWh)
January	1526	6104
February	1625	6500
March	1635	6540
April	1879	7516
May	1621	6484
June	1463	5852
July	1799	7196

August	1517	6068
September	1514	6056
October	1851	7404
November	1492	5968
December	1746	6984
TOTAL	19,667	78,668

Similar to the KLIA CSP plant, a CO_2 gas emission index of 170 gCO2eq/kWh was taken. By multiplying this number with the energy produced by the CSP plant, the reduction in CO_2 gas emissions was found. The approximated reduction in emission by utilizing the designed CSP plant in the first year instead of combined cycle gas turbine process is shown in Table 4.19. The total amount of CO_2 emissions reduced is 9859.96 ton CO_2.

Table 4.19: Monthly CO_2 emission reduction for Gaya Island CSP plant

Month	Energy production (kWh)	CO_2 emission reduction (tonCO_2)
January	4,654,170	791.21
February	6,072,200	1032.27
March	6,204,530	1054.77
April	5,425,670	922.36
May	5,990,430	1018.37
June	3,720,820	632.54
July	4,271,910	726.22
August	4,4951,70	764.18
September	4,447,540	756.08
October	5,024,900	854.23
November	4,165,770	708.18
December	3,526,630	599.53
TOTAL	57,999,736	9859.96

4.3.2.2 Gaya CSP Financial Simulation Results

Similar to the KLIA CSP plant, the current O&M fixed cost was estimated to be USD 77.44/kW-yr. The contingency cost was set to 7% of the subtotal cost, which is USD 5,059,891. The total direct cost totaled up to USD 77,344,048. The indirect capital cost was not considered as Gaya Island is part of the Tunku Abdul Rahman Park and any usage of such land size would have to be through an agreement with the local authorities. The installation cost for a reverse osmosis desalination facility is approximately USD 1,000,000 per 1000 m^3/day of capacity. The highest daily water consumption occurs in August with a value of 0.97 m^3 and, assuming heliostat washing occurs on the same day as well, the required capacity is 149.97 m^3/day. A capacity value of 200 m^3/day was selected as a safety measure. Thus, the installation cost for the desalination facility is USD 200,000. As there were no options to include additional cost in SAM, the installation cost for the facility was added to the "Heliostat cost fixed" column instead, which does not alter the value of the other parameters and costs. By adding the direct capital costs and desalination facility cost, the total installed cost was found to be USD 77,344,048. The estimated total installed cost per net capacity was found to be USD 6,272.83. Figure 4.53 below shows the breakdown for the direct capital costs and the total installed cost for the CSP plant. Figure 4.54 shows the operation and maintenance cost for the CSP plant.

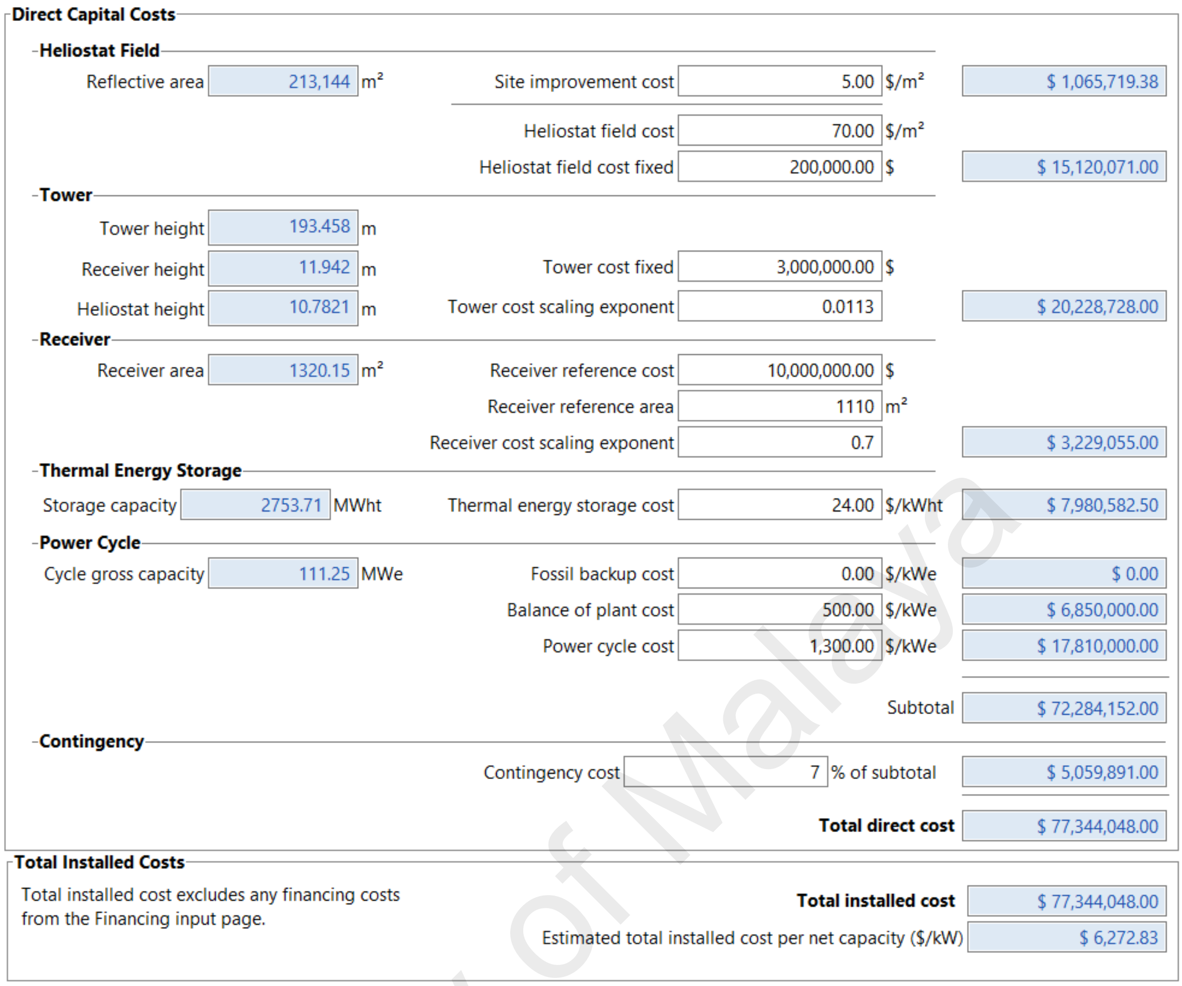

Figure 4.53: Direct capital costs and total installed cost for Gaya Island CSP plant

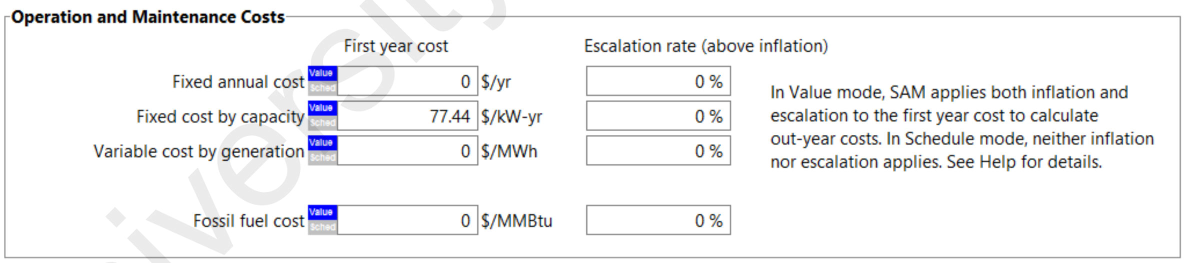

Figure 4.54: Operation and maintenance cost for Gaya Island CSP plant

An IRR target of 11% and a target year of year 20 was selected for this CSP project. At year 20, it is expected that the total installed cost has been paid and the CSP plant will start making a profit.

The analysis period of the project is 35 years. The inflation rate was set at 2.5% per year and the real discount rate to be 8% per year. The annual insurance rate was set at 0.5% of the installed cost. Lastly, the net salvage value of the plant when decommissioned was set at 10% of the installed cost with the end of analysis period value of USD 7,734,405. Project and property tax are not included in this paper. Figure 4.55 salvage value of the CSP plant.

Figure 4.55: Financial parameters for Gaya Island CSP plant

The project term debt and solution mode for revenue calculations are identical to the KLIA CSP plant.

4.3.2.3 Summary of Results and Cash Flow for Gaya Island CSP Plant

Table 4.20 shows the summary of results which includes both the performance and financial metrics. The capacity factor of the plant in year 1 was found to be 53.7%. The nominal LCOE and real LCOE was found to be 19.44 cents/kWh and 15.65 cents/kWh respectively after factoring in the power consumption of the desalination facility. The net present value of the project was found to be a positive value of USD 7,304,002.

Table 4.20: Summary of results for Gaya Island CSP plant

Metric	Value
Annual energy (year 1)	57,999,736 kWh
Capacity factor (year 1)	53.7%
Annual water usage	19,688 m^3
PPA price (year 1)	19.67 cents/kWh (with desalination cost)
Levelized COE (nominal)	19.44 cents/kWh (with desalination cost)
Levelized COE (real)	15.65 cents/kWh (with desalination cost)
Net present value	USD 7,304,002
Internal rate of return (IRR)	11.00%
Year IRR is achieved	20
IRR at end of project	12.36%
Net capital cost	USD 78,225,360

Equity	USD 54,759,336
Size of Debt	USD 23,466,024

The project after-tax cash flow is shown in Figure 4.56. The cash flow trend is identical to the KLIA CSP plant with Year 0 having a negative cash flow. The remaining years show a gradual decline in revenue and in year 35, the salvage value was added to the revenue. The details of the project cash flow were tabulated in Table 4.21 for the project's lifetime revenue and Table 4.22 for the project's lifetime O&M costs. The energy consumption by the desalination facility was subtracted from the annual energy production to reflect the actual amount of energy available for sale.

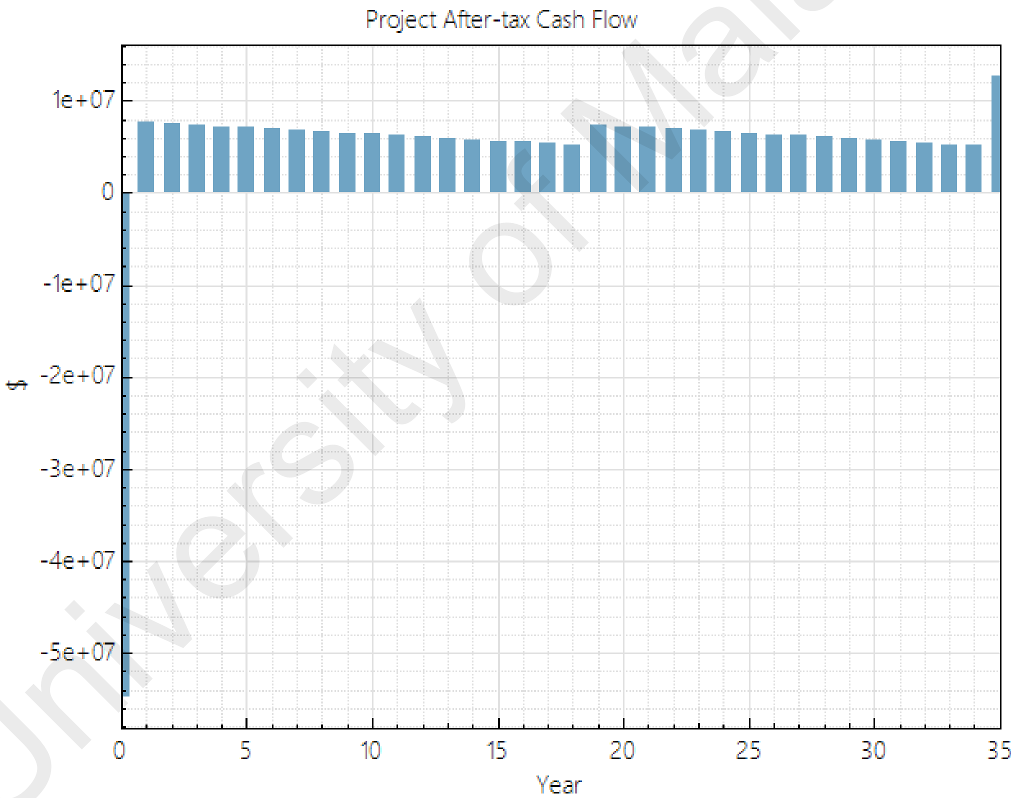

Figure 4.56: Project after-tax cash flow for Gaya Island CSP plant

Table 4.21: Gaya Island CSP plant lifetime revenue

Year	Energy production – desali. (kWh)	PPA price (cents/kWh)	PPA revenue (USD)	Salvage value (USD)	Total gross revenue (USD)
0	0	0	0	0	0
1	57,921,068	19.67	11,390,460	0	11,390,460

2	57,341,072	19.67	11,276,555	0	11,276,555
3	56,766,872	19.67	11,163,790	0	11,163,790
4	56,198,416	19.67	11,052,152	0	11,052,152
5	55,635,648	19.67	10,941,630	0	10,941,630
6	55,078,504	19.67	10,832,214	0	10,832,214
7	54,526,932	19.67	10,723,892	0	10,723,892
8	53,980,876	19.67	10,616,653	0	10,616,653
9	53,440,280	19.67	10,510,486	0	10,510,486
10	52,905,092	19.67	10,405,382	0	10,405,382
11	52,375,252	19.67	10,301,328	0	10,301,328
12	51,850,712	19.67	10,198,314	0	10,198,314
13	51,331,420	19.67	10,096,331	0	10,096,331
14	50,817,320	19.67	9,995,368	0	9,995,368
15	50,308,360	19.67	9,895,414	0	9,895,414
16	49,804,488	19.67	9,796,460	0	9,796,460
17	49,305,656	19.67	9,698,496	0	9,698,496
18	48,811,816	19.67	9,601,511	0	9,601,511
19	48,322,908	19.67	9,505,496	0	9,505,496
20	47,838,892	19.67	9,410,441	0	9,410,441
21	47,359,720	19.67	9,316,336	0	9,316,336
22	46,885,336	19.67	9,223,173	0	9,223,173
23	46,415,696	19.67	9,130,941	0	9,130,941
24	45,950,752	19.67	9,039,632	0	9,039,632
25	45,490,456	19.67	8,949,235	0	8,949,235
26	45,034,764	19.67	8,859,743	0	8,859,743
27	44,583,632	19.67	8,771,146	0	8,771,146
28	44,137,008	19.67	8,683,434	0	8,683,434
29	43,694,852	19.67	8,596,600	0	8,596,600
30	43,257,116	19.67	8,510,634	0	8,510,634
31	42,823,756	19.67	8,425,527	0	8,425,527
32	42,394,732	19.67	8,341,272	0	8,341,272
33	41,970,000	19.67	8,257,860	0	8,257,860
34	41,549,512	19.67	8,175,281	0	8,175,281
35	41,133,232	19.67	8,093,528	7,713,005	15,806,533

Table 4.22: Gaya Island CSP plant lifetime O&M costs

Year	O&M expenses (USD)	Insurance expenses (USD)	Total operating	Total installed cost/debt	Total net revenue (USD)

			expenditure (USD)	related costs (USD)	
0	0	0	0	-78,225,364	0
1	954,835	385,650	1,340,485	-1,642,622	8,407,353
2	978,706	395,292	1,373,998	-1,594,308	8,308,250
3	1,003,174	405,174	1,408,348	-1,542,612	8,212,830
4	1,028,253	415,303	1,443,556	-1,487,298	8,121,298
5	1053959	425686	1479645	-1,428,111	8,033,874
6	1,080,308	436,328	1,516,636	-1,364,782	7,950,796
7	1,107,316	447,236	1,554,552	-1,297,019	7,872,321
8	1,134,999	458,417	1,593,416	-1,224,513	7,798,724
9	1,163,374	469,877	1,633,251	-1,146,932	7,730,303
10	1,192,458	481,624	1,674,083	-1,063,920	7,667,379
11	1,222,270	493,665	1,715,935	-975,097	7,610,296
12	1,252,827	506,007	1,758,833	-880,056	7,559,425
13	1,284,147	518,657	1,802,804	-778,363	7,515,165
14	1,316,251	531,623	1,847,874	-669,551	7,477,943
15	1,349,157	544,914	1,894,071	-553,122	7,448,221
16	1,382,886	558,537	1,941,423	-428,544	7,426,494
17	1,417,458	572,500	1,989,958	-295,244	7,413,293
18	1,452,895	586,812	2,039,707	-152,614	7,409,189
19	1,489,217	601,483	2,090,700	0	7,414,796
20	1,526,448	616,520	2,142,967	0	7,267,474
21	1,564,609	631,933	2,196,542	0	7,119,795
22	1,603,724	647,731	2,251,455	0	6,971,718
23	1,643,817	663,924	2,307,742	0	6,823,200
24	1,684,912	680,523	2,365,435	0	6,674,197
25	1,727,035	697,536	2,424,571	0	6,524,665
26	1,770,211	714,974	2,485,185	0	6,374,558
27	1,814,466	732,848	2,547,315	0	6,223,831
28	1,859,828	751,170	2,610,998	0	6,072,437
29	1,906,324	769,949	2,676,273	0	5,920,328
30	1,953,982	789,198	2,743,179	0	5,767,455
31	2,002,831	808,927	2,811,759	0	5,613,769
32	2,052,902	829,151	2,882,053	0	5,459,220
33	2,104,225	849,879	2,954,104	0	5,303,756
34	2,156,830	871,126	3,027,957	0	5,147,324
35	2,210,751	892,905	3,103,656	0	12,702,877

CHAPTER 5: DISCUSSION

In this chapter, the results for both the KLIA and Gaya Island will be compared to each other as well as other studies and data regarding solar tower power plants. The feasibility of each plant will also be analyzed.

As mentioned previously, both CSP plants were restricted to the identical land boundary size, solar field design power, HTF parameters, power cycle parameters and financial parameters for an accurate comparison between both CSP plants. Based on the SolarPILOT results, it can be seen that the KLIA plant has a higher value for power absorbed by the receiver and HTF with 115,203kW and 106,140kW respectively in comparison with 110,910kW and 102,557kW from the Gaya plant. The KLIA plant also has a higher solar field optical efficiency of 70.15% compared to the Gaya plant with 66.06%. This is an anomaly as the design-point DNI for Gaya Island is higher at 780 W/m^2 as compared to 660 W/m^2 for KLIA and the power incident on field is 178,597kW and 174,716kW for Gaya Island and KLIA, respectively. A possible reason for this occurrence is due to the heliostats size difference. The KLIA plant utilizes larger heliostats which combined for a total simulated heliostat area of 213851 m^2 as compared to the Gaya plant's value of 212110 m^2. However, the rough total cost of USD 88,344,823,34 for the Gaya plant is lower than the total cost KLIA plant, which is USD 92,797,035.44. This is mainly due to the fact that the Gaya plant requires smaller heliostats, a slightly smaller receiver, and a lower solar tower due to the higher design-point DNI input. A high design-point DNI generally translates to a smaller equipment as there is more solar irradiation per unit area.

The SAM simulation gives a more detailed outlook on the performance and financial characteristics of both CSP plants. It was found that the Gaya plant generates a total of 57,999,736 kWh in its first year of operation, which is 29% higher than KLIA plant's value of 41,145,964 kWh. The higher energy production also resulted in a higher CO2 reduction and higher water consumption for the Gaya plant. The higher water consumption for the Gaya plant is due to the higher temperatures and higher rate of energy generation. The capacity factor for the Gaya plant is higher at 53.7% as compared to 38.1% for the KLIA plant which is due to the higher DNI values for Gaya Island. With a net capital cost of USD 81,903,032 and USD 78,225,360 for the KLIA and Gaya Island CSP plants respectively and an IRR target year of 20 years, the PPA price for the KLIA plant is significantly higher at 26.31 cents/kWh compared to 19.67 cents/kWh for the Gaya plant. With a real discount rate of 5.5%, the KLIA plant has a nominal and real LCOE value of 26.61 cents/kWh and 21.06 cents/kWh while the values for the Gaya plant are 19.44 cents/kWh and 15.65 cents/kWh. Do note that the values for the Gaya plant were adjusted to reflect the remaining available energy after subtracting the energy consumption for the desalination facility. It was also found that the cost for water for the KLIA plant, which obtains its water from Air Selangor, is higher over 35 years compared to the Gaya plant's desalination facility's cost. However, the calculation for the cost of the desalination facility did not include the cost of the energy consumed. The net present value for the KLIA and Gaya plant are USD 7,701,224 and USD 7,304,002 respectively, which a nearly identical end of project IRR value of 12.37% and 12.36% respectively. A positive net present value usually indicates that a project is economically feasible, however it is not the only determining factor.

When compared to the study done by the researchers at UTM Malaysia on CST (Rafeq et al., 2013), it was found that the average cosine efficiency obtained from the SolarPILOT simulation for the KLIA CSP plant (84.63%) and Gaya Island CSP plant (82.38%) are 21% and 19% higher than the average Malaysia value of 63%. However, these values are nearly identical to the average cosine efficiency value of 85% for Aswan, Egypt. The total optical efficiency values show the same trend with the KLIA plant (70.15%) and Gaya plant (66.06%) having efficiency values similar to Aswan at 70% as compared to the Malaysian average of 52%.

In another study, done by researchers from Macquarie University, Sunway University and American University of Ras Al Khaimah (Islam, Huda, & Saidur, 2019), it was mentioned that the national average of a SPT plant's unit cost of energy or electricity is 0.78 RM/kWh with a discount rate of 8%. By converting the nominal LCOE values using the 1 USD to 4.35 RM conversion rate, it was found that both the KLIA plant and Gaya plant exceed the average value with a LCOE of RM 0.92kWh and RM 0.68/kWh, respectively. It was also mentioned that the present FiT system provides electricity producer with RM 0.95/kWh for plants with a generation capacity of over 10 MW. By converting the PPA price for both plants, it was found that the KLIA plant exceeds this value with a PPA price of RM 1.14/kWh while the Gaya plant has a PPA price of RM 0.86/kWh. In the study, only Labuan, Sabah has a positive NPV, which is a large contrast compared to the NPV values obtained from the SAM simulation which were positive for both CSP plants. Another location included in the study is Kota Kinabalu, which is essentially the same location as Gaya Island. The values for annual electricity generation and LCOE for Kota Kinabalu in the study are 23.53 GWh and RM 0.90/kWh, respectively. The Gaya plant has a simulated annual electricity generation of 57.9 GWh which is more than double the value stated in the study.

The installed cost per net capacity of USD 6,551.29/kW for the KLIA plant and USD 6,272.83/kW is considered towards the lower end for current towers with TES. The LCOE value for the KLIA plant is on the high end as it is above the usual range of 17-24 cents/kWh whereas the LCOE for Gaya plant is towards the low end and well within the expected range.

In comparison to the solar PV farms such as the SunEdison Inc./MAHB solar farm in KLIA with a LCOE value of RM 0.10/kWh, the LSS2 bidding prices of RM 0.33 – 9.53/kWh and the LSS3 bidding prices of RM 0.24 – 0.32/kWh, it can be seen that the LCOE for both the KLIA and Gaya CSP plants are much higher. Besides the LCOE, the maintenance cost of solar PV panels is also much lower, at a rate of RM 33.75/kW per year compared to RM 336.86/kW per year for both CSP plants. However, despite the low cost of PV electricity in comparison to CSP, the weather and high humidity climate in Malaysia would become a major concern in maintaining a constant output. The long-term degradation factor of the solar PV panels also needs to be taken into consideration during the design stage. The fact that CSP relies on mirror would render the maintenance easier to handle and conduct.

CHAPTER 6: CONCLUSION

The feasibility study on Concentrated Solar Power (CSP) plants in Malaysia was performed based on climate data obtained from the Solcast API Toolkit, which included parameters such as GHI, DNI, DHI, normal and dewpoint temperature, relative humidity, atmospheric pressure, wind speed and direction and albedo. This study focused only on the solar tower technology (SPT) and the study was done with the SolarPILOT and SAM simulation software for two selected locations, namely KLIA and Gaya Island. The KLIA and Gaya CSP plants were compared based on performance and financial metrices such as optical efficiency, annual energy production, water consumption, capacity factor, PPA price, net capital cost, net present value and levelized cost of energy (LCOE) values. With a land area of 620,156 m^2, a thermal power rating of 100 MWt, and a 10-hour thermal storage, the KLIA and Gaya CSP plant both has a capacity of 13.7 MWe and produce an annual value of 41,145,964 kWh and 57,999,736 kWh of electrical energy respectively. The capacity factor for the KLIA and Gaya plant are 38.1% and 53.7% respectively. The cosine efficiency and optical efficiency for both plants were found to be above the Malaysian average found in another study (Rafeq et al., 2013) and on par with the Aswan averages. The water consumption for the KLIA and Gaya plant are 18,649 m^3 and 19,667 m^3 respectively. The KLIA plant obtains water from the Selangor state's water supplier, Air Selangor, and the total 35-year cost for water usage is USD 342,646.69. The Gaya plant uses a reverse osmosis desalination facility instead, which costs USD 200,000 to install and consumes 78,668 kWh annually. Based on these results, it can be said that a solar tower CSP plant is feasible in the Malaysian environment in terms of performance.

With a 8% discount rate, 11% IRR target with a target year of 20 years, a 35 year lifespan and a salvage value that is 10% of the installed cost, this study showed that the KLIA plant requires a PPA price that exceeds the government's FiT rate of 0.95 RM/kWh to meet the 20 year IRR target while the Gaya plant has a PPA price 9 sens below the stated FiT rate. The LCOE values for both plants exceeded the national average value of 0.78 RM/kWh stated in another study (Islam et al., 2019). It was also found that the installed cost per net capacity for both plants are within the expected range for current solar tower CSP systems. The net capital cost for the KLIA and Gaya plant were found to be USD 81,903,032 and USD 78,225,360 while the net present value for both plants are USD 7,701,224 and USD 7,304,002, respectively. Based on the values for the net present value, it can be said that both CSP plants are economically feasible, provided the PPA price is equal or more than the simulated values.

However, as shown in a previous study (Islam et al., 2019), the parabolic trough collector (PTC) is superior to the solar tower technology in many parameters, such as the capacity factor, annual energy generation, unit cost of electricity, net present value, and IRR. Improvements in photovoltaic (PV) technology which allows for an increased in efficiency at a lower cost for PV panels might also be a viable option compared to the more expensive solar tower CSP plants. As an example, the SunEdison solar power system installed in KLIA cost RM 200 million and has a capacity of 19MW while the simulated KLIA and Gaya plant cost RM 368,563,644 (USD 81,903,032) and RM 352,014,120 (USD 78,225,360) respectively with a 13.7 MWe capacity. The simulated LCOE and maintenance cost for both CSP plants are also much higher compared to solar PV farms. Another disadvantage of a solar tower CSP plant when compared to solar PV energy farms, is that the operation of a CSP plant requires a team of people and the maintenance cost is very high while a solar PV energy farm requires minimal staff and maintenance activities. However, the weather and high humidity climate in Malaysia would become a major concern in maintaining a constant output for a solar PV farm. The long-term degradation factor of the solar PV panels also needs to be taken into consideration during the design stage. The fact that CSP relies on mirror would render the maintenance easier to handle and conduct. Besides that, a solar tower CSP plant, or any other CSP technology, have the edge of having 24-hour power generation due to thermal storage.

As such, the solar power tower CSP plant is feasible to be implemented in Malaysia, provided the PPA price required is agreed upon. However, it may not be the best option for clean and renewable energy due to the higher cost and labor requirements compared to technologies such as the solar PV panels.

CHAPTER 7: FUTURE RECOMMENDATIONS

In this study, financial parameters such as taxes, construction financing, reserve accounts, and depreciation were not considered. As such, future studies could focus on the financial aspects of a CSP plant in detail which includes the aforementioned parameters. This study is also done based on the cost of components in the USA or Europe, which might not reflect the actual cost of the components in the Malaysian market. Future studies could be done on the costs for each components of a solar tower CSP plant in the Malaysian market and to compare the different variations of each component. Future studies should also be done on land availability, exact land cost and site preparation as these factors were not considered or is only an approximation in this study.

CHAPTER 8: REFERENCES

Affandi, R., Gan, C. K., & Ab Ghani, M. R. (2014). Prospective of implementing concentrating solar power (CSP) in Malaysia environment. *World Applied Sciences Journal*. https://doi.org/10.5829/idosi.wasj.2014.32.08.895

Aichmayer, L. (2011). *Solar Receiver Design and Verification for Small Scale Polygeneration Unit*.

Ali, M. H., Chakrabarty, C. K., Abdalla, A. N., Gamil, A. M., Gilani, S. I., & Al - Kayiem, H. H. (2013). *Simulation and Evaluation of Small Scale Solar Power Tower Performance under Malaysia Weather Conditions* . https://doi.org/10.1088/1755-1315/16/1/012031

ASEAN Centre for Energy. (2015). The 4th ASEAN Energy Outlook 2013-2035. In *ACE*. Retrieved from https://aseanenergy.sharepoint.com/PublicationLibrary/Forms/AllItems.aspx?id=%2FPublicationLibrary%2F2015%2FACE

ASEAN Centre for Energy. (2017). The 5th ASEAN Energy Outlook 2015 - 2040. *ACE*, *66*, 142. Retrieved from https://aseanenergy.sharepoint.com/PublicationLibrary/Forms/AllItems.aspx?id=%2FPublicationLibrary%2F2017%2FACE

Ávila-Marín, A. L. (2011). Volumetric receivers in Solar Thermal Power Plants with Central Receiver System technology: A review. *Solar Energy*, *85*(5), 891–910. https://doi.org/10.1016/j.solener.2011.02.002

Azhari, A. W., Sopian, K., Zaharim, A., & Al Ghoul, M. (2008). A new approach for predicting solar radiation in tropical environment using satellite images - Case study of Malaysia. *WSEAS Transactions on Environment and Development*.

Aziz, H., Said, S., Won, P., On, S., Salamun, H., & Yaakob, R. (2017). The Change of Malaysian Standard Time: A Motion and Debate in the Malaysian Parliament. *International Journal of Academic Research in Business and Social Sciences*, *7*(12). https://doi.org/10.6007/IJARBSS/v7-i12/3725

Bellini, E. (2020). Five bidders set to secure 490 MW in Malaysia's third solar auction – pv magazine International. Retrieved August 12, 2020, from https://www.pv-magazine.com/2020/01/09/five-bidders-set-to-secure-490-mw-in-malaysias-third-solar-auction/

Bergman, T. L., Lavine, A. S., Incropera, F. P., & Dewitt, D. P. (2011). Fundamentals of Heat and Mass Transfer. 7th Edition. In *R. R. Donnelley (Jefferson City)*. https://doi.org/10.1007/s13398-014-0173-7.2

Bienert, W. B. (1980). The heat pipe and its application to solar receivers. *Electric Power Systems Research*, *3*(1–2), 111–123. https://doi.org/10.1016/0378-7796(80)90027-9

Bouaddi, S., Fernández-García, A., Sansom, C., Sarasua, J. A., Wolfertstetter, F., Bouzekri, H., … Azpitarte, I. (2018, October 29). A review of conventional and innovative- sustainable methods for cleaning reflectors in concentrating solar power plants. *Sustainability (Switzerland)*, Vol. 10. https://doi.org/10.3390/su10113937

BP. (2019). BP Statistical Review of World Energy 2019|68th Edition. *BP World Energy*. https://doi.org/10.2307/3324639

Brussels, E., & Ce, O. (2011). *Concentrating solar power: its potential contribution to a sustainable energy future ea sac building science into EU policy*. Retrieved from www.easac.eu

Buck, R., Bräuning, T., Denk, T., Pfänder, M., Schwarzbözl, P., & Tellez, F. (2002). Solar-hybrid gas turbine-based power tower systems (REFOS). *Journal of Solar Energy Engineering, Transactions of the ASME*, *124*(1), 2–9. https://doi.org/10.1115/1.1445444

Carbon Footprint of Electricity Generation. (n.d.). Retrieved from www.parliament.uk/post

Concentrating Solar Power. (2016). Retrieved from http://www.sbcenergyinstitute.com/Publications/SolarPower.html

Ctein. (n.d.). Ctein's Online Gallery. Retrieved August 5, 2020, from http://ctein.com/postlist2.htm

Darwish, M., Hassabou, A. H., & Shomar, B. (2013). Using Seawater Reverse Osmosis (SWRO) desalting system for less environmental impacts in Qatar. *Desalination*, *309*, 113–124. https://doi.org/10.1016/j.desal.2012.09.026

Deign, J. (2012). CSP storage: Phase-change materials quest continues | New Energy Update. Retrieved August 12, 2020, from https://analysis.newenergyupdate.com/csp-today/technology/csp-storage-phase-change-materials-quest-continues

Deng, R., Xie, L., Lin, H., Liu, J., & Han, W. (2010). Integration of thermal energy and seawater desalination. *Energy*, *35*(11), 4368–4374. https://doi.org/10.1016/j.energy.2009.05.025

ELBEH, M. B. (2017). *Concentrated Solar Power Plant for Key Locations in Doha Qatar*.

Energy Agency, I. (2019). *Key World Energy Statistics 2019*.

Energy Commission. (2018). 2018 Malaysia Energy Statistics Handbook. *Malaysia Energy Statistics Handbook*. Retrieved from https://meih.st.gov.my/documents/10620/c7e69704-6f80-40ae-a764-ad0acf4a844d

Evans, G., Houf, W., Greif, R., & Crowe, C. (1987). Gas-particle flow within a high temperature solar cavity receiver including radiation heat transfer. *Journal of Solar Energy Engineering, Transactions of the ASME*, *109*(2), 134–142. https://doi.org/10.1115/1.3268190

Exclusive: Why Malaysia uses drones to monitor power lines | GovInsider. (n.d.). Retrieved August 3, 2020, from https://govinsider.asia/smart-gov/malaysia-tnb-power-lines-drones-fauzan-mohamad/

Fernández-García, A., Álvarez-Rodrigo, L., Martínez-Arcos, L., Aguiar, R., & Márquez-Payés, J. M. (2014). Study of different cleaning methods for solar reflectors used in CSP plants. *Energy Procedia*, *49*, 80–89. https://doi.org/10.1016/j.egypro.2014.03.009

Ghaffour, N., Missimer, T. M., & Amy, G. L. (2013). Technical review and evaluation of the economics of water desalination: Current and future challenges for better water supply sustainability. *Desalination*, *309*, 197–207. https://doi.org/10.1016/j.desal.2012.10.015

Gorjian, S., & Ghobadian, B. (2015, August 1). Solar desalination: A sustainable solution to water crisis in Iran. *Renewable and Sustainable Energy Reviews*, Vol. 48, pp. 571–584. https://doi.org/10.1016/j.rser.2015.04.009

Guidelines on GITA Assets. (2019). Retrieved August 10, 2020, from https://www.myhijau.my/wp-content/uploads/2019/05/Guidelines-on-GITA-Assets-29May19.pdf

Guidelines on GITA Projects. (2019). Retrieved August 10, 2020, from https://www.myhijau.my/wp-content/uploads/2019/05/Guidelines-on-GITA-Projects-29May19.pdf

Hall, M. (2019). Latest Malaysian tender attracts bids for 6.7 GW of capacity – pv magazine International. Retrieved August 12, 2020, from https://www.pv-magazine.com/2019/09/05/latest-malaysian-tender-attracts-bids-for-6-7-gw-of-capacity/

HECTOR successfully completes qualification tests. (2012). Retrieved August 10, 2020, from http://www.sener.es/revista-sener/en/n44/up-to-date__new_markets.html

Heller, P. (2011). *SOLHYCO_Final Public Report*.

Ho, Z. Y., & Bahar, R. (2018). *Performance Analysis of a Solar Desalination System with Concentrated Solar Power (CSP) Performance*. https://doi.org/10.1088/1755-1315/268/1/012023

Hoffmann, J. E. (n.d.). *ON THE OPTIMIZATION OF A CENTRAL RECEIVER SYSTEM*.

Hoffschmidt, B, Alexopoulos, S., Göttsche, J., Sauerborn, M., & Kaufhold, O. (2012). High concentration solar collectors. In *Comprehensive Renewable Energy*. https://doi.org/10.1016/B978-0-08-087872-0.00306-1

Hoffschmidt, B, Alexopoulos, S., Rau, C., Sattler, J., Anthrakidis, A., Boura, C., … Hilger, P. (2012). Concentrating solar power. In *Comprehensive Renewable Energy*. https://doi.org/10.1016/B978-0-08-087872-0.00319-X

Hoffschmidt, Bernhard. (2014). *Receivers for Solar Tower Systems*.

Hwang, J. J. (2010). Promotional policy for renewable energy development in Taiwan. *Renewable and Sustainable Energy Reviews*. https://doi.org/10.1016/j.rser.2009.10.029

IEA-ETSAP & IRENA. (2013). Concentrating Solar Power Technology Brief. In *Energy Committee of the Royal Swedish Academy of Sciences*. https://doi.org/10.1063/1.2993731

Incorporating Renewables Into The Electric Grid: Expanding Opportunities For Smart Market and Energy Storage. (2016).

International Renewable Energy Agency (IRENA). (2018). Renewable Energy Market Analysis: Southeast Asia. In *Irena*.

IRENA. (2019). Renewable Energy Statistics 2019. In *International Renewable Energy Agency*.

Islam, M. T., Huda, N., & Saidur, R. (2019). Current energy mix and techno-economic analysis of concentrating solar power (CSP) technologies in Malaysia. *Renewable Energy*, *140*, 789–806. https://doi.org/10.1016/j.renene.2019.03.107

Jali, M. H., Bohari, Z. H., Izzuddin, T. A., Sarkawi, H., Sulaima, M. F., & Ibrahim, A. (2015). Numeric Model Analysis of a Large Scale Solar PV Generations. In *International Journal of Innovative Technology and Exploring Engineering (IJITEE)*.

Kalogirou, S. A. (2012). Solar thermal systems: Components and applications - introduction. In *Comprehensive Renewable Energy* (Vol. 3, pp. 1–25). https://doi.org/10.1016/B978-0-08-087872-0.00301-2

Kami, J., Kribu, A., Doron, P., Rubin, R., Fiterman, A., & Sagie, D. (1997). The diapr: A high-pressure, high-temperature solar receiver. *Journal of Solar Energy Engineering, Transactions of the ASME*, *119*(1), 74–78. https://doi.org/10.1115/1.2871853

Kim, K., Siegel, N., Kolb, G., Rangaswamy, V., & Moujaes, S. F. (2009). A study of solid particle flow characterization in solar particle receiver. *Solar Energy*, *83*(10), 1784–1793. https://doi.org/10.1016/j.solener.2009.06.011

KLIA installs RM200mil solar power system | The Star. (n.d.). Retrieved August 10, 2020, from https://www.thestar.com.my/business/business-news/2014/01/28/country-first-rm200mil-airport-solar-power-system-launched/

Kodama, T. (2018). Development of Thermochemical Water-Splitting Hydrogen Production System utilizing Concentrated Solar High-Temperature Heat. *Japanses Society for the Promotion of Science*.

Kohli, R., & Mittal, K. L. (2016). Developments in Surface Contamination and Cleaning. In *Developments in Surface Contamination and Cleaning* (Vol. 10). https://doi.org/10.1016/c2013-0-19237-9

Korzynietz, R., Brioso, J. A., Del Río, A., Quero, M., Gallas, M., Uhlig, R., … Teraji, D. (2016). Solugas - Comprehensive analysis of the solar hybrid Brayton plant. *Solar Energy*, *135*, 578–589. https://doi.org/10.1016/j.solener.2016.06.020

Kribus, A., Doron, P., Rubin, R., Reuven, R., Taragan, E., Duchan, S., & Karni, J. (2001). Performance of the Directly-Irradiated Annular Pressurized Receiver (DIAPR) operating at 20 bar and 1,200°C. *Journal of Solar Energy Engineering, Transactions of the ASME*, *123*(1), 10–17. https://doi.org/10.1115/1.1345844

Kutscher, C., Mehos, M., Turchi, C., Glatzmaier, G., & Moss, T. (2011). *Line-Focus Solar Power Plant Cost Reduction Plan (Milestone Report)*. Retrieved from http://www.osti.gov/bridge

Largest solar park in Malaysia starts operation | The Star. (n.d.). Retrieved August 10, 2020, from https://www.thestar.com.my/business/business-news/2018/12/05/largest-solar-park-in-malaysia-starts-operation/

Levelized Cost of Electricity (LCOE) - Overview, How To Calculate. (n.d.). Retrieved August 12, 2020, from https://corporatefinanceinstitute.com/resources/knowledge/finance/levelized-cost-of-energy-lcoe/

Li, X., Wang, Z., Yu, J., Liu, X., Li, J., & Song, X. (2009). The power performance experiment of dish-stirling solar thermal power system. *Proceedings of ISES World Congress, 3*, 1858–1862. https://doi.org/10.1007/978-3-540-75997-3_379

Liu, M., Saman, W., & Bruno, F. (2012). Review on storage materials and thermal performance enhancement techniques for high temperature phase change thermal storage systems. *Renewable and Sustainable Energy Reviews*, Vol. 16, pp. 2118–2132. https://doi.org/10.1016/j.rser.2012.01.020

Liu, M., Steven Tay, N. H., Bell, S., Belusko, M., Jacob, R., Will, G., … Bruno, F. (2016, January 1). Review on concentrating solar power plants and new developments in high temperature thermal energy storage technologies. *Renewable and Sustainable Energy Reviews*, Vol. 53, pp. 1411–1432. https://doi.org/10.1016/j.rser.2015.09.026

Lovegrove, K., & Stein, W. (2012a). Concentrating Solar Power Technology: Principles, Developments and Applications. In *Concentrating Solar Power Technology: Principles, Developments and Applications*. https://doi.org/10.1533/9780857096173

Lovegrove, K., & Stein, W. (2012b). Concentrating solar power technology. In *Concentrating solar power technology*. https://doi.org/10.1533/9780857096173

Luzzi, A., & Lovegrove, K. (2004). Solar Thermal Power Generation. In *Encyclopedia of Energy* (pp. 669–683). https://doi.org/10.1016/B0-12-176480-X/00531-3

MAHB goes for renewable energy at KLIA. (2014). Retrieved August 12, 2020, from The Edge Market website: https://www.theedgemarkets.com/article/mahb-goes-renewable-energy-klia

Mathur, A. (2013). *Using Encapsulated Phase Change Material for Thermal Energy Storage for Baseload CSP*.

McGovern, R. (n.d.). How much does a water desalination plant cost? | SMIPP Ltd. Retrieved August 9, 2020, from https://smipp.wordpress.com/2017/02/13/how-much-does-a-water-desalination-plant-cost/

MetMalaysia: Iklim Malaysia. (n.d.). Retrieved August 10, 2020, from http://www.met.gov.my/pendidikan/iklim/iklimmalaysia?lang=en

Montes, M. J., Abánades, A., Martínez-Val, J. M., & Valdés, M. (2009). Solar multiple optimization for a solar-only thermal power plant, using oil as heat transfer fluid in the parabolic trough collectors. *Solar Energy*, *83*(12), 2165–2176. https://doi.org/10.1016/j.solener.2009.08.010

Neiman, R. (2009). Making the desert bloom with solar flower power. Retrieved August 7, 2020, from https://www.israel21c.org/making-the-desert-bloom-with-solar-flower-power-2/

Ng, K. M., Adam, N. M., & Azmi, B. Z. (2012). Numerical simulation on the reflection characterisation and performance of a solar collector - A case study of UPM Solar Bowl. *Pertanika Journal of Science and Technology*.

Noor, N., & Muneer, S. (2009). Concentrating Solar Power (CSP) and its prospect in Bangladesh. *Proceedings of 1st International Conference on the Developments in Renewable Energy Technology, ICDRET 2009*. https://doi.org/10.1109/icdret.2009.5454207

Norton, B. (n.d.). SOLAR ENERGY. In *A-to-Z Guide to Thermodynamics, Heat and Mass Transfer, and Fluids Engineering*. https://doi.org/10.1615/AtoZ.s.solar_energy

NREL. (n.d.). *System Advisor Model (SAM)*. Retrieved from https://sam.nrel.gov/

NREL. (2001). Concentrating Solar Power: Energy from Mirrors. Retrieved August 5, 2020, from https://www.nrel.gov/docs/fy01osti/28751.pdf

Obrey, S., Steoenheim, J., Mcbride, T., Hehlen, M., Reid, R., & Jankowski, T. (2015). *High Temperature Heat Pipe Receiver for Parabolic Trough Collectors*.

Omar, Z., Ruddin, M., Ghani, A., Gan, C. K., Affandi, R., & Kim, G. C. (2018). Feasibility of 25kw parabolic dish-sterling engine based concentrating solar power under Malaysia environment. *Article in International Journal of Engineering and Technology*, *7*(4), 3874–3878. https://doi.org/10.14419/ijet

Pacheco, J. E. (2002). *Final Test and Evaluation Results from the Solar Two Project*.

Pacio, J., & Wetzel, T. (2013). Assessment of liquid metal technology status and research paths for their use as efficient heat transfer fluids in solar central receiver systems. *Solar Energy*. https://doi.org/10.1016/j.solener.2013.03.025

Petinrin, J. O., & Shaaban, M. (2015, October 1). Renewable energy for continuous energy sustainability in Malaysia. *Renewable and Sustainable Energy Reviews*, Vol. 50, pp. 967–981. https://doi.org/10.1016/j.rser.2015.04.146

Pidaparthi, A., Landman, W., Hoffmann, J., & Dinter, F. (2017). *Optical performance considerations for analysis and simulation of power tower plants . 1850*, 30052. https://doi.org/10.1063/1.4984555

Pihl, E., & Frescativägen, L. (n.d.). *Concentrating Solar Power prepared for the Energy Committee of the Royal Swedish Academy of Sciences*.

Pitz-Paal, R. (2014). Solar Energy - Concentrating Solar Power. In *Future Energy: Improved, Sustainable and Clean Options for our Planet* (pp. 405–431). https://doi.org/10.1016/B978-0-08-099424-6.00019-3

Power Tower System Concentrating Solar Power Basics | Department of Energy. (n.d.). Retrieved July 31, 2020, from https://www.energy.gov/eere/solar/articles/power-tower-system-concentrating-solar-power-basics

Prieto, C., & Cabeza, L. F. (2019). Thermal energy storage (TES) with phase change materials (PCM) in solar power plants (CSP). Concept and plant performance. *Applied Energy*, *254*, 113646. https://doi.org/10.1016/j.apenergy.2019.113646

Rafeeu, Y., & Ab Kadir, M. Z. A. (2012). Thermal performance of parabolic concentrators under Malaysian environment: A case study. *Renewable and Sustainable Energy Reviews*. https://doi.org/10.1016/j.rser.2012.03.041

Rafeq, S. A., Zulfattah, Z. M., Najib, A. M., Rody, M. Z. M., Fadhli, S., Abdollah, M. F. Bin, & Hafidzal, M. H. M. (2013). Preliminary study of CST in malaysia based on field optical efficiency. *Procedia Engineering*, *68*, 238–244. https://doi.org/10.1016/j.proeng.2013.12.174

Renewable Energy Agency, I. (2012). *Concentrating Solar Power Volume 1: Power Sector Issue 2/5 Acknowledgement*. Retrieved from www.irena.org/Publications

Romero, M., Buck, R., & Pacheco, J. E. (2002). An Update on solar central receiver systems, projects, and technologies. *Journal of Solar Energy Engineering, Transactions of the ASME*, *124*(2), 98–108. https://doi.org/10.1115/1.1467921

Santos, J. J. C. S., Palacio, J. C. E., Reyes, A. M. M., Carvalho, M., Freire, A. J. R., & Barone, M. A. (2018a). Concentrating Solar Power. In *Advances in Renewable Energies and Power Technologies*. https://doi.org/10.1016/B978-0-12-812959-3.00012-5

Santos, J. J. C. S., Palacio, J. C. E., Reyes, A. M. M., Carvalho, M., Freire, A. J. R., & Barone, M. A. (2018b). Concentrating Solar Power. In *Advances in Renewable Energies and Power Technologies*. https://doi.org/10.1016/B978-0-12-812959-3.00012-5

Singh, B., Tan, L., Ezriq, Z., & Narayana, P. A. A. (2012). Small parabolic solar cooker for rural communities in Malaysia. *PECon 2012 - 2012 IEEE International Conference on Power and Energy*. https://doi.org/10.1109/PECon.2012.6450189

SOLGATE Final Publishable Report. (2002). *Publication Office of European Comission*. Retrieved from http://www.cordis.lu/sustdev/energy

Stekli, J., Irwin, L., & Pitchumani, R. (2013). Technical challenges and opportunities for concentrating solar power with thermal energy storage. *Journal of Thermal Science and Engineering Applications, 5*(2). https://doi.org/10.1115/1.4024143

Stoffel, T., Renné, D., Myers, D., Wilcox, S., Sengupta, M., George, R., & Turchi, C. (2012). Concentrating solar power: Best practices handbook for the collection and use of solar resource data. In *Concentrating Solar Power: Data and Directions for an Emerging Solar Technology*.

System Advisor Model (SAM). (n.d.). Retrieved August 10, 2020, from https://sam.nrel.gov/concentrating-solar-power/csp-videos.html

Vignarooban, K., Xu, X., Arvay, A., Hsu, K., & Kannan, A. M. (2015). Heat transfer fluids for concentrating solar power systems - A review. *Applied Energy*. https://doi.org/10.1016/j.apenergy.2015.01.125

William, B. S., & Richard, B. D. (1994). A Compendium of Solar Dish/Stirling Technology. *Sandia National Laboratories*. Retrieved from https://www.osti.gov/servlets/purl/10130410

Xiaohong, G., Xiange, S., Miao, Z., & Dawei, T. (2016). Influence of void ratio on thermal stress of PCM canister for heat pipe receiver. *Applied Thermal Engineering*, *94*, 615–621. https://doi.org/10.1016/j.applthermaleng.2015.10.003

Yang, P., Yao, L., Liu, Y., Ni, Q., & Tong, J. (2007). Development of the experimental bench for a research on solar-dish power genaration. *ISES Solar World Congress 2007, ISES 2007*. https://doi.org/10.1007/978-3-540-75997-3_365

Yousif, B. F., Al-Shalabi, A., & Rilling, D. G. (2010). On Integration of Mirror Collector and Stirling Engine for Solar Power System. In *Survival and Sustainability*. https://doi.org/10.1007/978-3-540-95991-5_47